

AD-601 728

AD 601 728

RIA-84-U69

TECHNICAL
LIBRARY



FINAL REPORT

CONCEPT AND FEASIBILITY STUDIES
OF MUZZLE BRAKE BLAST SUPPRESSION DEVICES
FOR 105MM AND 155MM HOWITZERS

**BEST
SCAN
AVAILABLE**

OEA

ORDNANCE ENGINEERING ASSOCIATES, INC.

AD 601728

OEA Project No. 2070

FINAL REPORT

CONCEPT AND FEASIBILITY STUDIES
OF MUZZLE BRAKE BLAST SUPPRESSION DEVICES
FOR 105MM AND 155MM HOWITZERS

Contract No. DA-11-070-AMC-11
OI-11-070-003-04909

Prepared for
ROCK ISLAND ARSENAL
Rock Island, Illinois

26 February 1964

OEA

ORDNANCE ENGINEERING ASSOCIATES, INC.

DISTRIBUTION LIST

	<u>No. of Copies</u>
Commanding Officer Rock Island Arsenal Rock Island, Illinois ATTN: SWERI-RDD-AR	9
Commanding General U. S. Army Weapons Command Rock Island Arsenal Rock Island, Illinois ATTN: AMS WE	1
Commanding Officer Rock Island Arsenal Rock Island, Illinois ATTN: SWERI-RDD-SE	1
Commanding Officer Rock Island Arsenal Rock Island, Illinois ATTN: SWERI-RDD-TS	1
Commanding Officer Rock Island Arsenal Rock Island, Illinois ATTN: SWERI-ASP	1
Commanding General Army Materiel Command ATTN: AMC RD Director of R & D Washington, D. C.	1
Commanding Officer Watervliet Arsenal Watervliet, New York ATTN: Mr. E. Ryan, R&D	1
Commander Armed Forces Technical Information Agency Arlington Hall Station Arlington 12, Virginia ATTN: TIPDR	5
Chicago Procurement District U. S. Army 623 South Wabash Avenue Chicago 5, Illinois	1

OEA

ORDNANCE ENGINEERING ASSOCIATES, INC.

FINAL REPORT
OEA Project No. 2070

CONCEPT AND FEASIBILITY STUDIES
OF MUZZLE BRAKE BLAST SUPPRESSION DEVICES
FOR 105MM AND 155MM HOWITZERS

This final report, prepared by Ordnance Engineering Associates, Inc., under Contract DA-11-070-AMC-11 and OI-11-070-003-04909, covers the period 13 December 1962 through 26 February 1964. The objective of this program is to study and evaluate methods for the attenuation of overpressures resulting from the muzzle brake blast of the 105mm and 155mm Howitzers.

Personnel contributing to this program include: R. L. Chatry, A. D. Kafadar, Samuel Levin, N. Y. Olcer, R. L. Olson, B. E. Paul, E. K. Takata, and A. C. Eringen.

Your comments and suggestions concerning this report will be received with appreciation.

Respectfully submitted,

ORDNANCE ENGINEERING ASSOCIATES, INC.


Samuel Levin


A. D. Kafadar

SL/ADK/jam

OEA

ORDNANCE ENGINEERING ASSOCIATES, INC.

TABLE OF CONTENTS

<u>Section</u>	<u>Page</u>
1.0 INTRODUCTION	1
2.0 DETERMINATION OF OVERPRESSURE RESULTING FROM FIRING WEAPONS WITH MUZZLE BRAKES	3
2.1 Method of Computation	4
2.2 Brake Index Constraint	7
2.3 Comparison With Experimental Data	9
2.4 Effect of Thrust on Location of Overpressure	13
2.5 Summary	19
3.0 DESIGN CONSIDERATIONS	22
3.1 Application to 105mm Howitzer	23
3.2 Application to 155mm Howitzer	33
3.3 Summary	41
4.0 MUZZLE BRAKE BLAST SUPPRESSION DEVICE - 105mm HOWITZER	44
4.1 Design Description	44
4.2 Results - Stress Analysis of 360 Degree Muzzle Brake Blast Suppression Device	46
4.3 Summary	47
5.0 PRESSURE AND FLOW FIELD EXTERIOR TO A GUN BLAST	49
6.0 RECOMMENDATIONS	50
 APPENDICES	
A Interior Ballistics of Muzzle Brake and Blast Suppression Devices	
B Stress Analysis of Muzzle Brake Blast Suppression Device - 105mm Howitzer	
C Pressure and Flow Field Experior to a Gun Blast	



LIST OF ILLUSTRATIONS

<u>Fig. No.</u>		<u>Page</u>
2.1	Computed Overpressures Compared with Measured 105mm Howitzer XM103E1 Fired with 5/K Brake	10
2.2	Comparison of Computed with Experimental Blast Overpressure, 105mm Howitzer, XM103 with Brake D8259	11
2.3	Comparison of Computed with Experimental Blast Overpressure, 105mm Howitzer, XK103 with Brake F8241	12
2.4	Location of 4 psi Isobar; 105mm Howitzer Fired with Muzzle Brake of Index 1.2	17
2.5	Location of 4 psi Isobar; 155mm Howitzer Fired with Muzzle Brake of Index 1.2	21
3.1	Brake Port Angle Versus A_p/A with "a" as a Parameter, 105mm Howitzer	24
3.2	Effect of Muzzle Brake Index on Brake Port Angle, 105mm Howitzer	25
3.3	Computed Isobars Obtained as a Result of Firing Howitzer with a Muzzle Blast Suppression Device, $a = 1/3$	27
3.4	Computed Isobars Obtained as a Result of Firing 105mm Howitzer with a Muzzle Blast Suppression Device, $a = 2/3$	28
3.5	Brake Port Angle Versus A_p/A for 105mm Howitzer Shoring Effect of Time Parameter	31
3.6	Effect of Design Parameters on Dimensionless Brake Pressure for 105mm Howitzer	34
3.7	Effect of Design Parameters on Rate of Gas Discharge for 105mm Howitzer	35
3.8	Brake Port Angle Versus A_p/A for 155mm Howitzer	37
3.9	Computed Isobars Obtained as a Result of Firing the 155mm Howitzer with a Muzzle Blast Suppression Device	39

LIST OF ILLUSTRATIONS Continued

<u>Fig. No.</u>		<u>Page</u>
3.10	Brake Port Angle Versus A_p/A for 155mm Howitzer Showing Effect of Time Parameter	40
3.11	Effect of Design Parameters on Blast Suppression Device Pressure, 155mm Howitzer	42
3.12	Effect of Design Parameters on Rate of Gas Discharge for 155mm Howitzer	43
4.1	Muzzle Brake, 105mm Howitzer	45
4.2	Location of Computed Stress And Deflections for 360° Muzzle Brake, 105mm Howitzer	48

LIST OF TABLES

<u>Table No.</u>		<u>Page</u>
2.1	Location of 4 psi Overpressure from 105mm Howitzer Fired with Muzzle Brake with no Additional Expansion	16
2.2	Location of 4 psi Overpressure from 105mm Howitzer Fired with Muzzle Brake with Additional Expansion	16
2.3	Location of 4 psi Overpressure from 105mm Howitzer Fired with Muzzle Brake with no Additional Expansion and Losses Considered	18
2.4	Location of 4 psi Overpressure from 155mm Howitzer Fired with Muzzle Brake with no Additional Expansion	20
2.5	Location of 4 psi Overpressure from 155mm Howitzer Fired with Muzzle Brake with Additional Expansion	20
3.1	Parameters Used to Map Overpressure 105mm Howitzer	26
3.2	Computed Location of 4 psi Overpressure, 105mm Howitzer, Showing Effect of Design Parameters	30
4.1	Summary of Maximum Stresses and Displacements for 360° Muzzle Blast Suppression Device	48

FINAL REPORT
OEA Project No. 2070
CONCEPT AND FEASIBILITY STUDIES
OF MUZZLE BRAKE BLAST SUPPRESSION DEVICES
FOR 105MM AND 155MM HOWITZERS

1.0 INTRODUCTION

Muzzle brakes are included in the new lightweight 105mm and 155mm Howitzers in order to reduce overall weapon weight. The weight savings, in the recoil system, results from diverting a portion of the propellant gases that normally discharge through the muzzle, after shot ejection, in a non-axial direction. Thus, the recoil system operates against a lesser thrust, resulting from the impulse of the discharging gases, and offers a reduction in the weight of the recoil system.

However, as the performance requirements of the brake increase, more propellant gas is diverted from passing through the weapon in the axial direction. The discharge of the diverted high pressure propellant gases produces blast waves which in turn increase the overpressure in the crew area of the weapon. At present, it is understood that 4 psi overpressure is the maximum level which the crew can tolerate without resorting to special protective devices.

This final report contains a summary of the work conducted by Ordnance Engineering Associates, Inc. under Contract Nos. DA-11-070-AMC-11 and OI-11-070-003-04909 relating to muzzle brake blast suppression in 105mm and 155mm Howitzers. The main objective of the program is attenuation of the blast overpressure in the gun crew servicing area without retarding the effectiveness of the recoil system.

OEA

ORDNANCE ENGINEERING ASSOCIATES, INC.

During the course of this program the results of the following studies were presented and when practical application was made to the 105mm and 155mm Howitzers:

1. Analytical determination of overpressure maps resulting from firing Howitzers with muzzle blast suppression devices.
2. Analyses for evaluating the effects of design parameters comprising the device.
3. Techniques for computing the dimensionless pressure and mass rate of discharge - dimensionless time histories in the suppression device.
4. The effect of time which the projectile remains in the suppression device.
5. Design parameters of the device which create attenuated overpressures in the crew area.
6. A proposed design for the 105mm Howitzer blast suppression device and the stress analysis of the design.

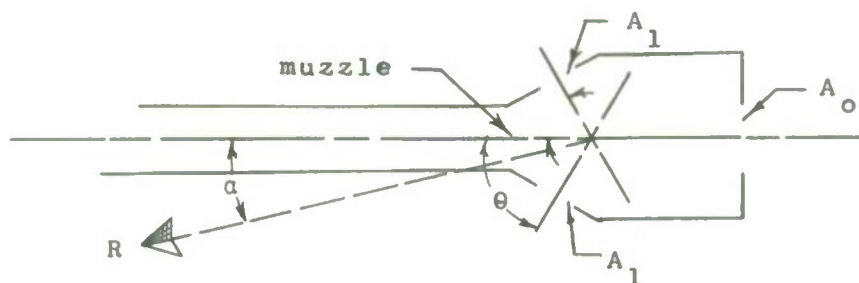
In addition to the above, an analytical study relating to the directional effects of blast waves was conducted. A summary of this work is presented in this report.

2.0 DETERMINATION OF OVERPRESSURE RESULTING FROM FIRING WEAPONS WITH MUZZLE BRAKES

Overpressures in the crew area increase as a result of firing Howitzers equipped with muzzle brakes. In general, the more efficient the device the greater the quantity of gas is discharged to the rear area; hence, increasing the magnitude of the overpressure. As an upper limit, an idealized brake having a maximum efficiency would be where all of the propellant gas is discharged opposite to the line of fire. This ideal system would achieve the maximum reduction in the recoil force, but would also produce the greatest overpressure in the rear area of the weapon. The magnitude of overpressure in the rear area under this condition would correspond to that encountered forward of the muzzle when the weapon is fired without a muzzle brake.

In this section of the report, a method is presented which enables one to predict the overpressure resulting from the blast of a muzzle brake. In addition, the effect of the performance index and other brake parameters on the overpressure are given.

It is necessary for a muzzle brake to have as a minimum two ports in addition to the shot ejection port in order to achieve non-axial force balance. Such a system is shown below:



OEA

ORDNANCE ENGINEERING ASSOCIATES, INC.

where

- A_o = ejection port area
- A_1 = recoil compensating port area
- θ = angle of normal to A_1 with axis
- R = distance from brake to specific reference point
- α = angle of reference point vector with respect to axis

2.1 Method of Computation

The overpressure, Δp , induced by energy flow, E_e , from a sonic orifice, has been shown^{1/} to be given by:

$$\Delta p = \left[\frac{p_o \gamma_o (\gamma_o - 1)}{144 R^3 \pi (\gamma_o + 1)} \right]^{1/2} \left[\Phi E_e \right]^{1/2} = K_o^{1/2} \left[\Phi E_e \right]^{1/2} \quad (2.1)$$

where:

- p_o = ambient pressure, psi
- γ_o = specific heat ratio of ambient medium
- R = distance from nozzle exit, ft.
- E_e = energy of gas discharged from orifice, ft.-lb
- Φ = directional function dependent on angle of position vector, R , with orifice axis.

If the blast results from a point source detonation, the resulting shock wave is spherical as described by Eq. (2.1), and $\Phi = 1.0$ for a given energy release, E_e . Because the energy flow from an orifice is not instantaneous, and is also directed in a conical fashion, the function Φ becomes strongly dependent on the angle from the nozzle axis, as well as a factor which may reduce the effective energy. This function has been determined experimentally^{2/} for the flow from a recoilless

^{1/} Summary Report. Investigation of the Effect of Blast from Recoilless Rifles, Contract DA-11-022-ORD-1227, April 1953 by B. E. Paul and A. D. Kafadar.

^{2/} Ibid.

rifle orifice, and may be accurately represented by:

$$\Phi = \Phi_0 \left(1 - \frac{\theta}{\theta_0}\right)^n \quad (2.2)$$

where:

$$\begin{aligned} \Phi_0 &= 6.25 \\ \theta_0 &= 83^\circ \\ n &= 3.23 \end{aligned}$$

This can be shown to account for about 60% of the energy as contributing to the shock structure developed. Of the remaining 40%, some of the energy contributes to the formation of very weak shock waves at angles greater than 83° from the orifice axis. The remainder simply does not enter the primary shock formation due to its time lag in the flow phenomenon.

However, Eq. (2.1) does not yet lend itself to application to the muzzle brake situation, since there are at least two orifices to be considered in the blast pressure developed. It is possible to extend the argument to include a multiple orifice system. In general, energy is a scalar additive property. Based on this characteristic, and assuming R large with respect to the maximum orifice-to-orifice distance, the energy function in Eq. (2.1) may be replaced by the summation of directional energies, $\Phi_1 E_1$, contributed by each port flow. This further assumes the flow to occur in the same time period, which is of course the case experienced with the muzzle brake blast suppression device.

Although the energy term, E_1 , is equal for each set of symmetric brake ports, the directional functions, Φ_1 , are equal only for a point, R , on a plane containing the gun axis and perpendicular to the plane containing the gun and brake port axis. For the case depicted in the sketch, the Φ_1 functions would be

$$\left. \begin{aligned}
 \Phi_1 &= \Phi_0 \left[1 - \frac{\theta_1}{\theta_0} \right]^n \\
 \theta_1 &= \left| \theta - \alpha \right| \\
 \theta_2 &= \theta + \alpha
 \end{aligned} \right\} (2.3)$$

whereas the energy flow terms, E_1 , would be equal, $E_1 = E_2$. The effect of the angle α may be readily shown, however, by referencing the overpressure to the gun axis for which $\alpha = 0$. The dual port condition may then be defined by

$$\left. \begin{aligned}
 \Delta p &= (\Delta p_0) G \\
 G^2 &= \frac{\left(1 - \frac{\theta_1}{\theta_0}\right)^n + \left(1 - \frac{\theta_2}{\theta_0}\right)^n}{2 \left(1 - \frac{\theta}{\theta_0}\right)^n} \\
 \Delta p_0 &= (K_0 \Phi_0)^{1/2} \left[2 \left(1 - \frac{\theta}{\theta_0}\right)^n E_1 \right]^{1/2}
 \end{aligned} \right\} (2.4)$$

where

E_1 = energy flow from each brake port

The angles, (θ_1, θ_2) are defined by Eq. (2.3), which makes G a function of the brake port angle, θ , and position angle, α . The function, G , enables an axial pressure study Δp_0 to be extended to any position angle, α . Equations (2.3) and (2.4) therefore describe the pressure distribution in the crew area for a double ported brake. Additional ports at angles $\theta > \alpha + 83^\circ$ make negligibly small contributions. In any case, the technique is readily extended to include any number of brake ports, however, the energy flows will, in general, be unequal and will then enter as ratios in the G function.

2.2 Brake Index Constraint

The primary purpose of the muzzle brake is of course to afford a particular degree of recoil momentum compensation, defined by the brake index, i , as

$$i = 1 - \frac{I_b}{I_g} \quad (2.5)$$

where:

I_b, I_g = port shot-ejection recoil momentum contribution of propellant gases with and without brake, respectively,

and the resulting total recoil momentum of the gun, I_r , is

$$I_r = m V_m - (i - 1) I_g \quad (2.6)$$

where:

m = projectile mass
 V_m = muzzle velocity

It can be shown that the momentum contribution of the flow through an orifice is proportional to the energy flow, or

$$I_i = B C_{fi} E_i \quad (2.7)$$

where:

B = proportionality constant
 C_{fi} = thrust coefficient of orifice
 E_i = energy flow through orifice
 I_i = orifice axial momentum

Without the brake, this is

$$I_g = B C_{fg} E_g \quad (2.8)$$

$C_{fg} \approx 1.0$, for flow from a straight tube.

With a muzzle brake, the total energy flow out of the system is less than E_g due to losses in the brake. Taking this as a function, b , of E_g , yields the energy flow balance as

$$E_o + 2 \sum E_i = (1 - b) E_g \quad (2.9)$$

where:

E_o = energy flow out of ejection port

E_i = energy flow out one of the i^{th} brake port orifice pairs

During the period of projectile base travel from the muzzle to the brake ejection port, there will be flow through the areas A_1 , however, there is essentially no flow through the projectile port, A_o ^{1/}. Its contribution to the total flow area is therefore reduced, so that the energy flow distribution may be written as:

$$E_o = \frac{\lambda A_o}{2 \sum A_1 + \lambda A_o} (1-b) E_g$$

$$E_K = \frac{A_K}{2 \sum A_1 + \lambda A_o} (1-b) E_g \quad (2.10)$$

λA_o = effective area for flow system, < 1

which is seen to satisfy the energy balance given by Eq.(2.9).

Taking the gun axial components of momentum from Eq. (2.7) the brake impulse, I_b , is given by

$$I_b = I_o - 2 \sum I_i \cos \theta_i$$

or

$$I_b = BC_{fo} E_o - 2B \sum C_{fi} E_i \cos \theta_i \quad (2.11)$$

^{1/} Each set of ports may further be separated by partitions.

Substituting Eq. (2.10) into (2.11), and taking the ratio of the result with I_g from Eq. (2.8), yields the brake index as:

$$i = 1 - \frac{(1 - b)}{2 \sum a_1 + \lambda} \left[C_{fo} \lambda - 2 \sum C_{fi} a_1 \cos \theta_i \right] \quad (2.12)$$

where:

$$a_i = \frac{A_i}{A_0}$$

The above equation represents the brake index constraint which must be satisfied.

2.3 Comparison With Experimental Data

Overpressures computed for the 105mm Howitzer XM103 based on Eqs. (2.4) and (2.10) were compared with experimental data reported^{1/} for this Howitzer when fired with three different muzzle brakes.

Figs. 2.1, 2.2, and 2.3 compare the above data and were based on the following parameters:

<u>Brake</u>	<u>5/K</u>	<u>D8259</u>	<u>F8241</u>
λ	1	1	1
β	0	0	0
E_g ft-lb	2.71×10^6	2.71×10^6	2.71×10^6
C_{fg}	1	1	1
C_{fi}	1	1	1
a_1	2.78	1.28	3.23
θ , degrees	25	30	25
p_o , psi	14.7	14.7	14.7
γ_o	1.4	1.4	1.4
Φ_o	6.25	6.25	6.25
θ_o , degrees	83	83	83
<u>n</u>	<u>3.23</u>	<u>3.23</u>	<u>3.23</u>

^{1/} Muzzle Blast Measurement on Howitzer, 105mm, XM103E1.
H. H. Holland, Jr., U.S. Army Human Engineering Laboratories,
APG, TM23-62, Oct. 1962.

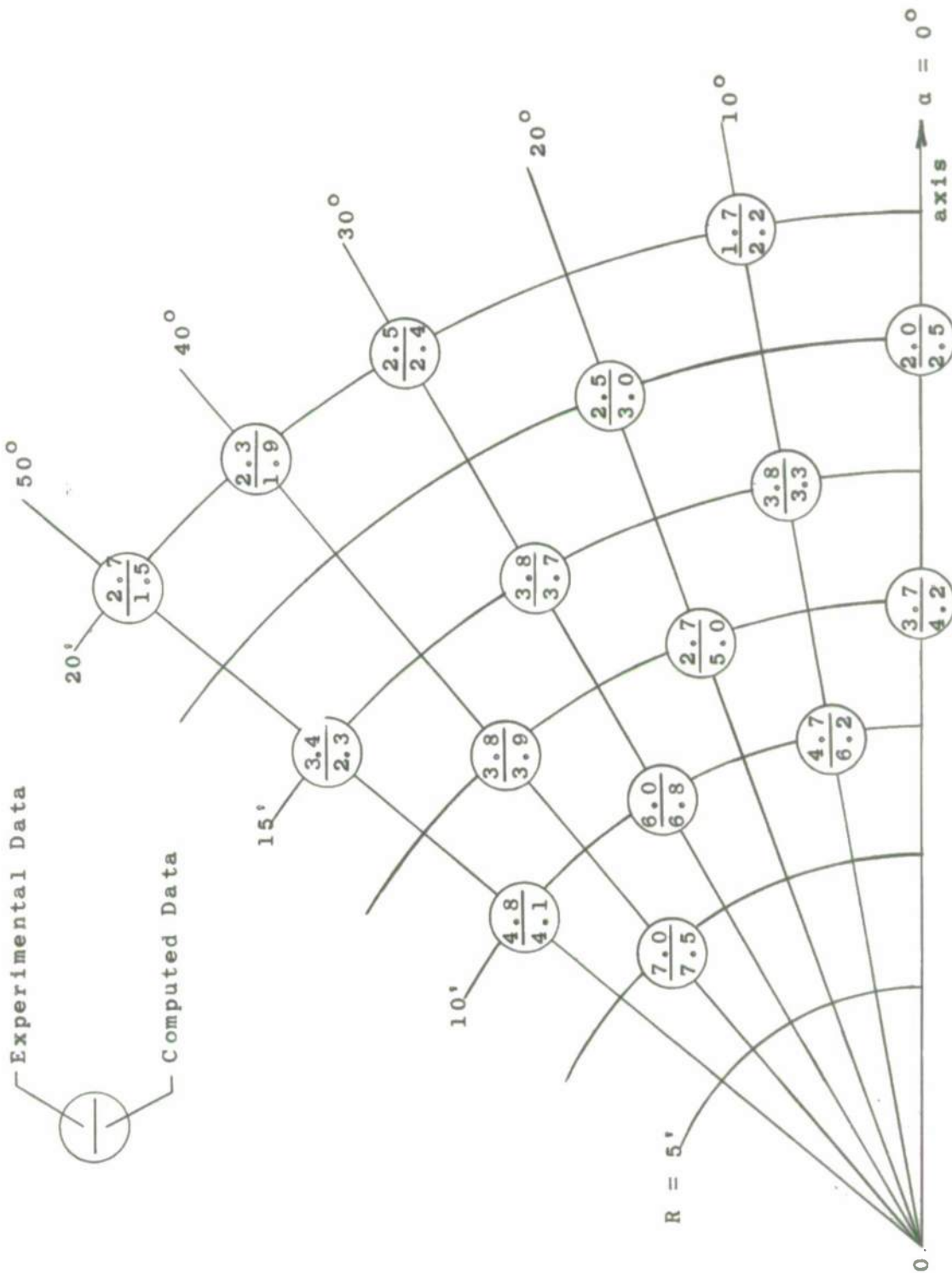


Fig. 2.1 - COMPUTED OVERPRESSURES COMPARED WITH MEASURED
105MM HOWITZER XM103E1 FIRED WITH 5/K BRAKE

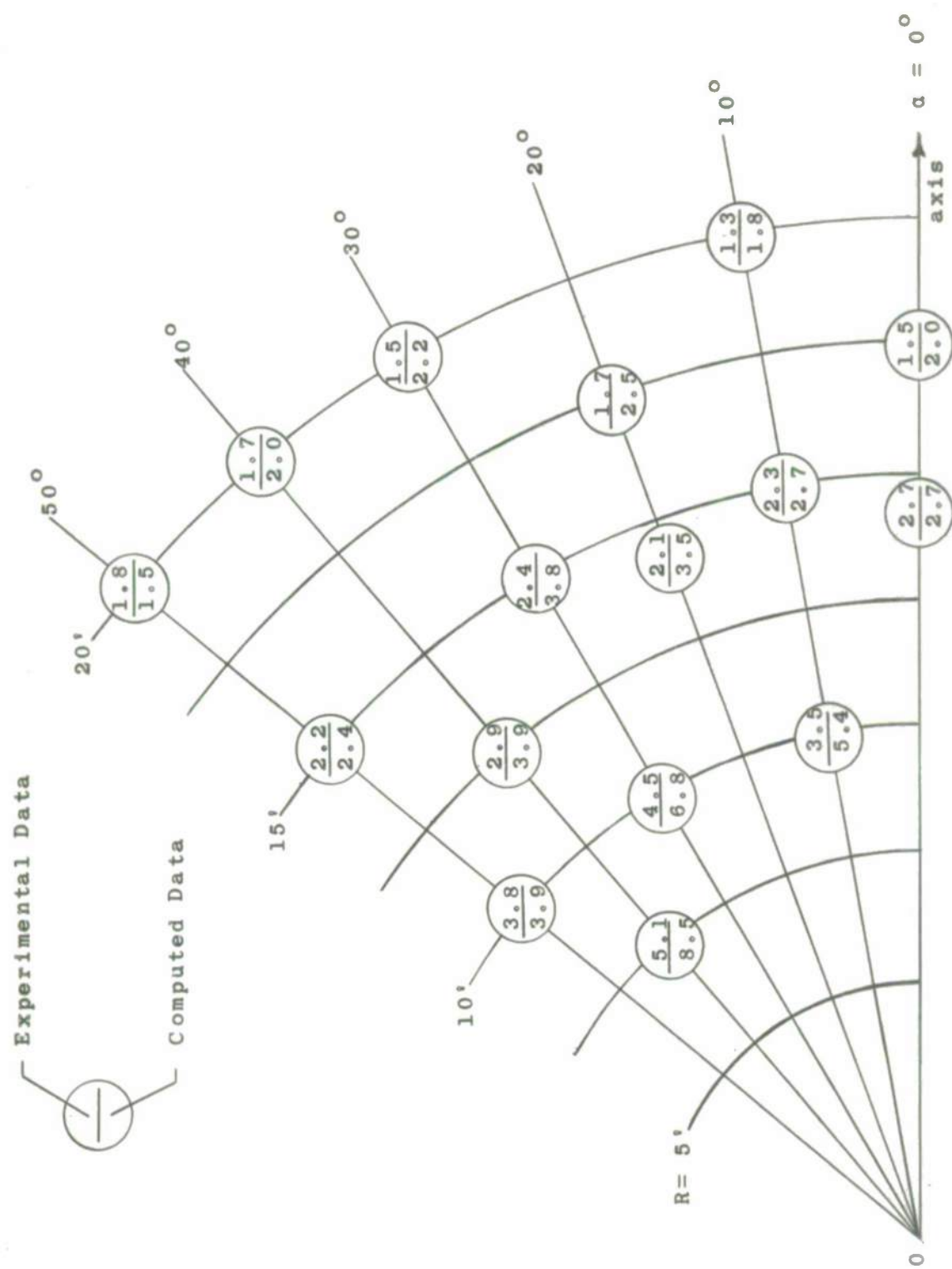


FIG. 2.2 - COMPARISON OF COMPUTED WITH EXPERIMENTAL BLAST OVERPRESSURE, 105MM HOWITZER, XM103 WITH BRAKE D8259



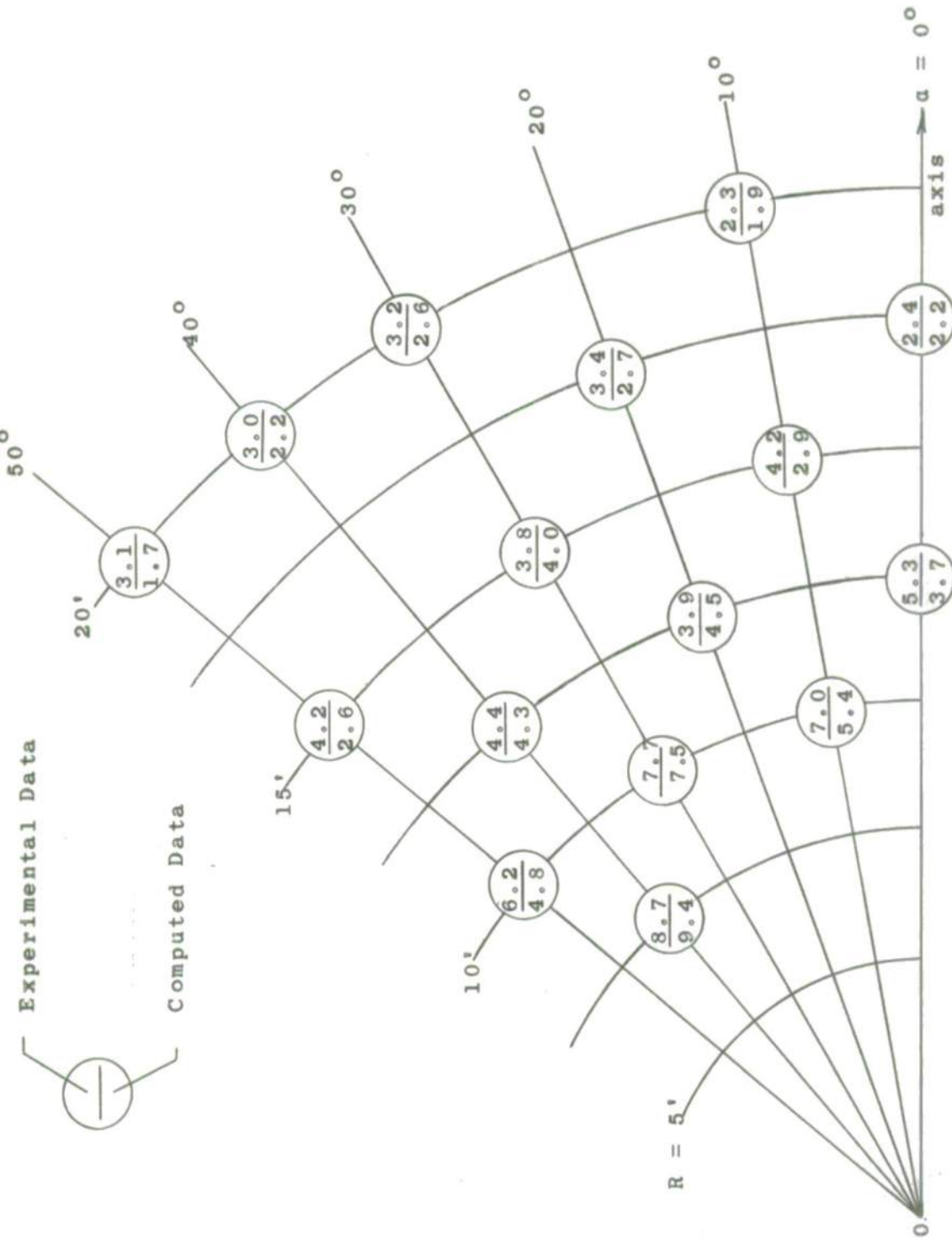


Fig. 2.3 - COMPARISON OF COMPUTED WITH EXPERIMENTAL BLAST OVERPRESSURE, 105MM HOWITZER, XM103 WITH BRAKE F8241



It can be seen in these figures that the mathematical model used to predict overpressures provides sufficiently good agreement with the experimental data to warrant its application to the evaluation of muzzle brake blast suppression devices.

2.4 Effect of Thrust on Locations of Overpressure

The following analysis was made to show the effect of expanding the discharged propellant gas, and thereby obtain additional thrust to reduce the recoil forces, on the location of the blast overpressure:

From Eq. (2.12) the port area ratio corresponding to a bi-ported brake is obtained as:

$$a_1 = \frac{\lambda}{2} \left[\frac{(1 - 1) + (1 - b) C_{fo}}{(1 - b) C_{f1} \cos \theta - (1 - 1)} \right] \quad (2.13)$$

and from Eq. (2.10) the energy passing through each side port is given by:

$$E_1 = \frac{a_1}{2 a_1 + \lambda} (1 - b) E_g \quad (2.14)$$

The location of a selected overpressure, Δp , as obtained from Eq. (2.4) is

$$R = \Phi_o^{1/3} \left[\frac{p_o \gamma_o (\gamma_o - 1)}{144\pi (\gamma_o + 1) (\Delta p)^2} \right]^{1/3} \left[\left(1 - \frac{\theta_1}{\theta_o}\right)^n + \left(1 - \frac{\theta_2}{\theta_o}\right)^n \right]^{1/3} E_1^{1/3} \quad (2.15)$$

Thus, from Eq. (2.15)

$$\frac{dR}{R} = \frac{1}{3} \frac{dE_1}{E_1}$$

from Eq. (2.14)

$$\frac{dE_1}{E_1} = \frac{\lambda}{\lambda + 2a_1} \frac{da_1}{a_1}$$

and from Eq. (2.13)

$$\frac{da_1}{a_1} = - \frac{(1-b) \cos \theta}{(1-b) C_{fi} \cos \theta - (i-1)} dC_{fi}$$

Therefore, from the above obtain

$$\frac{\Delta R}{R} = - \frac{1}{3} \left(\frac{\lambda}{\lambda + 2a_1} \right) \left[\frac{(1-b) \cos \theta}{(1-b) C_{fi} \cos \theta - (i-1)} \right] \Delta C_{fi} \quad (2.16)$$

which shows the expected variation in location of a particular overpressure as a function of the change in the thrust coefficient of the recoil compensating ports, C_{fi} .

2.4.1 Application to 105mm Howitzer

The location of 4 psi overpressure for 105mm Howitzer fired with a biported muzzle brake was determined for the following cases:

	<u>Case I</u>	<u>Case II</u>
E_g =	2.714×10^6 ft-lb	2.714×10^6 ft-lb
λ =	1.0	1.0
b =	0	0
C_{fi} =	1	1.175
i =	1.2	1.2

Case I corresponds to the condition of equal propellant gas expansion in the axial and side ports while Case II represents an increase in the propellant gas expansion in

the side ports over that in the axial ports. The results obtained for these cases are shown in Table 2.1 and Table 2.2 for Case I and II, respectively.

Comparison of the data in these tables shows that the location of 4 psi changes about 3 per cent when the C_{fi} is increased from unity to 1.175. From Eq. (2.16) it can be found that the expected change in overpressure location, $\frac{\Delta R}{R}$, would be about 25 per cent.

Fig. 2.4 shows a plot of 4 psi isobar as a function of the port angle θ and the location angle α . It is seen that as the port angle θ increases, the region of 4 psi overpressure occurs closer to the muzzle of the Howitzer.

The effect of the parameters λ and b were checked by re-evaluating Case I, above, for $\lambda = 0.8$ and $b = 0.05$. Table 2.3 shows the results of this study and comparison of these data with those in Table 2.1 shows negligible variation in the location of the isobar.

2.4.2 Application to 155mm Howitzer

A study, similar to that conducted for the 105mm Howitzer, was repeated for the 155mm Howitzer for the following cases:

	<u>Case I</u>	<u>Case II</u>
$E_g =$	14.56×10^6	14.56×10^6
$\lambda =$	1.0	1.0
$b =$	0	0
$C_{fi} =$	1	1.175
$i =$	1.2	1.2

These cases correspond to the condition of equal expansion in the side and axial ports (Case I) and to greater expansion in side ports than in axial ports (Case II). The

Table 2.1

LOCATION OF 4 PSI OVERPRESSURE FROM 105MM HOWITZER
FIRED WITH MUZZLE BRAKE WITH NO ADDITIONAL EXPANSION

Location of Overpressure, ft

θ a	0°	20°	40°	60°	78.27°
0°	16.9	12.7	8.7	4.7	0
10°	14.7	13.1	9.2	5.6	2.4
20°	12.6	14.1	10.5	7.3	5.4
30°	10.4	11.9	13.8	9.1	6.2
40°	8.3	10.2	14.0	11.0	8.1
50°	6.3	8.4	13.8	14.6	10.2
a_1	.75	.8108	1.06	2.00	∞

Table 2.2

LOCATION OF 4 PSI OVERPRESSURE FROM 105MM HOWITZER
FIRED WITH MUZZLE BRAKE WITH ADDITIONAL EXPANSION

Location of Overpressure, ft

θ a	0°	20°	40°	60°	80.13°
0°	16.4	12.3	8.5	4.6	0
10°	14.3	12.7	9.0	5.5	2.1
20°	12.2	13.7	10.2	7.2	3.9
30°	10.2	11.6	13.5	6.9	5.8
40°	8.1	9.9	13.6	10.8	7.8
50°	6.1	8.2	13.5	14.3	9.8
a_1	0.61	0.66	0.05	1.54	∞



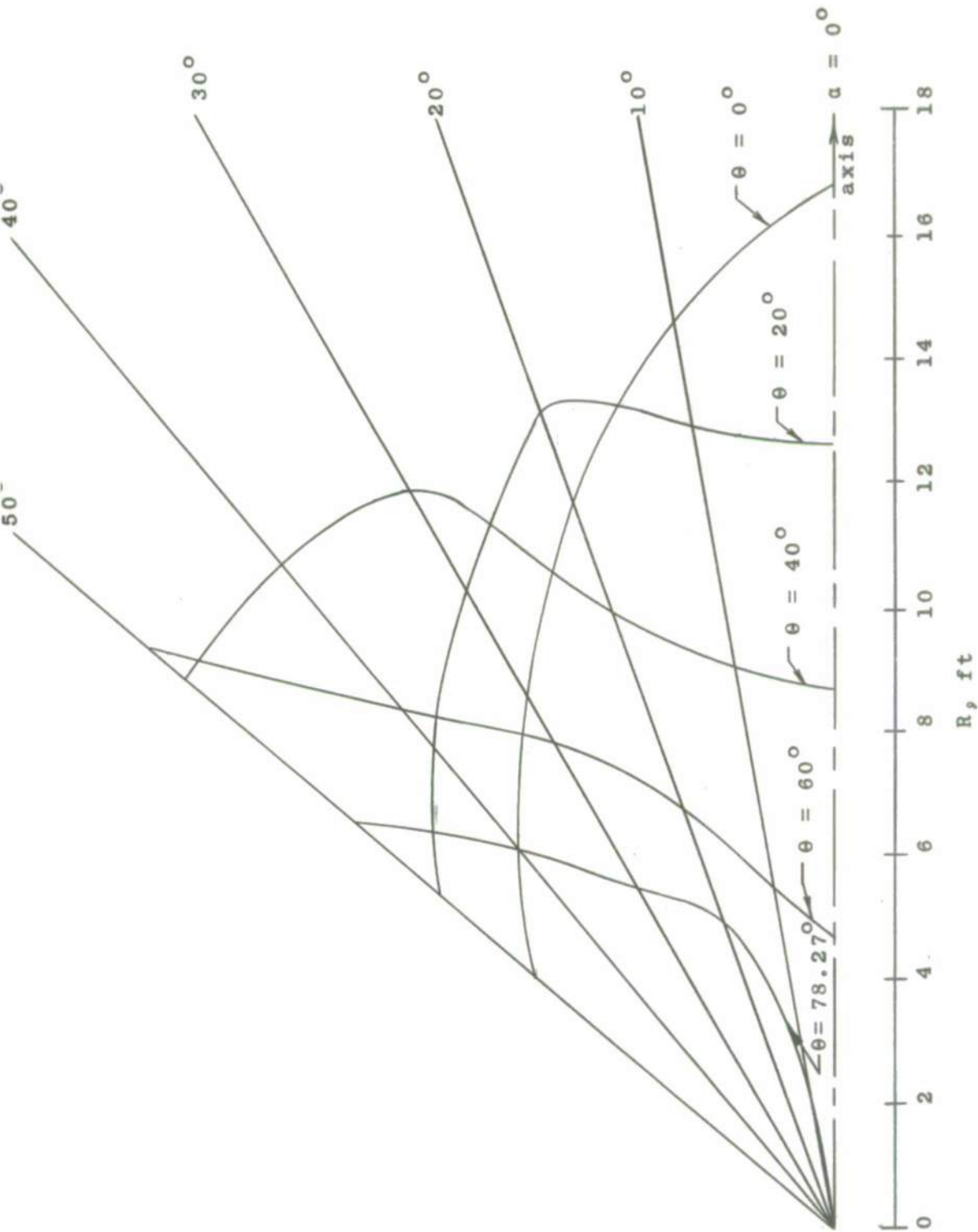


FIG. 2.4 - LOCATION OF 4 PSI ISOBAR; 105MM HOWITZER FIRED
WITH MUZZLE BRAKE OF INDEX 1.2



Table 2.3

LOCATION OF 4 PSI OVERPRESSURE FROM 105MM HOWITZER
FIRED WITH MUZZLE BRAKE WITH NO ADDITIONAL
EXPANSION AND LOSSES CONSIDERED

Location of Overpressure, ft

$\frac{\theta}{a}$	0°	20°	40°	60°	78.27°
0°	17.1	12.8	8.7	4.7	0
10°	14.9	13.2	9.3	5.5	2.3
20°	12.7	14.2	10.5	7.3	5.3
30°	10.6	12.0	13.9	9.1	6.8
40°	8.4	10.3	14.0	11.0	8.0
50°	6.3	8.5	13.9	14.5	10.0

OEA

ORDNANCE ENGINEERING ASSOCIATES, INC.

results are summarized in Tables 2.4 and 2.5 for Case I and II, respectively. Fig. 2.5 shows the plot of the 4 psi isobar as a function of the port angle θ and direction of angle α . These data in Tables 2.4 and 2.5 show that the effect of increasing the expansion as indicated above serves to alter the isobar location about 3 per cent. This range of variation is in agreement with that computed for the 105mm Howitzer.

2.5 Summary

The results of the studies conducted on the blast overpressure resulting from firing Howitzers with muzzle brakes are as follows:

1. Overpressure can be computed with the mathematical model presented with reasonable accuracy (generally about 20 per cent)
2. Directing the propellant gases away from the crew, without reducing the effectiveness of the brake, is a good method for reducing the overpressures in this region.
3. Providing additional thrust from the propellant gases as they are discharged through the recoil compensating ports should not seriously effect the magnitude of the overpressure in the crew area.

Table 2.4

LOCATION OF 4 PSI OVERPRESSURE FROM 155MM HOWITZER
FIRED WITH MUZZLE BRAKE WITH NO ADDITIONAL EXPANSION

Location of Overpressure, ft

θ a	0°	20°	40°	60°	78.27°
0°	29.6	22.2	15.2	8.2	0
10°	25.8	22.9	16.1	9.7	4.2
20°	22.0	24.6	18.4	12.8	9.5
30°	18.3	20.8	24.1	16.0	10.8
40°	14.6	17.8	24.5	19.2	14.2
50°	11.0	14.7	24.1	25.5	17.8

Table 2.5

LOCATION OF 4 PSI OVERPRESSURE FROM 155MM HOWITZER
FIRED WITH MUZZLE BRAKE WITH ADDITIONAL EXPANSION

Location of Overpressure, ft

θ a	0°	20°	40°	60°	80.13°
0°	28.8	21.6	14.8	8.0	0
10°	25.0	22.3	15.8	9.6	3.7
20°	21.4	24.0	18.0	12.5	6.9
30°	17.8	20.2	23.5	15.7	10.2
40°	14.2	17.3	23.9	18.8	13.6
50°	10.7	14.3	23.5	25.0	17.1



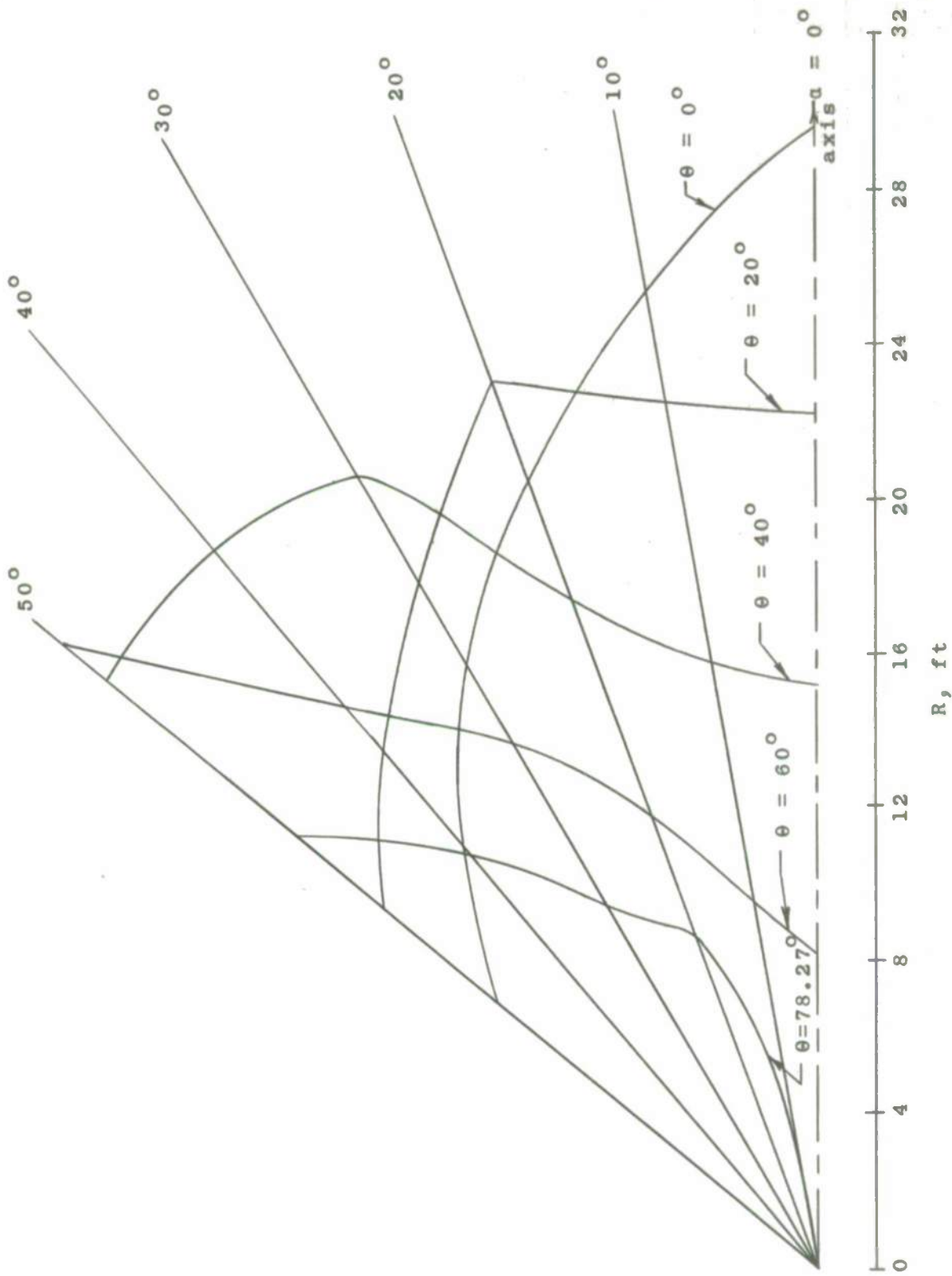
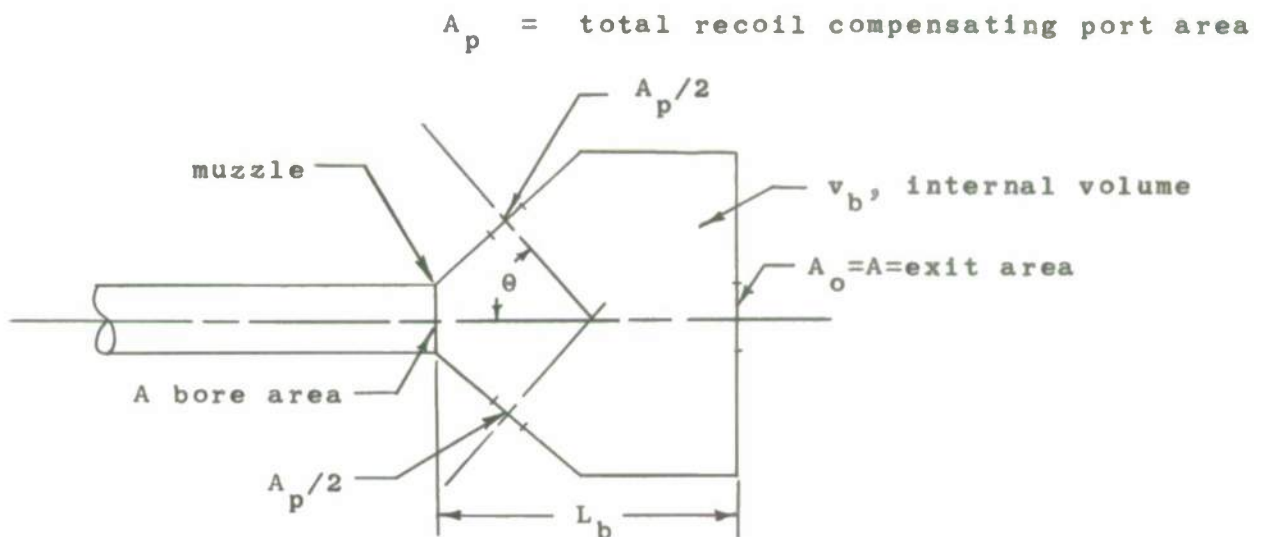


Fig. 2.5 - LOCATION OF 4 PSI ISOBAR: 155MM HOWITZER FIRED
WITH MUZZLE BRAKE OF INDEX 1.2

3.0 DESIGN CONSIDERATIONS

A study was conducted, based on the analysis given in Appendix A, to evaluate muzzle brakes and the effects of incorporating blast suppression provisions. The influence of the parameters comprising the device - internal volume, v_b , port angle, θ , total recoil compensating port area, A_p , pressure, p , and length, L_b - are evaluated as to their influence on the muzzle brake blast suppression device design. The factors which comprise the suppression device design are shown below:



3.1 Application to 105mm Howitzer

Figs. 3.1 and 3.2 were obtained from Eq. (A.17) and are based on the following parameters pertaining to a 105mm Howitzer:

θ_b	=	0.5, ratio of average gas temperature in brake to isochoric flame temperature
θ_g	=	0.6, ratio of average gas temperature discharged from muzzle to isochoric flame temperature
γ	=	1.24, ratio specific heat propellant gas
A	=	13.4 in. ² bore area
$C_d' = C_d'' = C_d'''$	=	0.85, discharge coefficients, muzzle, brake ports, and projectile exit
C_f'	=	1.3, thrust coefficient muzzle
C_f''	=	1.5, thrust coefficient brake port
C_f'''	=	1.1, thrust coefficient projectile exit
F	=	323,000 ft-lb/lb, propellant impetus
K	=	6.56×10^{-6} sec ⁻¹ , isentropic flow constant
L_b	=	12 in., brake length
p_m	=	4,950 psi, space mean pressure of gun at shot ejection
t_l	=	0.645×10^{-3} sec, time for projectile to traverse brake
v_T	=	1,578 in. ³ , effective total gun volume
V_m	=	1550 fps, muzzle velocity

The factor "a" indicated as a parameter on Fig. 3.1 and 3.2 is defined in Appendix A as follows:

$$a = \frac{AL_b}{v_b}$$

OEA

ORDNANCE ENGINEERING ASSOCIATES, INC.

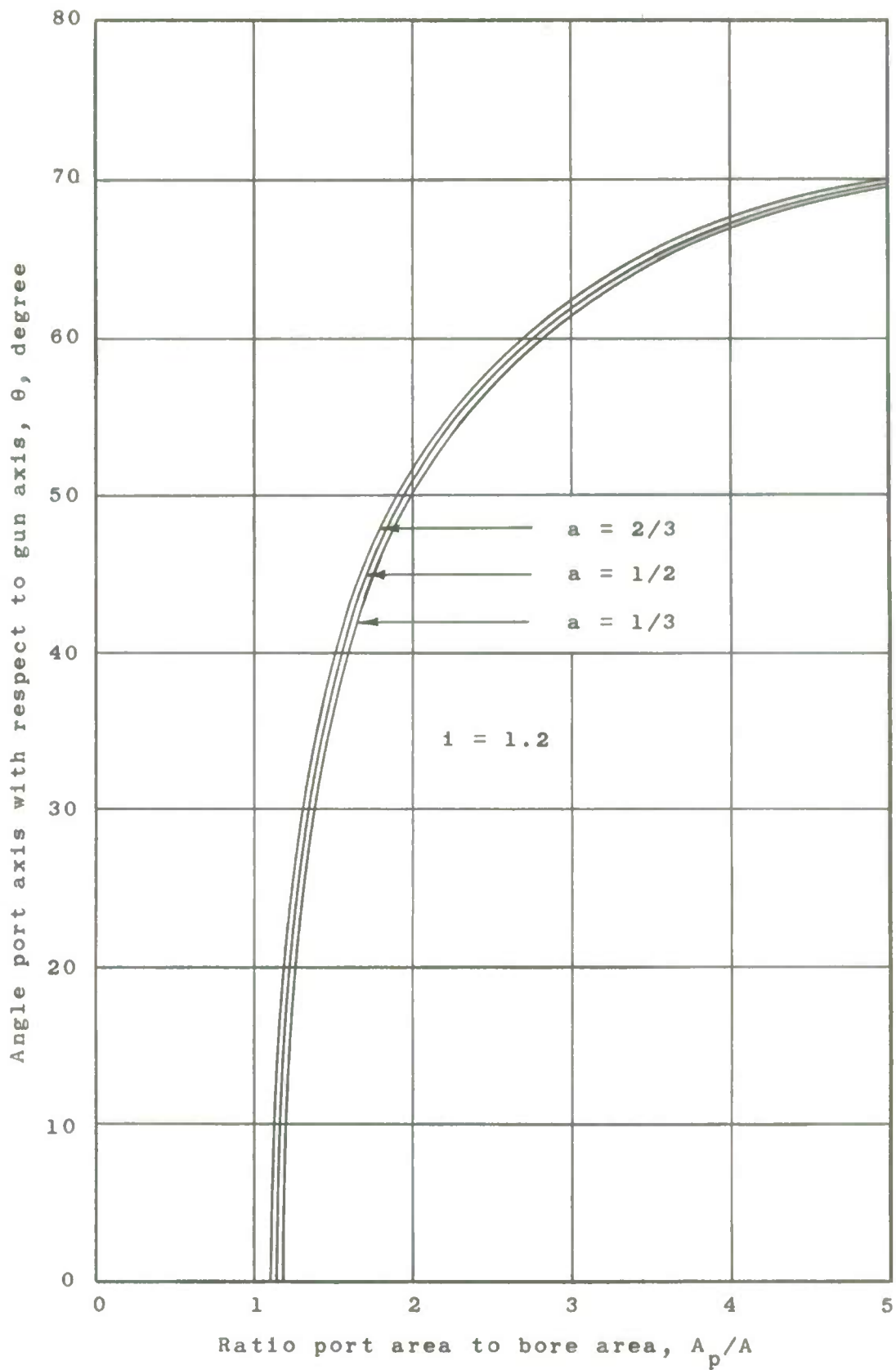


Fig. 3.1 - BRAKE PORT ANGLE VERSUS A_p/A WITH "a" AS A PARAMETER, 105MM HOWITZER



ORDNANCE ENGINEERING ASSOCIATES, INC.

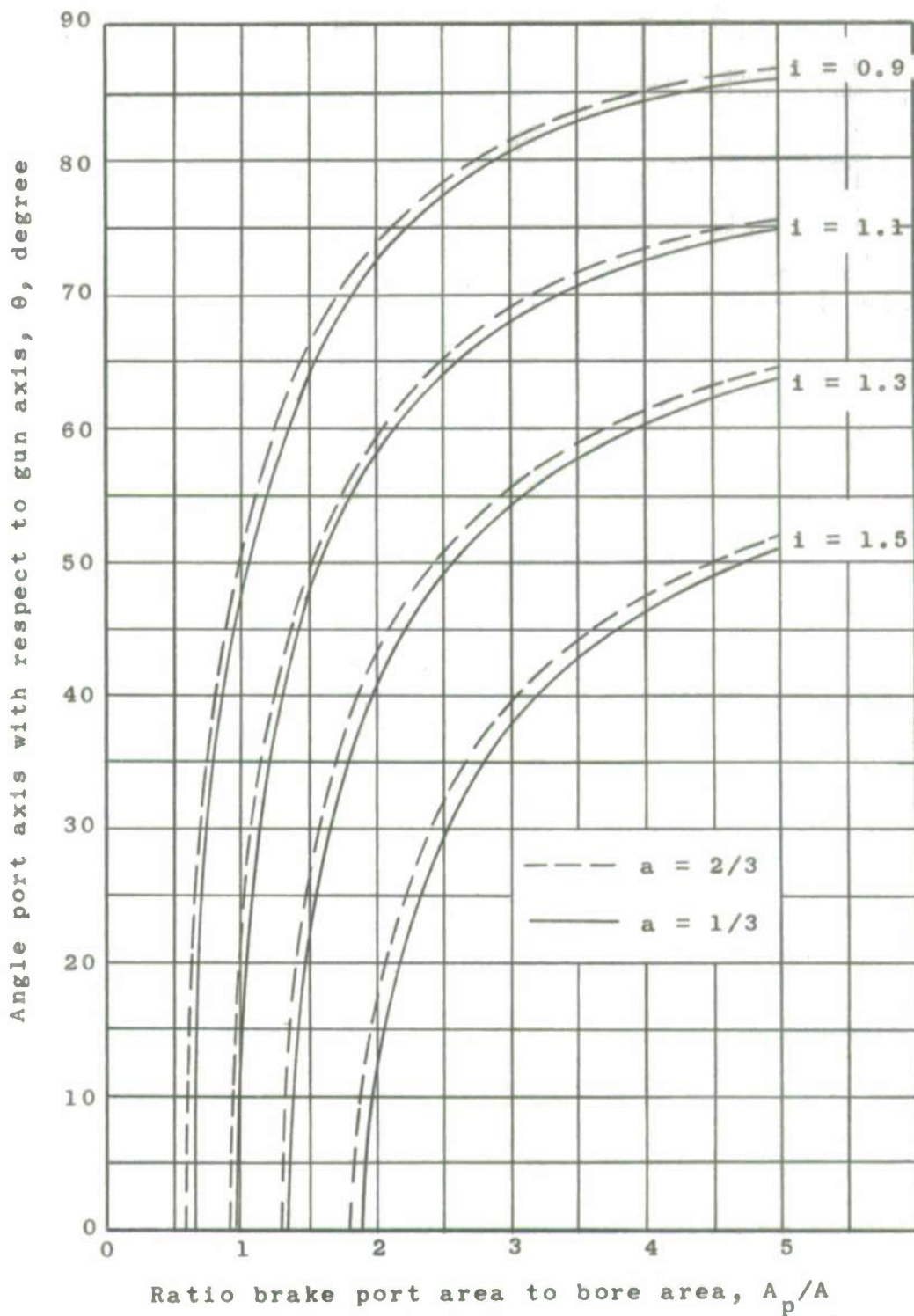


Fig. 3.2 - EFFECT OF MUZZLE BRAKE INDEX ON BRAKE PORT ANGLE, 105MM HOWITZER

It can be seen in Fig. 3.1 that the port angle required for a performance index of 1.2 is strongly dependent on the factor "a" in the region A_p/A between 1.25 and 2; for A_p/A greater than two, the dependence diminishes. It is also seen that the dependence of the angle on the A_p/A ratio diminishes for A_p/A greater than three. Similar data for other performance indices are shown in Fig. 3.2. It can be noted in this figure that for a fixed port area ratio the port angle must be reduced as the performance index is increased.

The above show that operation with a large port angle (Fig. 2.4 and 2.5 show that overpressures in the rear area of the weapon decrease as the port angle increases for a fixed performance index) requires that the port to bore area ratio incorporated in the muzzle brake blast suppression device be large; i.e., for an index of 1.2 A_p/A should be approximately three or greater. In these regions the "a" factor does not influence the port angle profoundly, but the maximum value of "a" will provide for an increase in port angle.

3.1.1 Effect of Design Parameters on Overpressure Field

The effect of the design parameters on the location of the overpressure was evaluated by application of the analyses presented in Section 2. The isobars mapped in Figs. 3.3 and 3.4 correspond to the parameters indicated in Table 3.1 for performance index of 1.2.

Table 3.1
PARAMETERS USED TO MAP OVERPRESSURE 105MM HOWITZER

$\frac{A_p/A}{a}$	Brake Port Angle, degree		Fig.No.
	1.5	3	
1/3	36.0	61.5	3.3
2/3	39.5	62.5	3.4



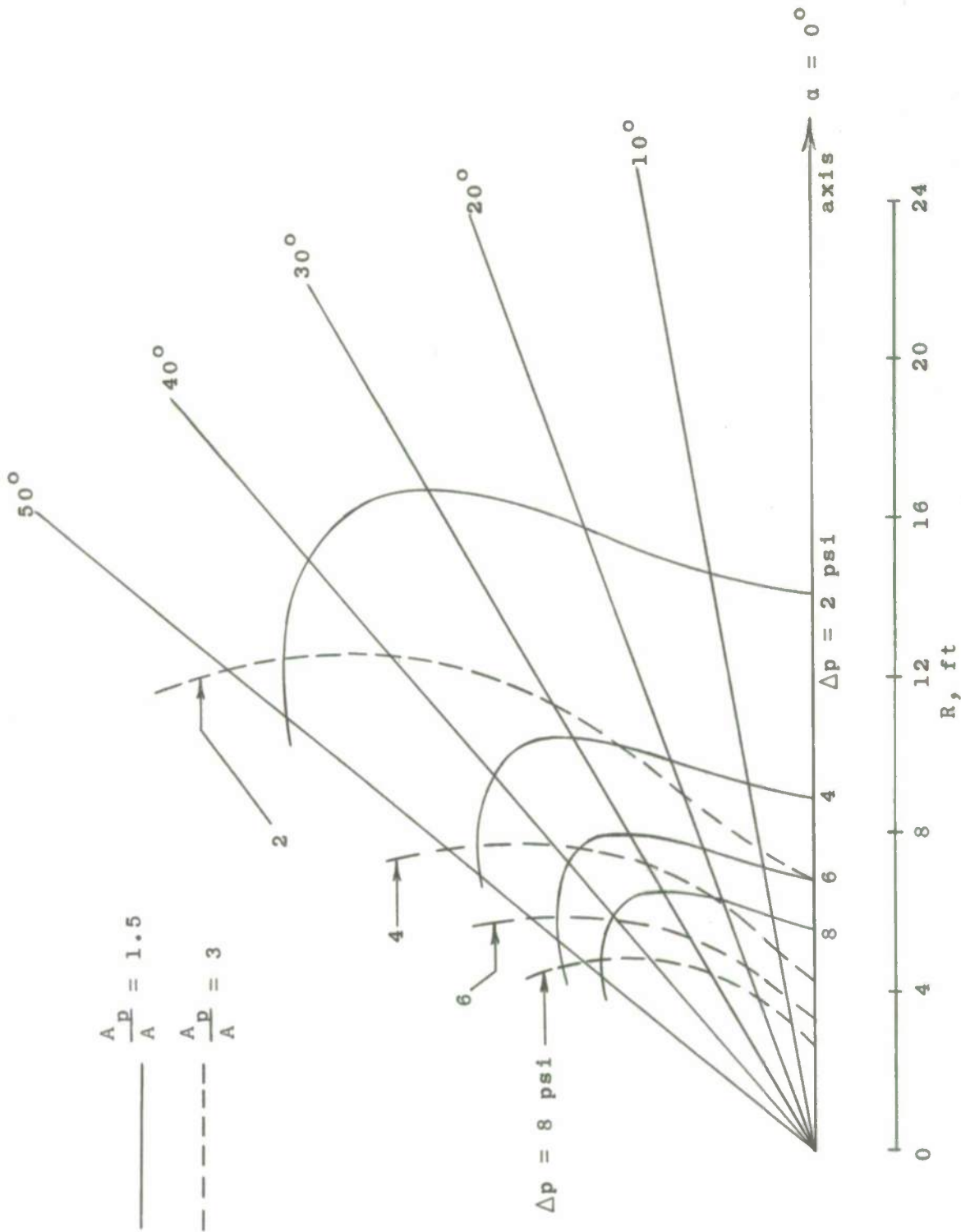


FIG. 3.3 - COMPUTED ISOBARS OBTAINED AS A RESULT OF FIRING 105MM
 HOWITZER WITH A MUZZLE BLAST SUPPRESSION DEVICE, $a = 1/3$

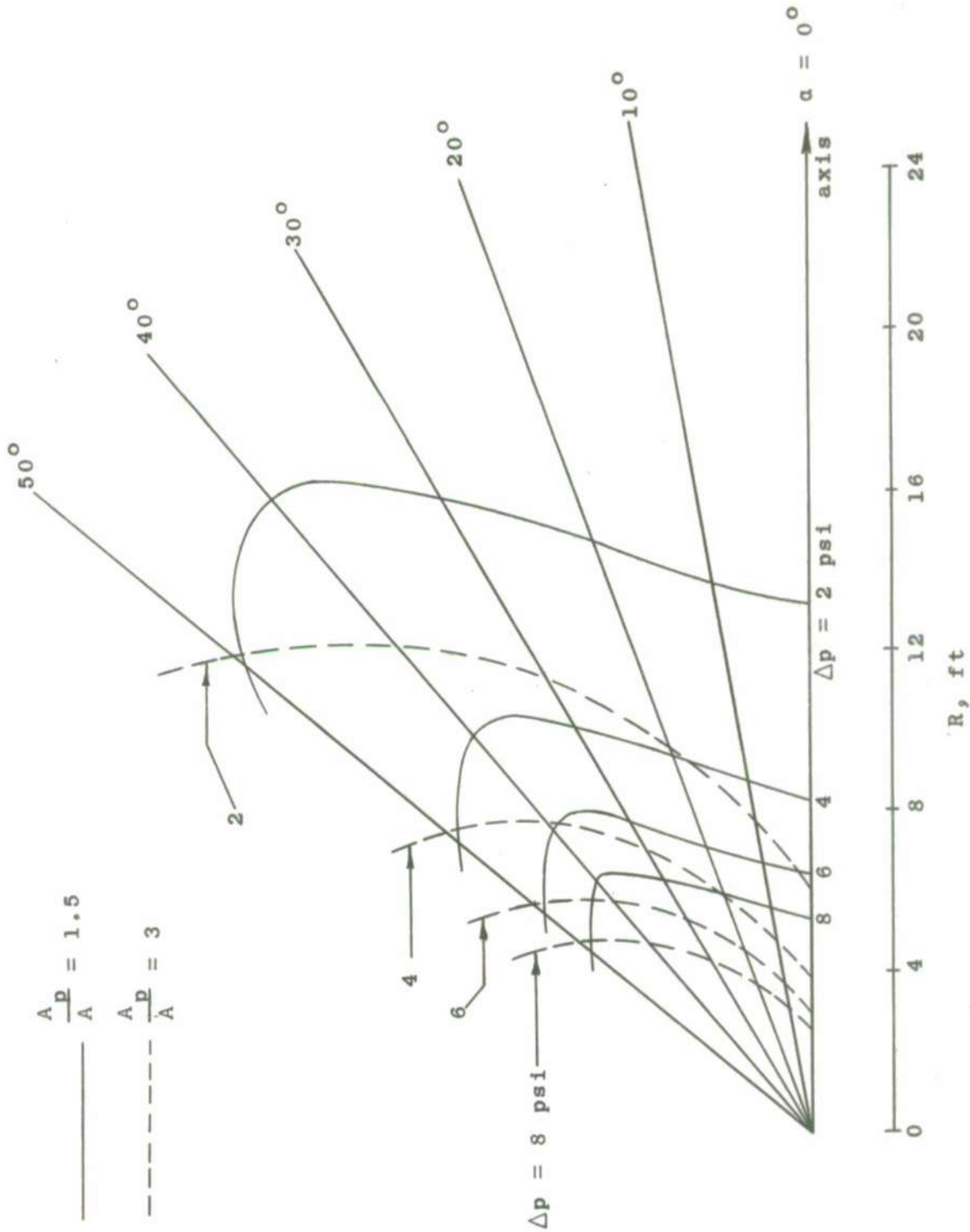


Fig. 3.4 - COMPUTED ISOBARS OBTAINED AS A RESULT OF FIRING 105MM HOWITZER WITH A MUZZLE BLAST SUPPRESSION DEVICE, $a = 2/3$

Review of the above figures shows that the overpressure at a fixed position is reduced for the larger value of A_p/A in a region subtended by an angle of approximately 50 degrees with respect to the Howitzer axis. Table 3.2 summarizes the data showing the location of 4 psi. It is apparent from the results given in this table that the overpressure in the crew area can be reduced, without impairing the performance of the muzzle brake suppression device, by (1) increasing the brake port area while maintaining the port angle consistent with the specified brake performance, i.e., Fig. 3.1, and (2) increasing the parameter "a."

3.1.2 Effect of Time that Projectile Is in Device

Fig. 3.5 was prepared for the 105mm Howitzer based on the equations and factors considered in Section 3.1. This figure shows the port angle, θ , as a function of the ratio of the port to bore area, A_p/A , for a fixed performance of the suppression device and for selected "time" and "a" factors. It can be noted that the port angle is more sensitive to the factor "a" the longer the projectile remains in the suppression devices.

It is seen in Fig. 3.5 that for an A_p/A ratio of 3.5, the angle θ will vary as follows:

Time (msec)	θ , degrees	
	1	0.3
a = 1/3	66.0	63.8
a = 2/3	66.9	64.0

Hence, when the projectile remains in the device for one msec, decreasing "a" from 2/3 to 1/3 corresponds to 1.4 per cent change in the angle θ . The corresponding angle change for a 0.3 msec time interval is 0.3 per cent.

Table 3.2

COMPUTED LOCATION OF 4 PSI OVERPRESSURE, 105MM
HOWITZER, SHOWING EFFECT OF DESIGN PARAMETERS

Angle with respect to Howitzer axis (degree)	Location of 4 psi			
	Measured for Exit of Brake, feet			
	a = 1/3		a = 2/3	
	$A_p/A=1.5$	$A_p/A=3$	$A_p/A=1.5$	$A_p/A=3$
10	9.3	5.1	8.8	4.9
20	10.5	7.8	10.0	6.4
30	12.2	8.5	11.6	8.1
40	12.5	10.3	13.1	10.1
50	11.0	12.1	11.3	11.8

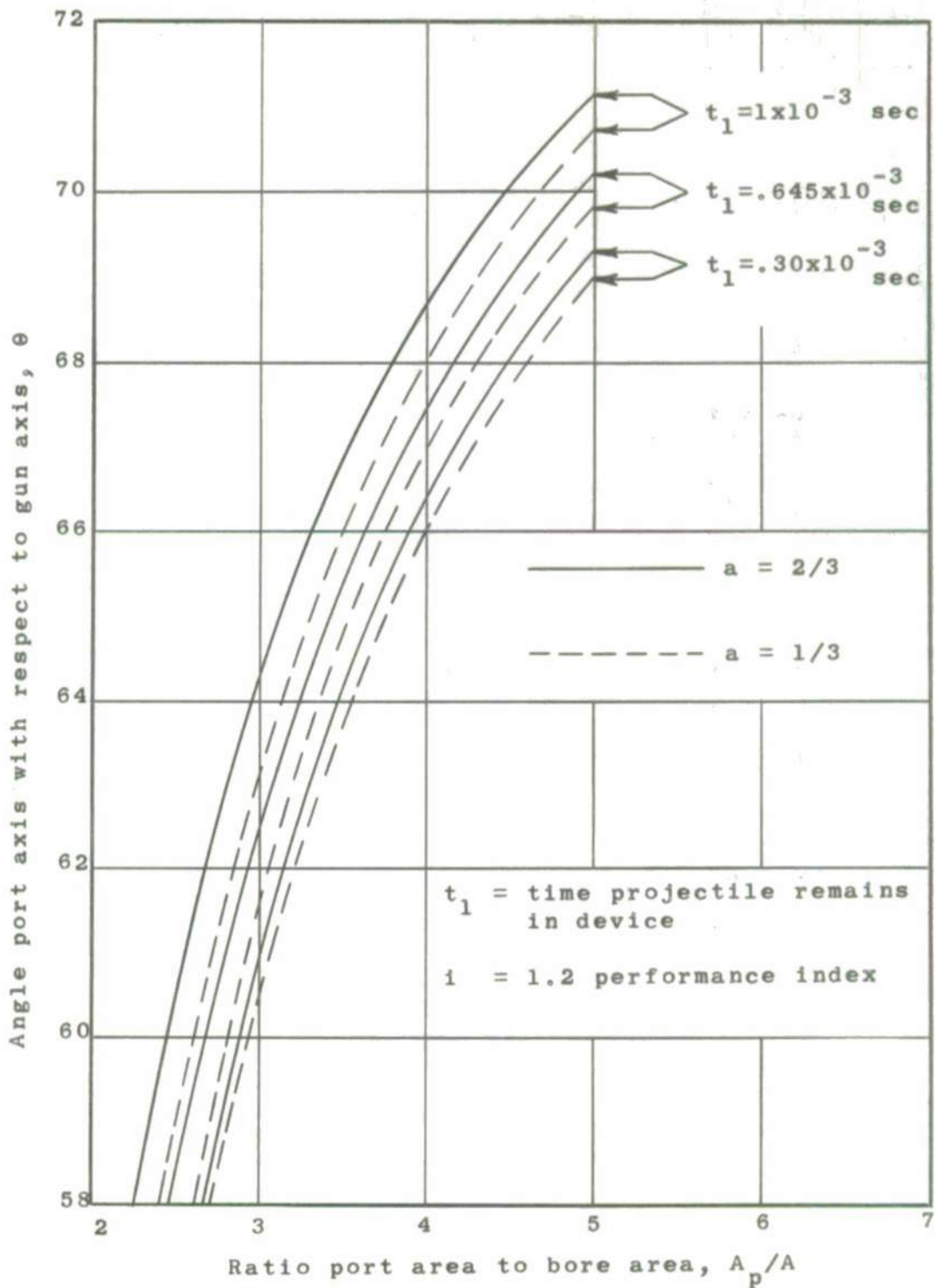


Fig. 3.5 - BRAKE PORT ANGLE VERSUS A_p/A FOR 105MM HOWITZER
SHOWING EFFECT OF TIME PARAMETER

It is seen that the longer the projectile remains in the device, the port angle required for the fixed performance index increases. (For a fixed muzzle velocity, the time that the projectile remains in the device is directly proportional to the length from the muzzle to the exit of the device.) Therefore, to reduce the overpressure in the crew area, the time which the projectile remains in the device should be maximized. This results from the observation that the overpressure in the crew area is reduced as the port angle is increased, thus directing the gases away from the service area.

3.1.3 Variation of Mass Rate of Discharge through Ports of Muzzle Brake Blast Suppression Device

The analysis as considered in this study on the rate of propellant gas discharge is based on one dimensional sonic flow through brake ports.

The mass rate of discharge from the recoil compensating ports can be expressed as follows:

$$\dot{m} = C_d'' K A_p \sqrt{\frac{T_o}{T_b}} P_m y \quad (3.1)$$

where

- A_p = total brake port area (for recoil compensation), in.²
- C_d'' = discharge coefficient of brake port
- K = isentropic flow constant, sec⁻¹
- P_m = space mean pressure in weapon at time projectile traverses muzzle, psi
- T_b = gas temperature in brake, °K
- T_o = isochoric flame temperature of propellant gas, °K
- y = dimensionless brake pressure

Considering the pressure history in the brake as developed in Appendix A, it can be seen from Eq. (3.1) that the rate of mass discharge is proportional to the brake pressure; other parameters remaining fixed.

Fig. 3.6 shows the dimensionless pressure versus dimensionless time for the following cases as obtained from Eqs. (A.11) and (A.12).

<u>Case</u>	<u>a</u>	<u>A_p/A</u>
I	1/3	3.0
II	1/3	1.5
III	2/3	3.0
IV	2/3	1.5

The mass rates of discharge from the brake ports corresponding to the above cases are shown in Fig. 3.7.

It can be seen in Fig. 3.7 comparing Case I with Case III that increasing the parameter "a" from 1/3 to 2/3 will provide a greater maximum rate of discharge. However, after the maximum is reached, it is seen that the rate of discharge is less for the larger value of "a" than for the value corresponding to Case I. Comparing Case III with Case IV, it is seen that Case III having the larger port area ratio maintains a greater rate of discharge than does the Case IV with the smaller port area ratio (This persists for about 15 msec ($T \approx 24$)).

3.2 Application to 155mm Howitzer

Fig. 3.8 was prepared for the 155mm Howitzer and shows the influence of the parameter "a" and the ratio of port area to bore area on the port angle for the indicated brake indices. The factors used in establishing these curves are as follows;

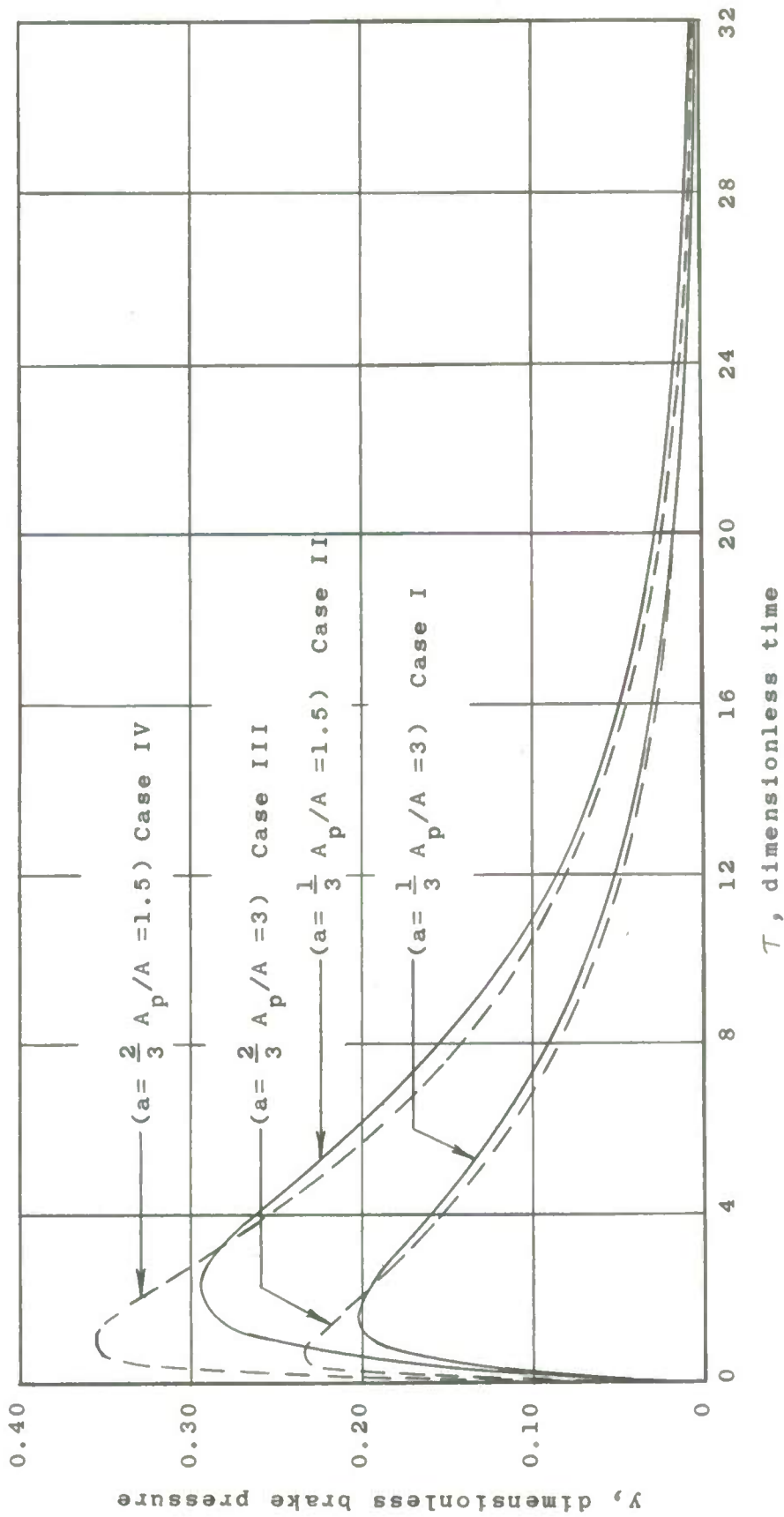


Fig. 3.6 - EFFECT OF DESIGN PARAMETERS ON DIMENSIONLESS BRAKE PRESSURE FOR 105MM HOWITZER

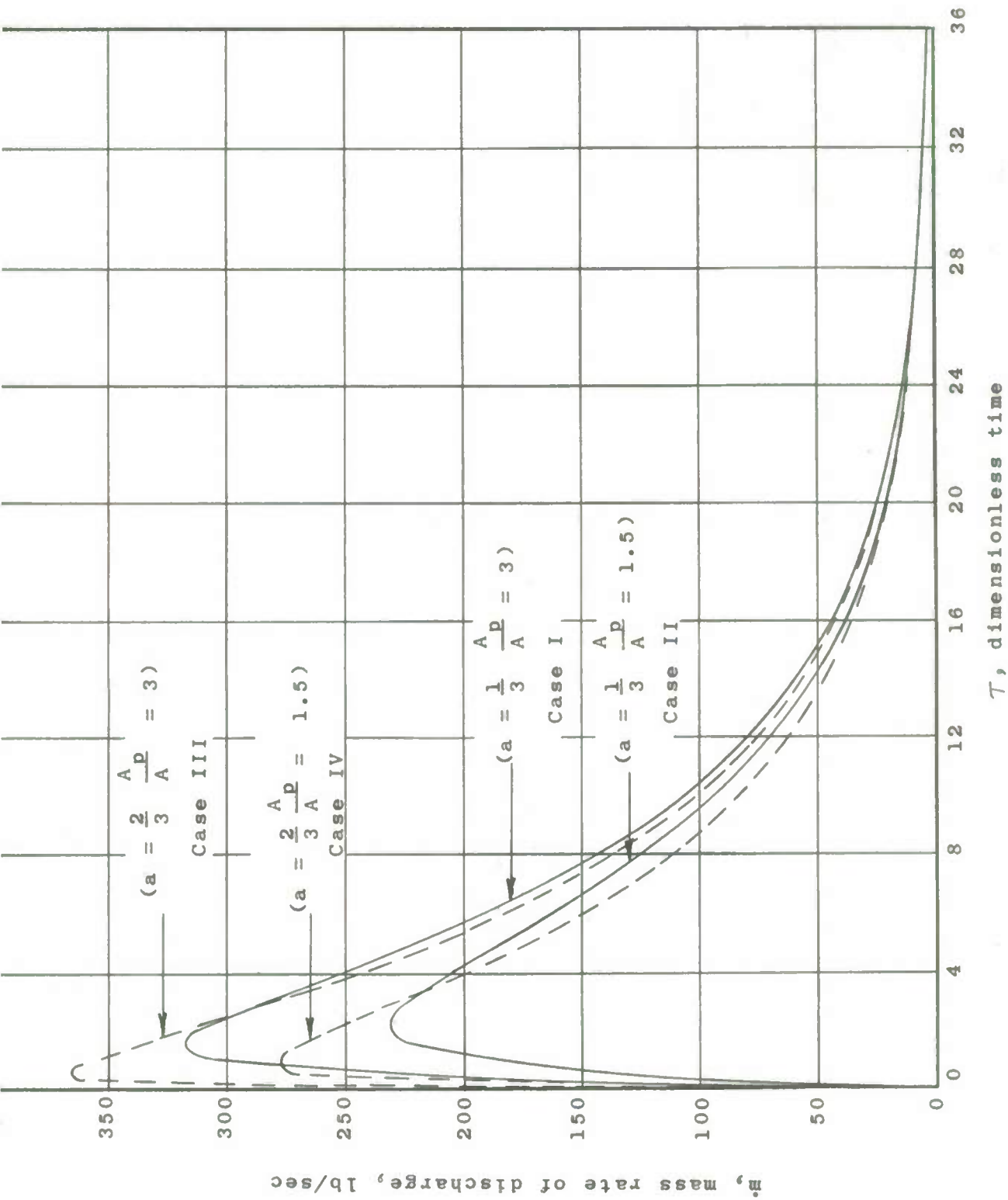


Fig. 3.7 - EFFECT OF DESIGN PARAMETERS ON RATE OF GAS DISCHARGE FOR 105mm HOWITZER

γ	=	1.24, specific heat ratio of propellant gas
θ_b	=	0.5, ratio average gas temperature in brake to isochoric flame temperature of propellant gas
θ_g	=	0.6, ratio of average gas temperature in weapon (after projectile passes muzzle) to isochoric flame temperature of propellant gas
A	=	29.8 in. ² , bore area
C_d	=	0.85, discharge coefficient
F	=	323,000 ft-lb/lb, propellant impetus
K	=	$6.56 \times 10^{-3} \text{ sec}^{-1}$, discharge coefficient
p_m	=	6,600 psi, space mean pressure in Howitzer at time projectile clears muzzle
t_l	=	$0.370 \times 10^{-3} \text{ sec}$, time for projectile to pass through suppression device
V_m	=	2700 fps, muzzle velocity
v_T	=	6050 in. ³ , total effective gun volume

It is seen here for a fixed performance requirement that as one increases the port to bore area ratio, the corresponding change in port angle decreases. The effect of changing the parameter "a" from 1/3 to 2/3 is seen to be insignificant in the regions where the slope of the curve is not near infinite. It can also be seen that as the performance index increases the required angle decreases. Comparison of these data for the 155mm Howitzer with those reported for the 105mm Howitzer (see Fig. 3.2) it can be seen that the general shape of the families of curves agree. However, the following exceptions are noted:

1. The 155mm data shows less sensitivity to variations in the factor "a," this is attributed to the difference in time which the projectile is in the brake.

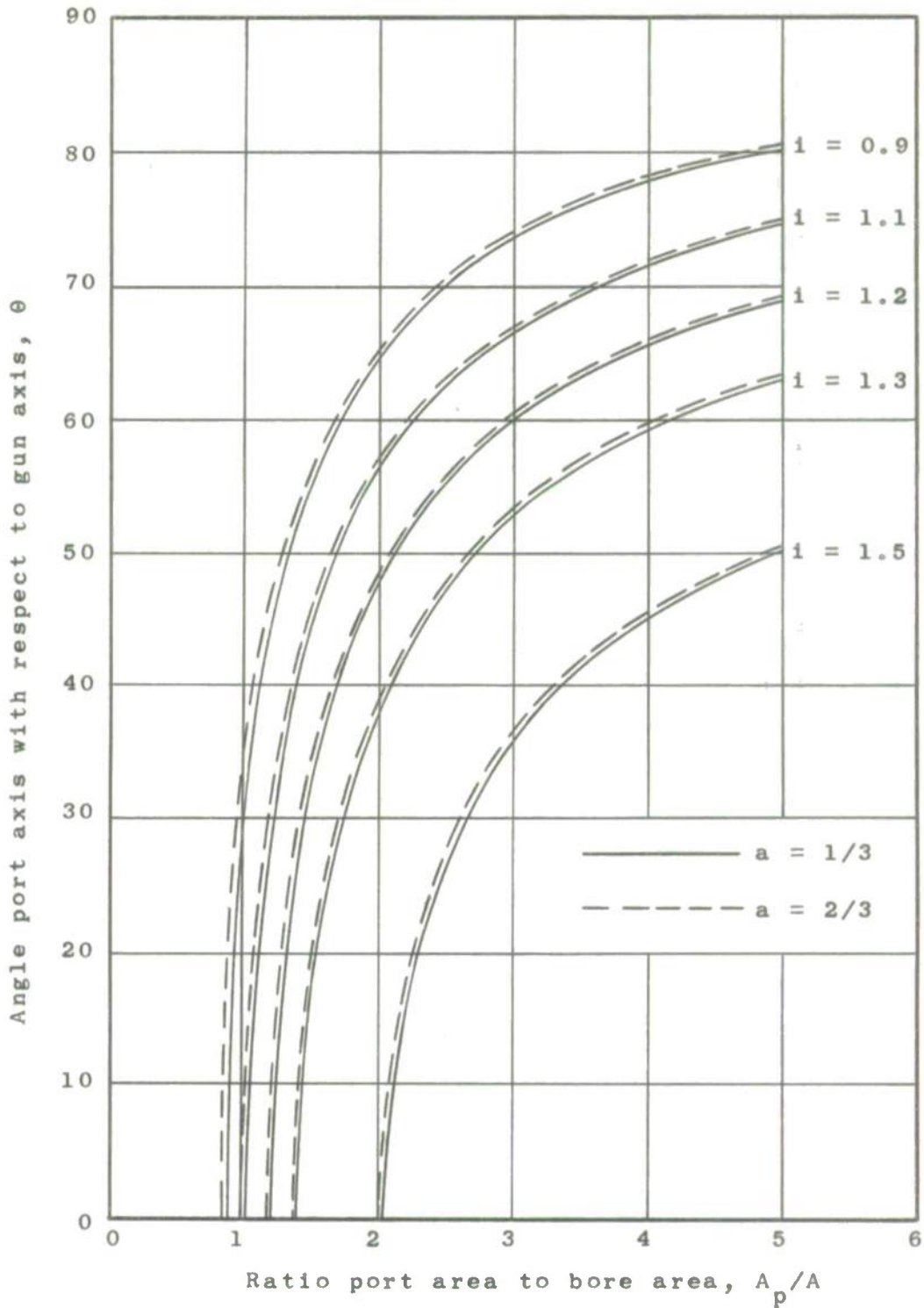


Fig. 3.8 - BRAKE PORT ANGLE VERSUS A_p/A FOR 155MM HOWITZER

OEA

ORDNANCE ENGINEERING ASSOCIATES, INC.

2. The 155mm requires a slightly larger port area ratio for a fixed port angle and performance index than does the 105mm Howitzer; this is attributed to the difference in the pressure histories in the weapons after shot ejection.

3.2.1 Effect of Design Parameters on Overpressure Field

The isobars resulting from firing the 155mm Howitzer with a muzzle blast suppression device were computed and are shown plotted in Fig. 3.9. These curves are consistent with the parameters considered for the 155mm Howitzers in this report. The overpressures as shown in Fig. 3.9 are plotted identically for both values of the factor "a" considered, 1/3 and 2/3. This occurs as a result of the insensitivity of the angle θ to the factor "a" as shown in Fig. 3.8. However, it can be seen in Fig. 3.9 that in the region subtended by an angle approximately 45° with respect to the howitzer axis, the overpressure is less for the A_p/A value of three than for a value of 1.5.

These results are in agreement with those obtained for the 105mm Howitzer (see Figs. 3.3 and 3.4).

3.2.2 Effect of Time that Projectile Is in Device

It was noted in Section 3.2 that the 155mm Howitzer shows less sensitivity to variations in the factor "a" than did the 105mm weapon. This was in part attributed to the difference in time considered, that the projectile remains in the suppression devices. Fig. 3.10, prepared for the 155mm, shows the port angle, θ , as a function of the ratio port to bore area for a fixed performance index of the suppression device and for selected "time" and "a" factors.

These data are in agreement with those shown in Fig. 3.5, that is; the shorter the time the projectile is in the devices the less sensitive is the angle to the factor "a" and for the longer the time the greater the required angle for a fixed A_p/A ratio.

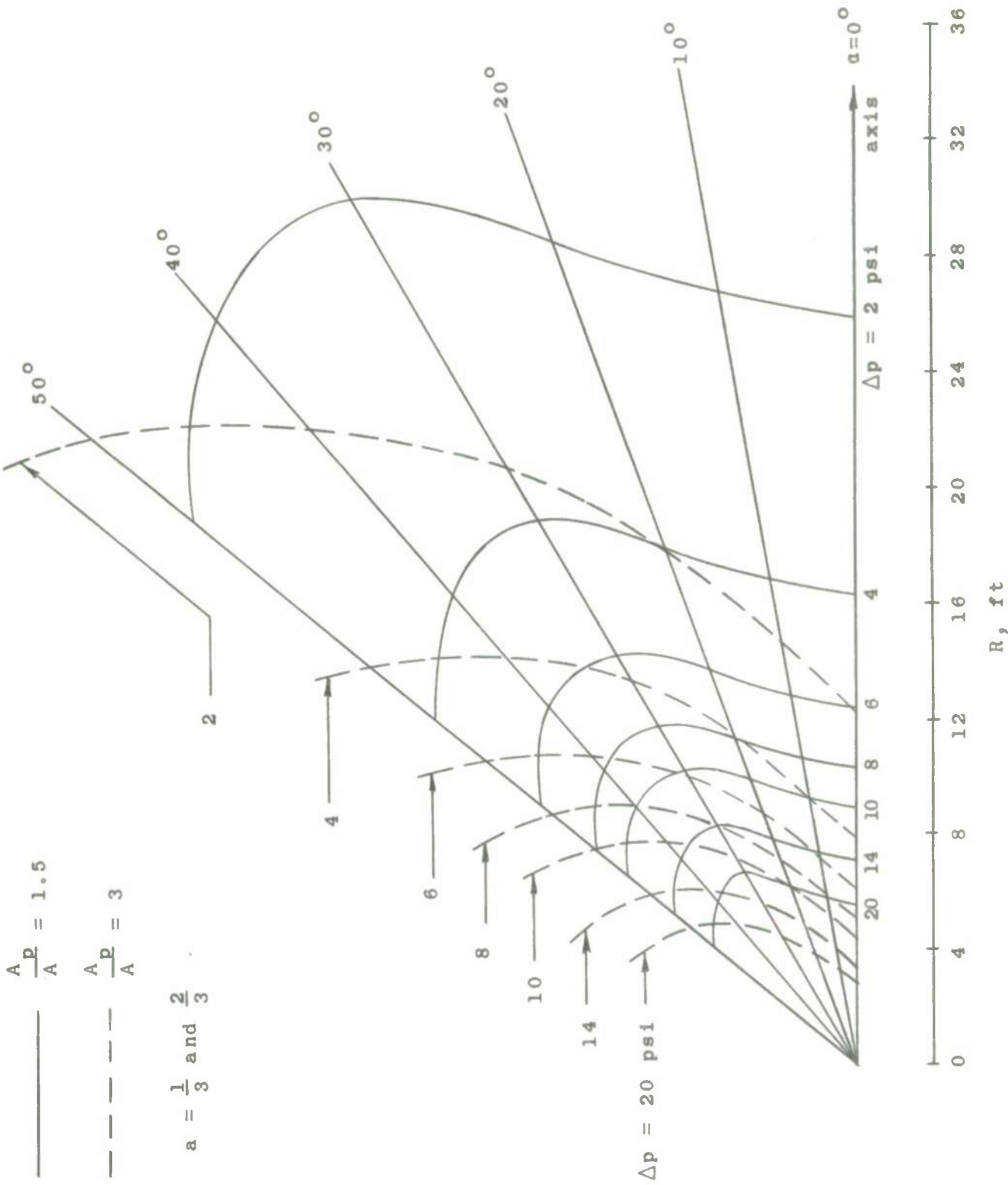


Fig. 3.9 - COMPUTED ISOBARS OBTAINED AS A RESULT OF FIRING THE 155MM HOWITZER WITH A MUZZLE BLAST SUPPRESSION DEVICE



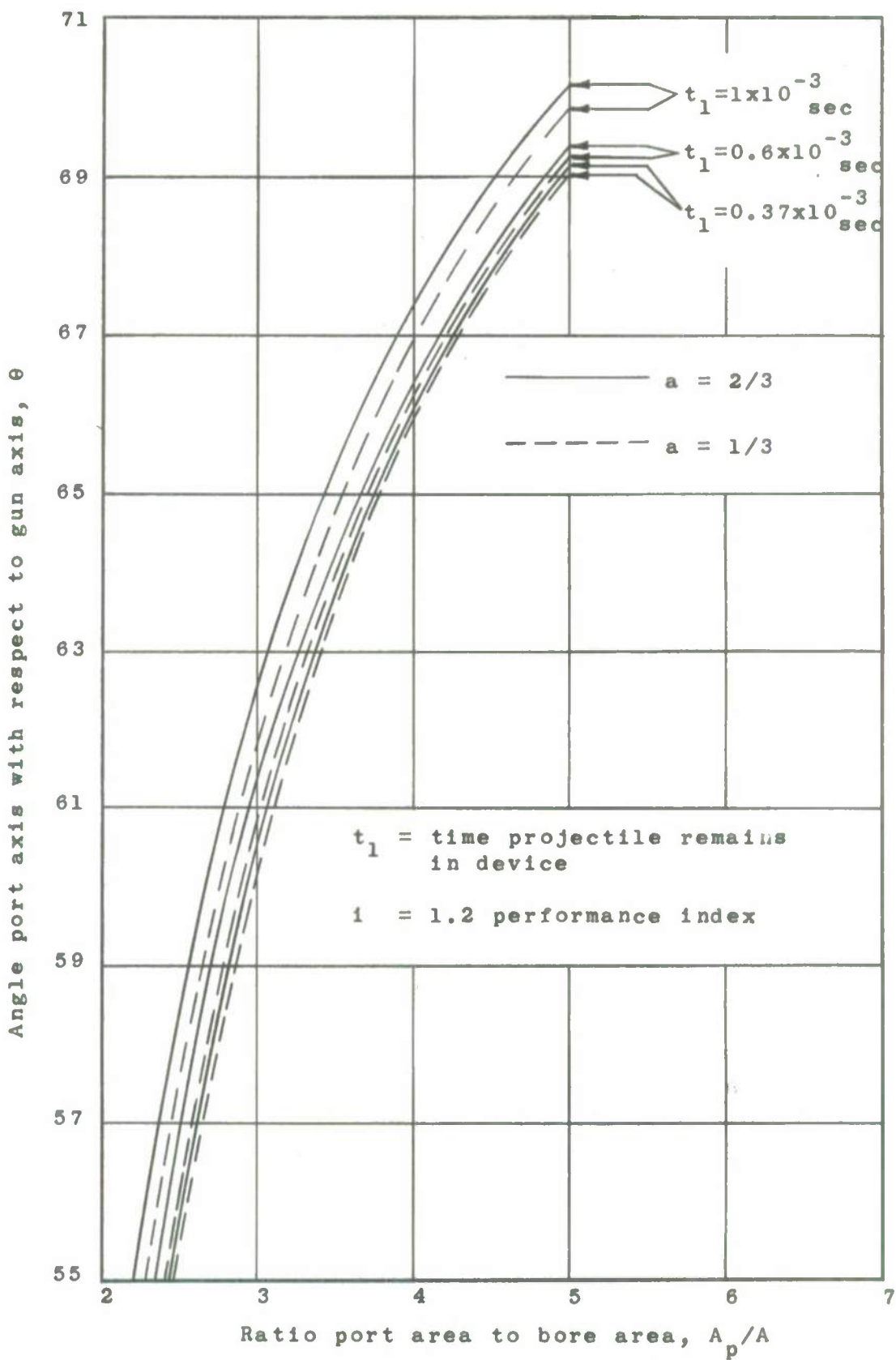


Fig. 3.10 - BRAKE PORT ANGLE VERSUS A_p/A FOR 155MM HOWITZER
SHOWING EFFECT OF TIME PARAMETER



3.2.3 Variation of Mass Rate of Discharge Through Ports of Muzzle Brake Blast Suppression Device

Dimensionless pressure-time and mass rate of discharge dimensionless time curves were obtained for the 155mm Howitzer based on Appendix A and Eq. (3.1). Fig. 3.11 contains the plot of the computed pressure curves while Fig. 3.12 shows the mass rate of discharge.

Comparison of the 155mm curves with those of the 105mm (see Figs. 3.6 and 3.7) shows that the effect of the variation in the factors "a" and A_p/A is identical for both systems. However, it is noted that the maximum values are greater, which is expected, for the 155mm weapon than for the 105mm Howitzer.

3.3 Summary

It has been shown that the overpressure in Howitzer crew areas can be attenuated by incorporating the following features in the design of the muzzle brake blast suppression device:

1. Of prime concern, maintain the largest realistic port area consistent with the required performance index (i.e., for the 105mm a port to bore area ratio of 2.5 would be realistic for an 0.9 performance index while a ratio of about 3.5 would correspond as maximum for an index of 1.3).
2. Of secondary importance, reduce or minimize the internal volume in order to maximize the factor "a".
3. Also as a secondary consideration, maintain a large length between the projectile exit and recoil compensating ports in order to increase the time the projectile remains in the device.

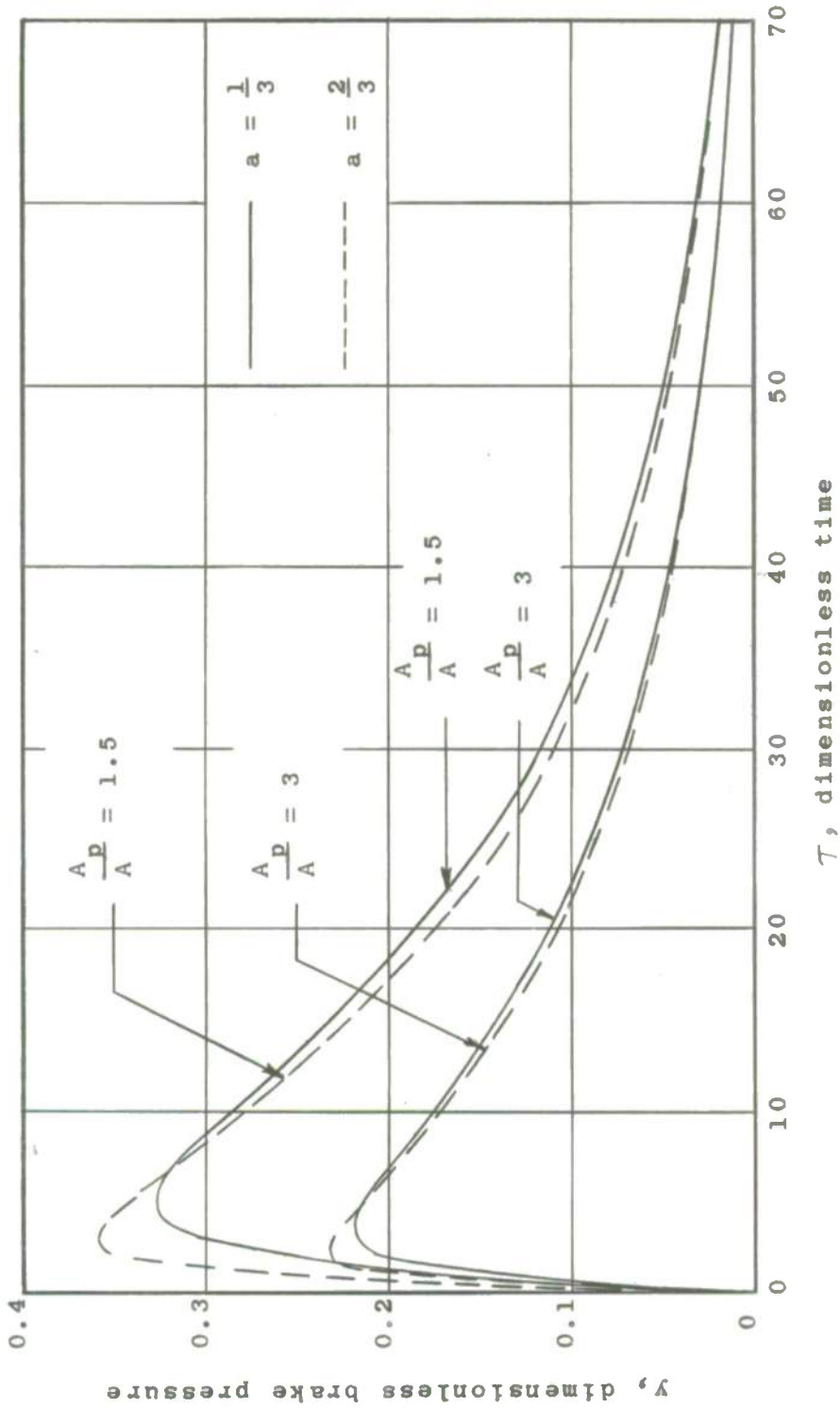


Fig. 3.11 - EFFECT OF DESIGN PARAMETERS ON BLAST SUPPRESSION
 DEVICE PRESSURE, 155MM HOWITZER

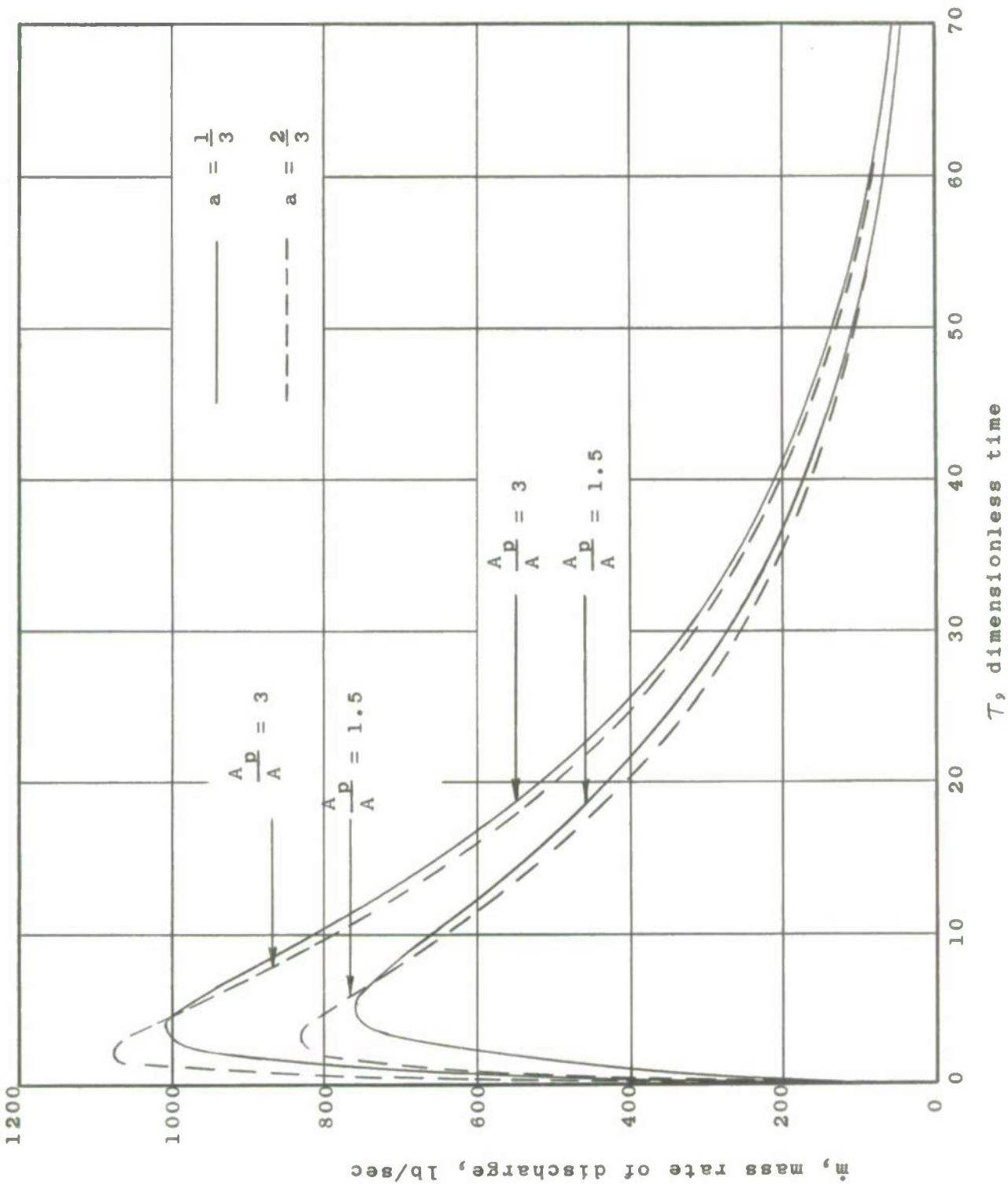


Fig. 3.12 - EFFECT OF DESIGN PARAMETERS ON RATE OF GAS DISCHARGE FOR 155mm HOWITZER

4.0 MUZZLE BRAKE BLAST SUPPRESSION DEVICE - 105mm HOWITZER

A muzzle brake blast suppression device was made incorporating those features which attenuate the overpressure in the crew area for a fixed performance index of 1.2. This device incorporates essentially 360 degrees of discharge at an angle 62 degrees with respect to the weapon axis. The design was based on the following:

1. Ratio of port to bore area of about three.
2. Internal volume minimized consistent with an overall length of 13.5 in. and yielding an "a" value of 0.59.
3. 62 Degree port angle selected to yield performance index of 1.2.

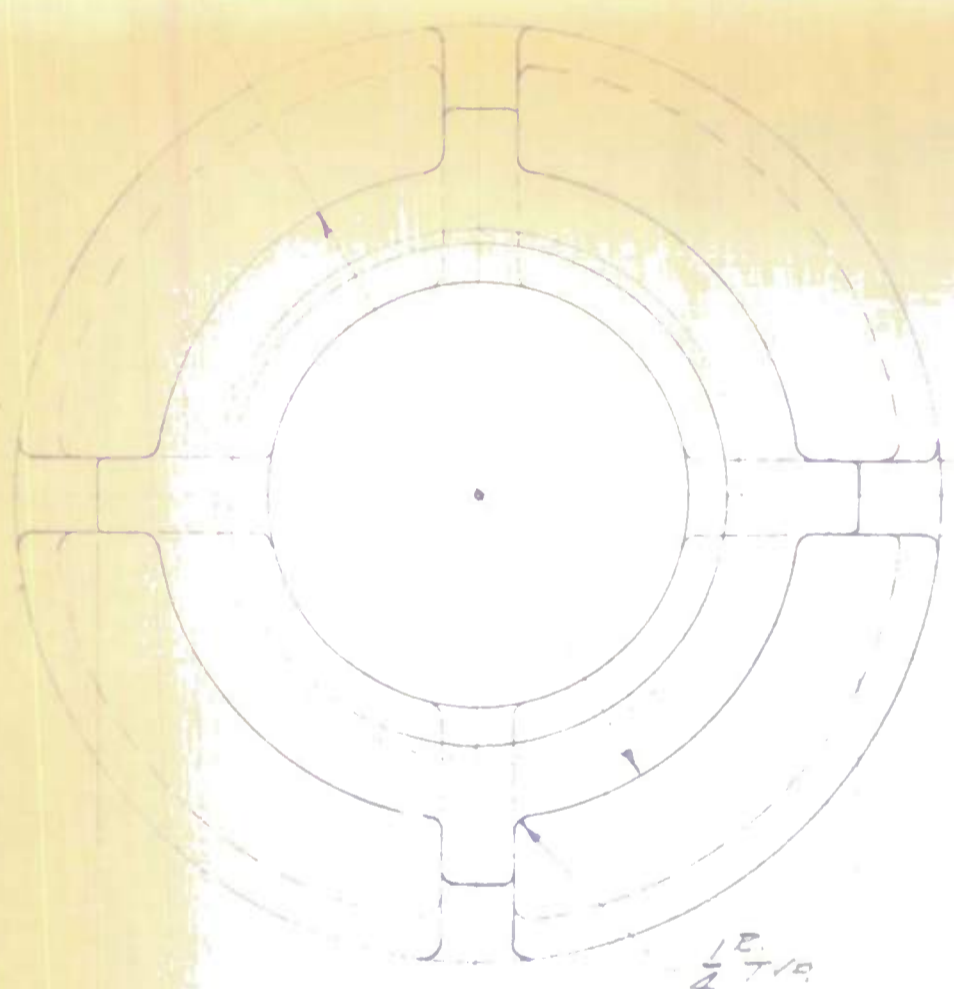
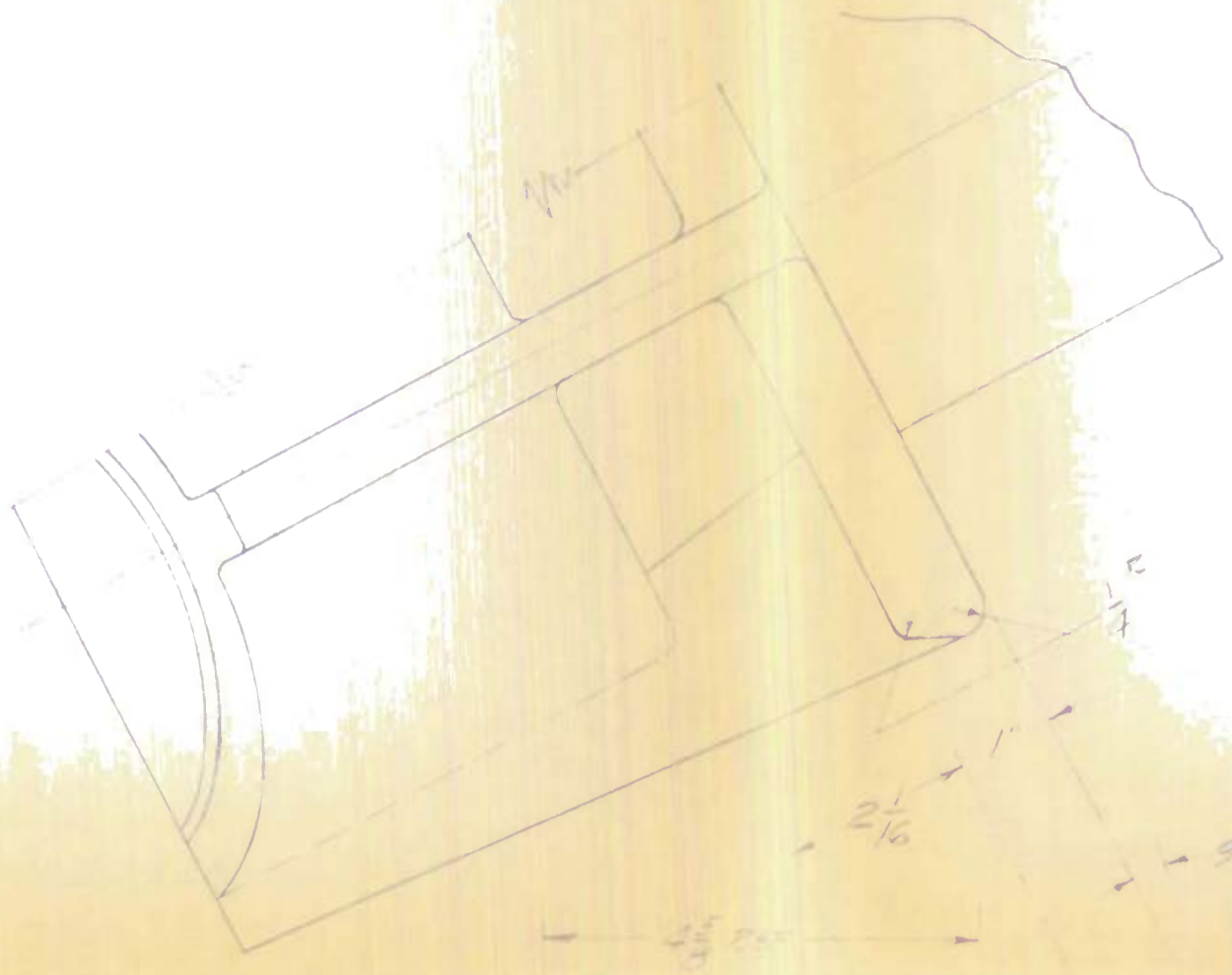
4.1 Design Description

The design of the 360° muzzle blast suppression device shown in Fig. 4.1, consists basically of a threaded ring for attachment to the Howitzer muzzle, a conical shaped baffle with a cylindrical extension and a set of four equally spaced gussets which join the ring and baffle. The port area is located between the baffle and ring in the axial direction and the gussets in the circumferential direction. Design values for the device are itemized below:

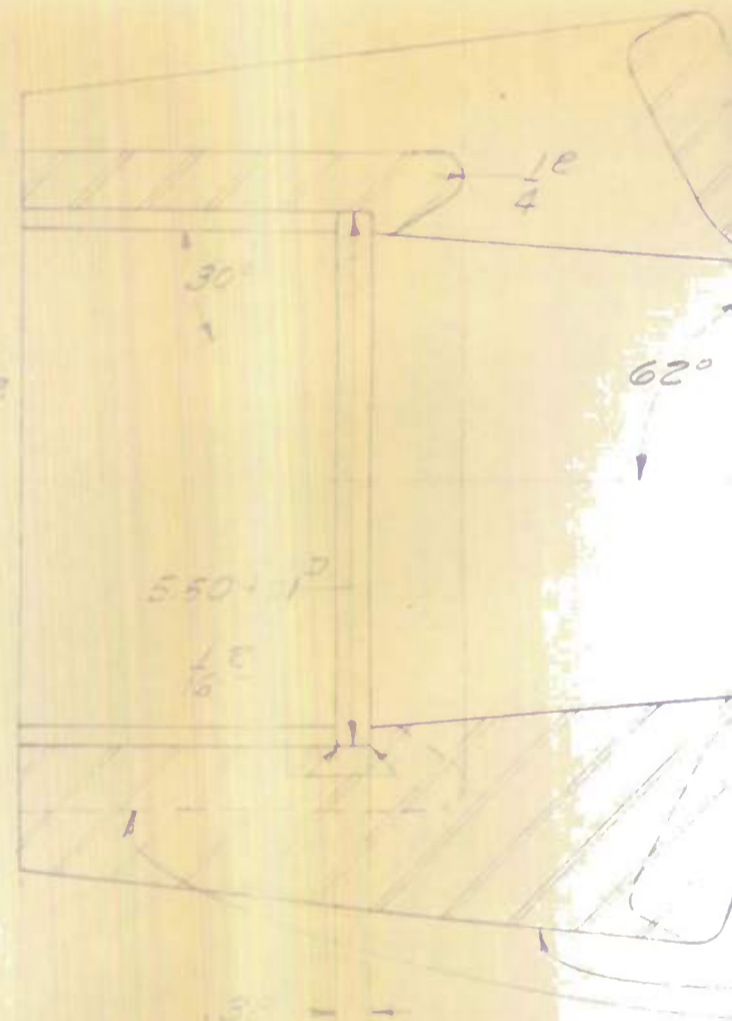
- | | | |
|----|-----------------------------------|-------------------------------|
| a. | Howitzer bore area | $A = 13.4 \text{ in.}^2$ |
| b. | Port area | $A_p = 41.3 \text{ in.}^2$ |
| c. | Entrance to port area | $A_e = 47.2 \text{ in.}^2$ |
| d. | Port to bore area ratio | $A_p/A = 3.08$ |
| e. | Internal volume | $v_b = 223 \text{ in.}^3$ |
| f. | Internal length | $L_b = 9.88 \text{ in.}$ |
| g. | Parameter "a" | $a = \frac{AL_b}{v_b} = 0.59$ |

REMOVE ALL BURRS
 ALL DIAMETERS TO BE CONCENTRIC WITHIN .005 EXCEPT AS NOTED
 ALL DIMENSIONS APPLY AFTER PLATING
 EDGES TO BE BROKEN .015 MAX
 MACHINE FINISH EXCEPT AS NOTED

✓

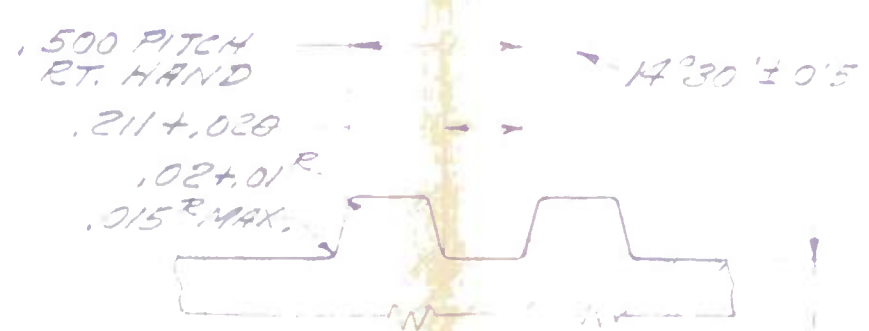


3.93
 7.87



3.68
 13.15

REVISIONS			
SYM	DESCRIPTION	DATE	APPROVAL



5.17±.01 MINOR DIA.
5.47±.01 MAJOR DIA.

THREAD DETAIL
PERMISSIBLE LEAD ERROR
±.002 INCH PER LENGTH
OF THREAD.
REMOVE 90° OF THREADS-
BOTH ENDS.
FIN. $\sqrt{3}$ SCALE-2:1

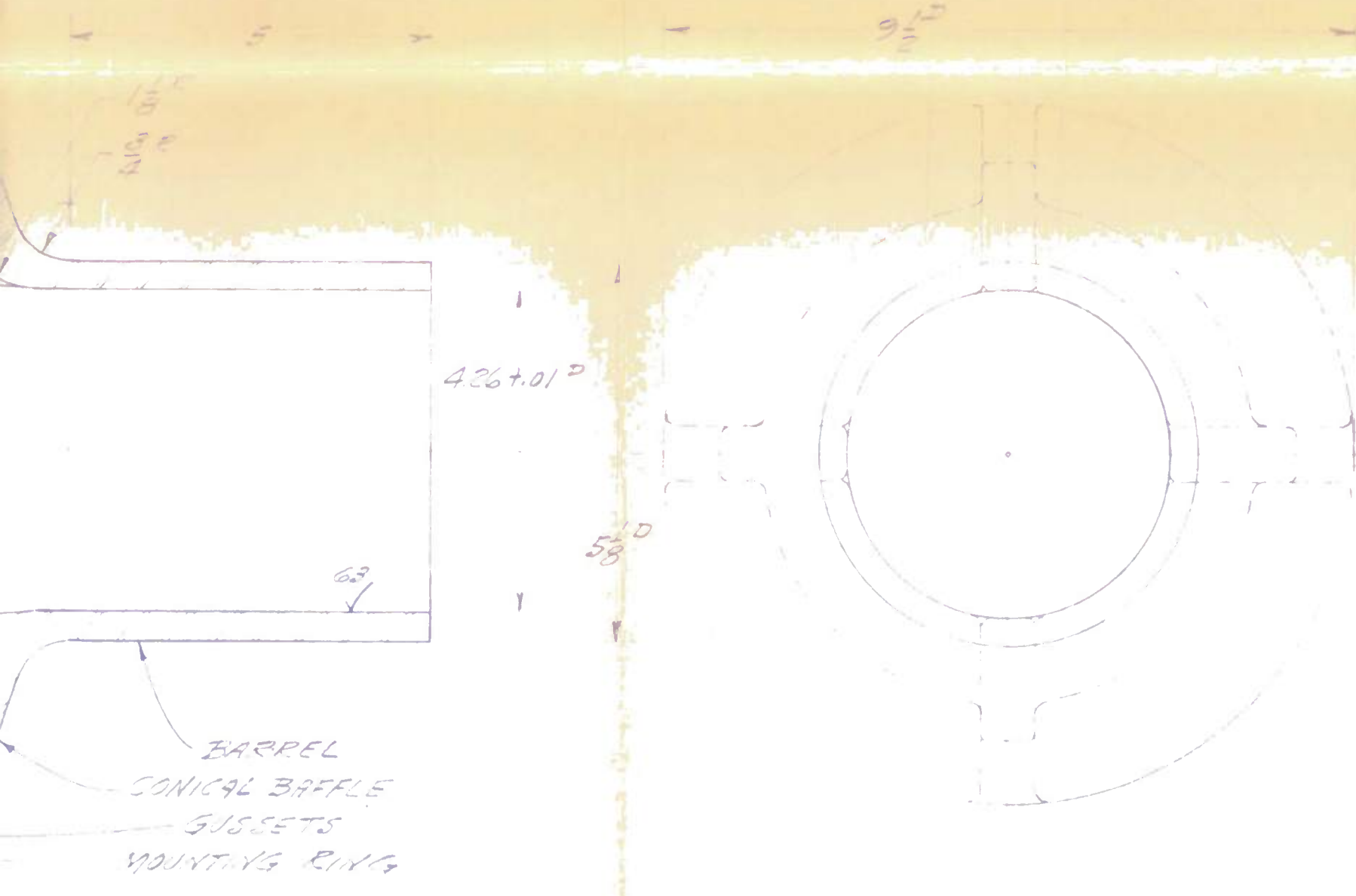



FIG. 4.1

REQ'D	PART NO.	DESCRIPTION	QTY	MATERIAL	FINISH	NOTE	PREPARED BY	REVISION
LIST OF MATERIAL								
UNLESS OTHERWISE SPECIFIED DIMENSIONS ARE IN INCHES			DRAWN					
FRAC	DEC	ANGLE	CHECK					
MATERIAL AND SPECIFICATION			STRESS					
HEAT TREATMENT AND SPECIFICATION			BALLISTICS					
PROTECTIVE FINISH AND SPECIFICATION			PROJECT ENG.					
			RELIABILITY					
			CHIEF ENG.					
			APPROVAL					

APPLICATION

ORDNANCE ENGINEERING ASSOCIATES, INC



DES PLAINES, ILLINOIS

- h. Port angle $\theta = 62^\circ$
- i. Approx. weight of device $W = 59 \text{ lb}$

In Fig. 4.1 the device is shown fabricated as a casting. As a weldment the gussets would be modified to permit access for welding to the baffle, increasing the weight of the device by approximately 4 lb.

The results of the stress analysis indicates a maximum tensile working stress of 57,100 psi; with a minimum yield stress of 120,000 psi for the material, a factor of safety of 2.1 is obtained.

4.2 Results - Stress Analysis of 360 Degree Muzzle Brake Blast Suppression Device

The stress analysis of the 360 degree device for the 105mm Howitzer, involved the determination of maximum stress levels and deflections when subjected to a maximum gas pressure of 5000 psi. Simplifying assumptions were made so that the stress distribution at the statically indeterminate junction between the gussets and baffle could be evaluated. It was assumed that

1. Uniform stress distribution exists between gussets and baffle in the axial direction. As a result of this assumption the longitudinal bending moment at the junction of gussets and baffle is neglected.
2. Localized baffle deflection in the radial direction at the gussets can be approximated by utilizing the ring theory.

In addition, the principle of stress superposition was incorporated in this analysis to find maximum combined stress levels.



The method of solution included evaluation of the maximum radial disparity between gussets and baffle when separated and gas pressure acting upon the baffle alone. The disparity is removed by introducing radial forces between gussets and baffle and a bending moment to the mounting ring. Maximum stresses are determined by methods of superposition of the resulting stresses. In addition, the tensile stress in the gussets resulting from the gas pressure impinging upon the baffle in the axial direction was included.

A summary of the computed stress levels and corresponding strains is given in Appendix B and is presented in Table 4.1, for the sections depicted in Fig. 4.2.

4.3 Summary

Selection of the circumferential type port was based on establishing the conditions in the device such that the gases passing through the port are directed at the greatest angle with respect to the Howitzer axis while maintaining a fixed performance index. This circumferential port arrangement provides the following conditions which are consistent with the above criteria:

1. Port to bore area ratio maximized consistent with minimum volume and realistic length.
2. Internal volume minimized.
3. Internal travel of the projectile while in the device maximized consistent with a reasonable length device and by providing the gas ports as close to the weapon muzzle as possible.

Table 4.1
SUMMARY OF MAXIMUM STRESSES AND DISPLACEMENTS
FOR 360° MUZZLE BLAST SUPPRESSION DEVICE

Location (See Fig. 4.2)	Maximum Combined Stress (psi)	Direction of Stress	Radial Displacement (in.)
(1)	53,000	Circumferential	0.0062
(2)	57,100	Longitudinal	0.0005
(3)	34,300	Longitudinal	0.0005
(4)	36,200	Circumferential	0.0029
(5)	16,500	Longitudinal	0.0005
(6)	19,400	Longitudinal	-

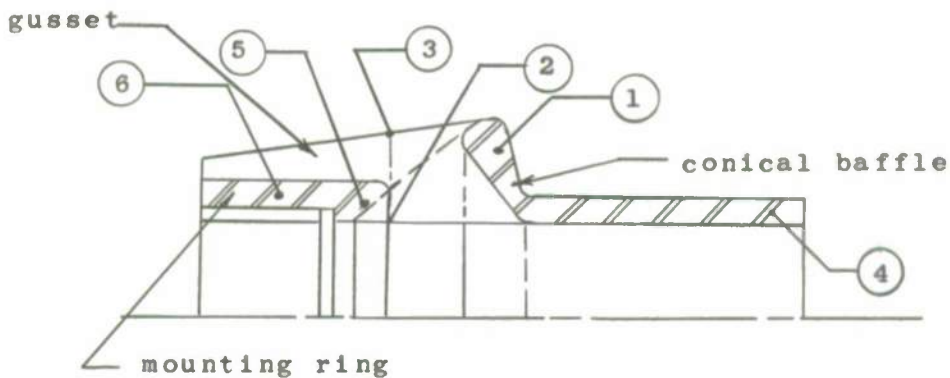


Fig. 4.2 - LOCATION OF COMPUTED STRESS AND DEFLECTIONS
FOR 360° MUZZLE BRAKE, 105MM HOWITZER

5.0 PRESSURE AND FLOW FIELD EXTERIOR TO A GUN BLAST

The axi-symmetric acoustical problem of a gun blast has been formulated as an initial value problem. The exact solution is obtained for a given initial pressure and velocity distribution. Special cases studied in detail include: (a) an initial velocity distribution with a semi-infinite cylinder, and (b) a constant pressure distribution within a finite cylinder.

An asymptotic representation for the pressure field is also developed to gain insight for the far field. Several plots for the acoustical pressure field are given.

The study of the problem is presented in Appendix C. This study was carried out by Dr. A. C. Eringen of Purdue University under OEA Purchase Order No. 5889. The analysis presented was reviewed by OEA personnel, especially by Dr. Nurettin Y. Olcer.

OEA

ORDNANCE ENGINEERING ASSOCIATES, INC.

6.0 RECOMMENDATIONS

The results of these analytical studies have shown that overpressures in the crew area can be reduced without affecting the performance of the muzzle brake by selection of those design parameters which allow the gases to be directed at the greatest angle with respect to the weapon axis. Based on the results obtained under this program it is recommended that additional studies be undertaken.

1. Verify experimentally the analytical results reported.
2. Modify analysis, if necessary, based on experimental results and prepare general design manual for muzzle brake blast suppression devices.

APPENDIX A

INTERIOR BALLISTICS OF MUZZLE BRAKE
AND BLAST SUPPRESSION DEVICES

OEA

ORDNANCE ENGINEERING ASSOCIATES, INC.

APPENDIX A

INTERIOR BALLISTICS OF MUZZLE BRAKE
AND BLAST SUPPRESSION DEVICES

A.1 BRAKE PRESSURE

The pressure-time history in the muzzle brake was developed based on the following:

1. Hugoniot form describes the pressure history in the weapon after the projectile has traversed the muzzle.
2. The projectile traverses the brake with uniform velocity.

From the Hugoniot Equation the space mean pressure in the weapon after the projectile has left the muzzle is given by:

$$\bar{p} = p_m (1 + B_1 t)^{-\frac{2\gamma}{\gamma-1}} \quad (\text{A.1})$$

where

- \bar{p} = space mean pressure^{1/}
- p_m = space mean pressure at the instant the projectile is discharged from the muzzle.
- $B_1 = (1+\beta) \left[\frac{12 FA}{v_T} \right] \left[\frac{\gamma-1}{2} \right] c_d' \sqrt{\frac{T_m}{T_o}} K$
- β = fraction of heat loss in weapon
- F = propellant impetus
- A = bore area

^{1/} The space mean pressure is the order of 90 per cent of the breech pressure for the type of weapon considered in this study. However, to simplify the analysis and without seriously affecting the results it shall be assumed that the ratio of space mean to breech pressure \bar{p}/p_c is equal to unity.

- v_T = total gun volume
 C_d' = discharge coefficient, muzzle
 γ = ratio of specific heats of propellant gas
 T_m = gas temperature at shot ejection
 T_o = isochoric flame temperature of propellant gas
 K = Isentropic flow constant
 $K = \left[\frac{\gamma g}{F} \left(\frac{2}{\gamma+1} \right)^{\frac{\gamma+1}{\gamma-1}} \right]^{1/2}$
 g = gravity acceleration

The pressure history in the brake during the period when the projectile is present can be obtained from the following:

Energy Balance

$$c_p N T_g = \beta_1 c_p N T_g + c_v (N - N_1) T_b + c_p N_1 T_b \quad (A.2)$$

Equation of State

$$p_b \left[v_b - AL_b + \frac{AL_b}{t_1} t \right] = 12F(N - N_1) \frac{T_b}{T_o}, \quad 0 \leq t \leq t_1 \quad (A.3)$$

$$\frac{dN}{dt} = C_d' KA \sqrt{\frac{T_o}{T_g}} \bar{p} \quad (A.4)$$

$$\frac{dN_1}{dt} = C_d'' KA_p \sqrt{\frac{T_o}{T_b}} p_b, \quad 0 \leq t \leq t_1$$

where

- N = quantity of gas entering the brake
 T_g = gas temperature leaving barrel
 T_b = gas temperature in brake
 c_p = isobaric specific heat of propellant gas
 c_v = isochoric specific heat of propellant gas
 C_d'' = discharge coefficient brake ports
 N_1 = quantity of gas discharged from the brake
 β_1 = fraction of heat loss in brake
 p_b = brake pressure
 A = bore area
 L_b = length of projectile traverse in brake
 t_1 = time for projectile to traverse L_b at constant velocity
 A_p = total port area of brake, does not include projectile exit area
 v_b = interior volume of brake

Combining Eq. (A.2) (A.3) and (A.4) one can obtain

$$\frac{dy}{dT} + \frac{h}{1+rT} y = \frac{g_1}{1+rT} (1+bT)^{-\frac{2\gamma}{\gamma-1}}, \quad 0 \leq T \leq 1 \quad (A.5)$$

where

$$y = \frac{p_b}{p_m}$$

$$T = \frac{t}{t_1}$$

$$h = \frac{a + \gamma f_2 \sqrt{\theta_b}}{1 - a}$$

$$r = \frac{a}{1 - a}$$

$$g_1 = \frac{\gamma (1 - \beta_1) f_1 \sqrt{\theta_g}}{1 - a}$$

OEA

ORDNANCE ENGINEERING ASSOCIATES, INC.

$$f_2 = \frac{12FC_d''KA_p t_1}{v_b}$$

$$f_1 = \frac{12FC_d'KA t_1}{v_b}$$

$$\theta_g = \frac{T_g}{T_o}$$

$$\theta_b = \frac{T_b}{T_o}$$

$$a = \frac{AL_b}{v_b}$$

$$b = B_1 t_1$$

During the period after the projectile has passed through the brake, the basic equations become:

Equation of State

$$p_b v_b = 12F (N - N_1) \frac{T_b}{T_o} \quad (A.6)$$

and

$$\frac{dN_1}{dt} = \left[C_d''A_p + C_d'A \right] K \sqrt{\frac{T_o}{T_b}} p_b, \quad t > t_1 \quad (A.7)$$

The energy balance and rate of gas discharge are as given above.

The corresponding differential equation resulting from the combination of the above system of equations is

$$\frac{dy}{dT} + My = (1-a) g_1 (1+bT)^{-\frac{2\gamma}{\gamma-1}}, \quad T \geq T_1 \quad (A.8)$$

where

$$M = \gamma (f_1 + f_2) \sqrt{\theta_b}$$

OEA

ORDNANCE ENGINEERING ASSOCIATES, INC.

The solution to Eq. (A.5) is given by:

$$y = c_1 (1+rT)^{-\frac{h}{r}} - (1+rT)^{-\frac{h}{r}} \int_0^T \left[g_1 (1+b\xi)^{-\frac{2\gamma}{\gamma-1}} (1+r\xi)^{\frac{h+r}{r}} \right] d\xi$$

$0 \leq T \leq 1$ (A.9)

and for Eq. (A.8) by

$$y = c_1 e^{-MT} - e^{-MT} g_1 (1-a) \int_1^T e^{M\xi} (1+b\xi)^{-\frac{2\gamma}{\gamma-1}} d\xi$$

$T \geq 1$ (A.10)

The integrals of Eq. (A.9) and (A.10) are obtained based on the following assumptions

$$(1+b\xi)^{-\frac{2\gamma}{\gamma-1}} = (1-m\xi), \quad 0 \leq T \leq 1$$

$$m = \frac{2\gamma}{\gamma-1} b$$

This assumption is justifiable since b is small; the order of 10^{-2} and

$$(1+b\xi)^{-\frac{2\gamma}{\gamma-1}} = e^{-m\xi}, \quad T > 1$$

The solution to the differential equations describing the dimensionless pressure-time history in the brake are as follows:

$$y(T) = \frac{g_1}{h} \left[1 + \frac{m}{r} \right] \left[1 - (1+rT)^{-\frac{h}{r}} \right] - \left[\frac{g_1}{(h+r)} \right] \left[\frac{m}{r} \right] \left[(1+rT)^{-\frac{h}{r}} - (1+rT)^{-\frac{h}{r}} \right]$$

$0 \leq T \leq 1$ (A.11)

$$y(T) = y_1 e^{-M(T-1)} + g_1 \left[\frac{1-a}{M-n} \right] \left[\begin{matrix} -mT & -M(T-1)-m \\ e & -e \end{matrix} \right], T > 1 \quad (\text{A.12})$$

and

$$y_1 = y(1) \text{ from Eq. (A.11)}$$

A.2 BRAKE PERFORMANCE

From the definition of brake index, the following can be written

$$\cos \theta = \frac{I_e + (i-1) I_g}{I_p} \quad (\text{A.13})$$

where

- θ = angle of gas deflection, through thrust reversing ports, with respect to the weapon axis
- i = muzzle brake index
- I_e = momentum produced by the gas flow through the shot exit port.
- I_p = momentum induced by the gas flow through the brake reversing ports
- I_g = momentum resulting from gas flow through muzzle with no brake present

The impulse as shown above are obtainable from the following

$$I_e = C_f' A \int_{t_1}^{\infty} p_b dt = C_f' A \Lambda_2 p_m t_1 \quad (\text{A.14})$$

$$I_p = C_f'' A_p \int_0^{\infty} p_b dt = C_f'' A_p (\Lambda_1 + \Lambda_2) p_m t_1 \quad (\text{A.15})$$

$$I_g = C_f''' A \int_0^{\infty} p_c dt = C_f''' A \Lambda_3 p_m t_1 \quad (\text{A.16})$$

OEA

ORDNANCE ENGINEERING ASSOCIATES, INC.

where

C_f = thrust coefficient corresponding to each of the ports; muzzle, brake reversing and shot exit

$$\Lambda_1 = \int_0^1 y dT$$

$$\Lambda_2 = \int_1^{\infty} y dT$$

$$\Lambda_3 = \int_0^{\infty} \left(\frac{P_c}{P} \right) \left(\frac{\bar{p}}{P_m} \right) dT$$

Substituting Eqs. (A.15) and (A.12) into Eq. (A.13), obtain

$$\cos \theta = \frac{C_f' \Lambda_2 + (1-1) C_f''' \Lambda_3}{C_f'' \frac{A_p}{A} (\Lambda_1 + \Lambda_2)} \quad (A.17)$$

The Λ terms are evaluated from Eqs. (A.1), (A.11) and (A.12) as

$$\Lambda_1 = \frac{g_1}{h} \left[1 + \frac{m}{r} \right] \left[1 - \frac{(1+r) \left(1 - \frac{h}{r} \right) - 1}{r \left(1 - \frac{h}{r} \right)} \right] - \frac{g_1}{h+r} \left[\frac{m}{r} \right] \left[\frac{2+r}{2} - \frac{(1+r) \left(1 - \frac{h}{r} \right) - 1}{r \left(1 - \frac{h}{r} \right)} \right] \quad (A.18)$$

$$\Lambda_2 = \frac{1}{M} \left[y_1 + \frac{(1-a) g_1}{m} e^{-m} \right] \quad (\text{A.19})$$

$$\Lambda_3 = \frac{1}{b} \left(\frac{p}{c} \right) \left(\frac{\gamma-1}{\gamma+1} \right) \quad (\text{A.20})$$

APPENDIX B

STRESS ANALYSIS OF MUZZLE BRAKE BLAST
SUPPRESSION DEVICE - 105mm HOWITZER

OEA

ORDNANCE ENGINEERING ASSOCIATES, INC.

APPENDIX B

STRESS ANALYSIS OF MUZZLE BRAKE BLAST
SUPPRESSION DEVICE - 105mm HOWITZER

The design of the muzzle brake blast suppression device shown in Fig. 4.1 was based on the stress analysis given in this appendix.

B.1 EQUATIONS FOR CONICAL BAFFLE

The circumferential stress^{1/} in a conical section with internal pressure is given by

$$S_1 = \frac{PR_1}{t_1 \cos \gamma} \quad (B.1)$$

where

- p = internal gas pressure, psi
- R₁ = mean radius of wall, in.
- t₁ = wall thickness, in.
- γ = wall slope, deg.

The corresponding radial displacement is given by

$$\Delta R_1 = \frac{S_1 R_1}{E} \quad (B.2)$$

or

$$\Delta R_1 = \frac{PR_1^2}{Et_1 \cos \gamma}$$

where E = modulus of elasticity, psi.

The conical baffle wall shape was proportioned so that the hoop stress is essentially constant; the radial displacement under pressure loading is then proportional to R₁. The

^{1/} Roark, R. J., Formulas for Stress Analysis and Strain, McGraw Hill, N.Y., 1954, page 269.

gussets act to restrain this displacement giving rise to inward forces at the junction between gussets and baffle. For each circular ring segment of the conical baffle the following equations were derived by superposition of 180° loading of a circular ring^{2/} giving the following equations for 90° loading of the ring.

$$M = 0.136 WR_1 \quad (B.3)$$

$$\Delta R_1' = -0.060 \frac{WR_1^3}{EI_1} \quad (B.4)$$

$$S_b' = \frac{6M'}{t_1^2} \quad (B.5)$$

where

- M = maximum bending moment in circumferential direction, in.-lb
- M' = maximum unit bending moment in circumferential directions, in.-lb per in. of baffle length
- W = radial inward loading of ring section, lb
- I₁ = area moment of inertia of ring section, in.⁴
- ΔR₁' = radial inward deflection of ring, in.
- S_b' = bending stress in circumferential direction, psi

B.2 EQUATIONS FOR GUSSETS

The gussets were considered to be short cantilever beams joined to the mounting ring and loaded in the vertical plane at the junction with the baffle. As a conservative estimate it was assumed that the mounting ring and gussets are not affected by the gas pressure or radial expansion of the howitzer muzzle.

^{2/} Ibid, page 156, case 2.

Radial displacement of the gussets at the junction with the baffle, considering the unloaded end fixed to the mounting ring, is given by

$$\Delta R_2 = \frac{W\ell^3}{3EI_2} + \frac{6W\ell}{5A_2G} \quad (B.6)$$

where the first term represents the contribution from bending and the second term represents the contribution from shear loading^{3/}, and

- W = end loading of gusset during radial displacement of baffle, lb
- ℓ = length of gusset to mounting ring, neglecting remainder of gusset, in.
- I_2 = area moment of inertia of gusset at support in vertical plane, in.⁴
- G = modulus of rigidity, psi

Tensile stress in the gussets in the axial direction during pressure loading of the baffle is given by

$$S_2 = \frac{PA_b}{A_g} \quad (B.7)$$

where

- P = muzzle brake pressure, psi
- A_b = net projected area of conical baffle in vertical plane, in.²
- A_g = cross-sectional area of four gussets in vertical plane, in.²

Bending stress in the gussets at the junction with the mounting ring is expressed as

$$S_{b2} = \frac{W\ell}{Z} \quad (B.8)$$

where Z = section modulus of gusset in vertical plane, in.³

^{3/} Ibid, page 119.

B.3 EQUATIONS OF MOUNTING RING

The mounting ring is loaded at the front edge with concentrated bending moments, radial shear forces and longitudinal tension forces located 90° apart. Outward flaring of this end of the ring serves to reduce the radial load W and consequently the bending moment M in the conical baffle section. As a conservative estimate it was assumed that the bending moments and shear forces transmitted from the gussets are uniformly distributed around the circumference of the front edge. Then the contributions to the radial displacement of the gusset baffle junction by deformation of the mounting ring is given by:

$$\Delta R_3 = \lambda \phi + K W_0 \quad (\text{B.9})$$

where

ϕ = angular displacement of front edge of mounting ring, radians

$K W_0$ = radial displacement of mounting ring resulting from shear load W , in.

However^{4/},

$$\phi = \frac{M_0}{\lambda D} + \frac{W_0}{2D\lambda^2} \quad (\text{B.10})$$

where

$$M_0 = \frac{2W\lambda}{\pi R_3} \text{ in.-lb/in.} \quad (\text{B.11})$$

$$W_0 = \frac{2W}{\pi R_3} \text{ lb/in.} \quad (\text{B.11})$$

$$K = \frac{1}{2D\lambda^2} \left(\frac{1}{\lambda} + \frac{M_0}{W_0} \right) \text{ in.}^2/\text{lb} \quad (\text{B.12})$$

^{4/} Ibid, page 271.

$$\lambda = \sqrt[4]{\frac{3(1-\nu^2)}{R_3^2 t_3^2}} \text{ per in.} \quad (\text{B.13})$$

$$D = \frac{Et_3^3}{12(1-\nu^2)} \text{ lb-in.} \quad (\text{B.14})$$

and

R_3 = mean radius of ring, in.

ν = Poisson's ratio

t_3 = wall thickness of ring, in.

The maximum bending stress in the front edge of the mounting ring is given by

$$S_{b3} = \frac{6H_0}{t_3^2} + \frac{1.932 W_0}{\lambda t_3^2} \text{ lb/in.}^2 \quad (\text{B.15})$$

The tensile stress in the longitudinal direction resulting from longitudinal forces transmitted from the gussets is assumed uniformly distributed and approximated by

$$S_{t3} = \frac{PA_b}{A_r} \text{ lb/in.}^2 \quad (\text{B.16})$$

where A_r = cross-sectional area of ring in vertical plane.

B.4 SUPERPOSITION OF DISPLACEMENTS AND STRESSES

B.4.1 Radial Displacement at Gusset-Baffle Junction

The maximum radial displacement of the conical baffle without gussets attached occurs at the outer diameter as given by Eq. (B.2). For determination of the load and bending moment required to join the gussets and baffle, the disparity ΔR_1 from Eq. (B.2) is equated to the sum of $\Delta R_1'$, ΔR_2 and ΔR_3 as given by Eqs. (B.4), (B.6) and (B.9) respectively, or

$$\Delta R_1 = \Delta R' + \Delta R_2 + \Delta R_3 \quad (B.17)$$

This allows evaluation of W , M , M' , M_o and W_o so that the combined stresses in the brake can be determined.

a) For the Conical Baffle:

With

$$\begin{aligned} P &= 5000 \text{ psi} \\ R_1 &= 4.16 \text{ in. (mean radius of 1" section} \\ &\quad \text{at outer diameter of baffle)} \\ t_1 &= 0.98 \text{ in.} \\ E &= 30 \times 10^6 \text{ psi} \\ \gamma &= 62^\circ \end{aligned}$$

from Eqs. (B.2) and (B.4)

$$\Delta R_1 = 0.0062 \text{ in.}; \quad \Delta R_1' = 6.45 \times 10^{-10} W$$

b) For the Gussets

With

$$\begin{aligned} \ell &= 2.5 \text{ in.} \\ I_2 &= 0.5 \text{ in.}^4 \\ A_2 &= 1.5 \text{ in.}^2 \\ G &= 11 \times 10^6 \text{ psi} \end{aligned}$$

from Eq. (B.6)

$$\Delta R_2 = 5.28 \times 10^{-7} W$$

c) For the Mounting Ring

With

$$\begin{aligned} \ell &= 2.5 \text{ in.} \\ R_3 &= 3.04 \text{ in.} \\ t_3 &= 0.70 \text{ in.} \\ \nu &= 0.25 \\ \lambda &= 0.891 \\ D &= 9.10 \times 10^5 \end{aligned}$$

$$\Delta R_3 = 25.0 \times 10^{-7} W$$

Substituting these values into Eq. (B.17) results in

$$\begin{aligned} W &= 2260 \text{ lb} \\ \Delta R_1' &= 14.7 \times 10^{-7} \text{ in.} \\ \Delta R_2 &= 0.0012 \text{ in.} \\ \Delta R_3 &= 0.0050 \text{ in.} \end{aligned}$$

This indicates radial deflection of the baffles is not appreciably restricted by the gussets and mounting ring.

B.4.2 Evaluation of Combined Stresses

a) Conical Baffle

From Eqs. (B.1) (B.3) and (B.5)

$$\begin{aligned} S_1 &= 45,000 \text{ psi} \\ S_b' &= 8,000 \text{ psi} \end{aligned}$$

Maximum circumferential tensile stress at inner surface of baffle, $S_1 + S_b' = 53,000 \text{ psi}$.

b) Gussets

From Eqs. (B.7) and (B.8)

$$\begin{aligned} S_2 &= 45,700 \text{ psi} \\ S_{b2} &= 11,400 \text{ psi} \end{aligned}$$

Maximum tensile stress at junction between gusset and mounting ring inner surface becomes

$$S_2 + S_{b2} = 57,100 \text{ psi}$$

OEA

ORDNANCE ENGINEERING ASSOCIATES, INC.

Tensile stress in same section, upper surface, becomes

$$S_2 - S_{b2} = 34,300 \text{ psi}$$

c) Mounting Ring

From Eqs. (B.15) and (B.16),

$$S_{b3} = 16,500 \text{ psi}$$

$$S_{t3} = 19,400 \text{ psi}$$

These maximum stresses occur at different locations in ring and cannot be combined.

d) Tube Extension

Using Eqs. (B.1) and (B.2) with subscripts 4, and

$$R_4 = 2.39 \text{ in.}$$

$$t_4 = 0.33 \text{ in.}$$

$$\gamma = 0^\circ$$

$$S_4 = 36,200 \text{ psi}$$

$$\Delta R_4 = 0.0029 \text{ in.}$$

APPENDIX C

PRESSURE AND FLOW FIELD
EXTERIOR TO A GUN BLAST

By

A. C. Eringen and J. D. Ingram

OEA

ORDNANCE ENGINEERING ASSOCIATES, INC.

APPENDIX C

PRESSURE AND FLOW FIELD EXTERIOR TO A GUN BLAST

By

A. C. Eringen and J. D. Ingram

C.1 PHYSICAL BASIS OF THE PROBLEM

The health and safety of a gun crew requires that the acoustic noise level produced by a gun blast not exceed a predetermined value. To a first approximation, the noise level is proportional to the pressure rise. The Human Engineering Laboratories(1) recommend that no persons should be subjected to an overpressure exceeding 7 psi. Thus the problem of determination of the pressure fields and flow exterior to the gun, following the blast, must be solved. The basic problem may be divided into two parts: (a) the flow and pressure field interior to the gun tube; and (b) the flow and pressure field exterior to the gun.

The solution of the problem (a) supplies us with the initial conditions necessary for the problem (b) as may be seen from the following consideration: Upon ignition, the shell moves as a piston in the gun tube, thus pushing the air. This air is compressed so that a shock wave proceeds toward the muzzle. The flow condition between the shock wave and the shell and the waves generated and reflected between the two must be studied in order to know the initial condition at the outlet of the muzzle. This problem has been studied extensively, (2) and (3), in the form of various simplified mathematical models. The full-fledged problem is highly complicated, but not impossible.

OEA

ORDNANCE ENGINEERING ASSOCIATES, INC.

When the shock first reaches the muzzle, suppose that the flow and pressure fields at the muzzle are known:

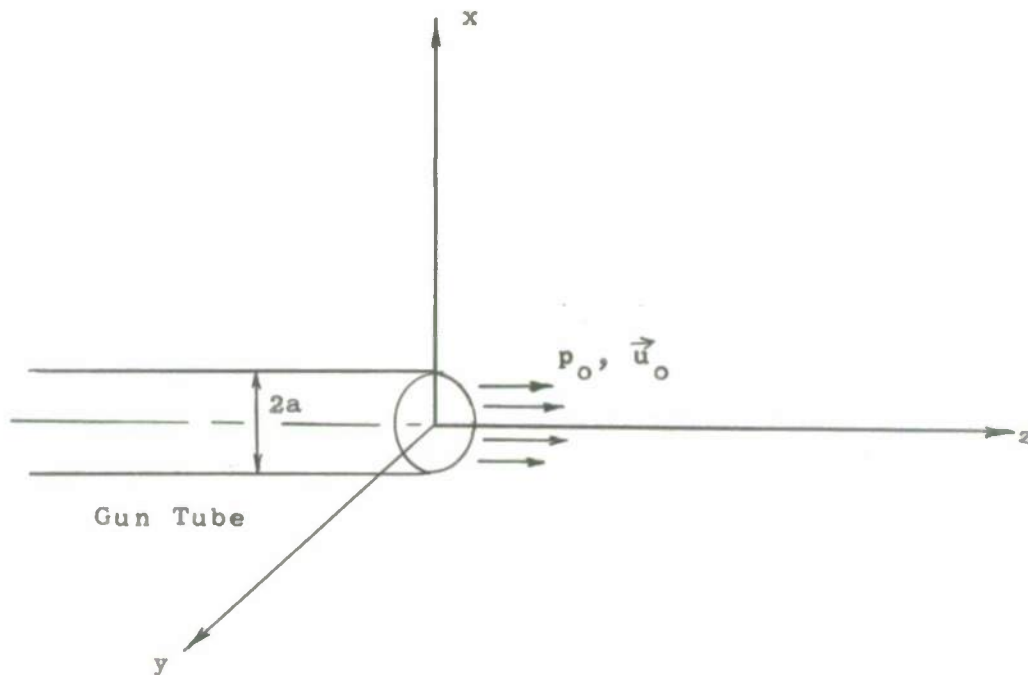


Figure C1

That is, suppose that the pressure p_0 , density ρ_0 , and velocity \vec{u}_0 at the origin of our rectangular coordinates x, y, z are determined through problem (a). We select the origin of time when shock waves reach the muzzle of the gun.

Given the initial state p_0, ρ_0, \vec{u}_0 the problem (b) is to determine p, ρ, \vec{u} at any space point as a function of time.

It is, therefore, clear that the problem (b) cannot be solved independently of problem (a), and that they are coupled through the muzzle shock. In the treatment of problem (b) we assume that p_0, ρ_0 and \vec{u}_0 at $t = 0$ are given. The exterior flow field now requires the solution of the basic equations of gas dynamics subject to some initial and boundary conditions.

The Initial Conditions require that we prescribe p, ρ, \vec{u} at time $t = 0$ throughout the region exterior to the gun tube.

The Boundary Conditions require that on the lateral surface of the gun and on any other rigid surface (such as the ground) the normal component of the velocity vanishes and at infinity the air be at rest at constant pressure and density.

The blast waves from a spherical explosion have been treated by Taylor (4) and others (5), (2). However, in the treatment of this problem, the so-called self similar motion forms have been employed. It is known that such solutions break down at pressure levels of 4kg/in.^2 . Moreover, the directional effect of the gun blast is not included in stationary point blast waves. Clearly the pressure at points which are mirror images of each other with respect to $z = 0$ plane are different. Therefore, spherical blast waves are not acceptable from the point of view of their lack of directionality.

The acoustic approximation treated in (6) on the other hand considers only motions due to density and heat addition inside a spatial region. The present problem, however, is basically an initial-value problem, requiring a different treatment. In order to cast light on the directionality of the problem and provide some intuitive basis for the most exact problem of finite amplitude waves, we give here a treatment of the limiting case of acoustical approximation.

C.2 ACOUSTICAL PROBLEM

The linearized equations of an axisymmetric acoustic field expressed in cylindrical coordinates (r, z) are (see Fig. C1):

$$\frac{\partial \rho}{\partial t} + \rho_a \left(\frac{\partial u}{\partial r} + \frac{u}{r} + \frac{\partial w}{\partial z} \right) = 0$$

$$\frac{\partial u}{\partial t} + \frac{1}{\rho_a} \frac{\partial p}{\partial r} = 0$$

$$\frac{\partial w}{\partial t} + \frac{1}{\rho_a} \frac{\partial p}{\partial z} = 0$$

$$p = c_a^2 \rho$$

(C2.1)

Here the first equation is the equation of conservation of mass; the next two are those of the balance of momentum and the last equation is the equation of state. The quantities p , ρ and (u, w) are respectively the pressure, the density and the velocity components. The ambient density and the constant velocity of sound are denoted by ρ_a and c_a respectively. In vector notation these equations may be written as

$$\frac{\partial \rho}{\partial t} + \rho_a \operatorname{div} \vec{u} = 0$$

$$\frac{\partial \vec{u}}{\partial t} + \frac{c_a^2}{\rho_a} \operatorname{grad} \rho = 0$$

$$p = c_a^2 \rho$$

(C2.2)

Initial Conditions require that at time $t = 0$ we prescribe the velocity and pressure fields, i.e.,

$$u(r, z, 0) = u_0(r, z)$$

$$w(r, z, 0) = w_0(r, z)$$

(C2.3)

$$p(r, z, 0) = p_0(r, z) = c_a^2 \rho(r, z, 0) = c_a^2 \rho_0(r, z)$$

where u_0 , w_0 and p_0 are given functions.

OEA

ORDNANCE ENGINEERING ASSOCIATES, INC.

The effect of the boundaries of gun tube will be neglected. The problem is, therefore, given an initial velocity and pressure (or density) distribution, to determine the resulting acoustical field. The solution is, further, subject to vanishing velocity field, constant atmospheric pressure, and density, at infinity.

C.3 THE SOLUTION OF THE ACOUSTIC PROBLEM

For the treatment of the initial-value problem at hand, the most appropriate tool is the Laplace transform as given in (7)

$$\bar{F}(r, z, s) = \int_0^{\infty} e^{-st} F(r, z, t) dt \quad (C3.1)$$

which has the inversion integral

$$F(r, z, t) = \frac{1}{2\pi i} \lim_{\beta \rightarrow \infty} \int_{\gamma - i\beta}^{\gamma + i\beta} e^{st} \bar{F}(r, z, s) ds \quad (C3.2)$$

where γ and β are real. For the region and conditions of validity of (C3.1) and (C3.2), see (7).

Applying the Laplace transform to (C2.2) we get

$$\begin{aligned} s\bar{\rho} + \rho_a \operatorname{div} \bar{\vec{u}} &= \rho_o \\ s\bar{\vec{u}} + \frac{c_a^2}{\rho_a} \operatorname{grad} \bar{\rho} &= \vec{u}_o \\ \bar{p} &= c_a^2 \bar{\rho} \end{aligned} \quad (C3.3)$$

where

$$\bar{p} = \bar{p}(r, z, s) = \int_0^{\infty} \rho(r, z, t) e^{-st} dt \quad (C3.4)$$

$$\bar{\vec{u}} = \bar{\vec{u}}(r, z, s) = \int_0^{\infty} \vec{u}(r, z, t) e^{-st} dt$$

etc., and

$$\bar{\vec{u}} = u \vec{e}_r + w \vec{e}_z, \quad \bar{\vec{u}}_0 = u_0 \vec{e}_r + w_0 \vec{e}_z \quad (C3.5)$$

are the velocity vectors and \vec{e}_r and \vec{e}_z are the unit vectors in r and z - directions.

From the last two of (C3.3) we solve for $\bar{\vec{u}}$:

$$\bar{\vec{u}} = \frac{1}{s} (\bar{\vec{u}}_0 - \frac{1}{\rho_a} \text{grad } \bar{p}) \quad (C3.6)$$

Substituting this into the first of (C3.3) we get

$$\nabla^2 \bar{p} - (s/c_a)^2 \bar{p} = \bar{F}(r, z, s) \quad (C3.7)$$

where

$$\nabla^2 \bar{p} = \frac{\partial^2 \bar{p}}{\partial r^2} + \frac{1}{r} \frac{\partial \bar{p}}{\partial r} + \frac{\partial^2 \bar{p}}{\partial z^2} \quad (C3.8)$$

$$\bar{F}(r, z, s) = P_a \text{div } \bar{\vec{u}}_0(r, z) - (s/c_a^2) p_0(r, z)$$

The problem is now reduced to solving the inhomogeneous Helmholtz equation (C3.7) for the infinite domain. This may be achieved by determining the Green's function

$G(r, \theta, z; \xi, \varphi, \zeta, t)$ whose Laplace transform satisfies (C3.7) with \bar{F} replaced by the three dimensional delta function, i.e.,

$$\nabla^2 \bar{G}(r, \theta, z; \xi, \varphi, \zeta, s) - (s^2/c_a^2) \bar{G} = \delta(r-\xi, z-\zeta, \theta-\varphi)$$

The solution to this equation in three dimensions is well-known. It is given by

$$\begin{aligned}\bar{G} &= \frac{-e^{-kR}}{4\pi R} \\ R^2 &= r^2 - 2r\xi \cos(\theta - \varphi) + \xi^2 + (z - \zeta)^2 \\ k &= (s/c_a)\end{aligned}\tag{C3.9}$$

The solution to equation (C3.7) may now be expressed as

$$\bar{p} = \iiint \bar{F}(\xi, \zeta, s) \bar{G}(r, \theta, z; \xi, \varphi, \zeta, s) \xi d\xi d\varphi d\zeta \tag{C3.10}$$

Since \bar{F} does not depend on φ we may integrate on φ directly. To this end we make use of the Sommerfeld representation of the point source at (ξ, φ, ζ) , i.e.,

$$\frac{e^{-kR}}{R} = \int_0^\infty J_0(\tau\rho) e^{-|\zeta - \zeta'| \sqrt{\tau^2 + k^2}} \frac{\tau}{\sqrt{\tau^2 + k^2}} d\tau \tag{C3.11}$$

where

$$\begin{aligned}\sqrt{\tau^2 + k^2} &= \gamma^2 \\ \rho^2 &= r^2 - 2r\xi \cos(\theta - \varphi) + \xi^2\end{aligned}$$

The addition formula for Bessel functions is

$$J_0(\tau\rho) = \sum_{n=0}^{\infty} \epsilon_n J_n(\tau\xi) J_n(\tau r) \cos n(\theta - \varphi) \tag{C3.12}$$

$$\begin{aligned}\epsilon_n &= 1 & n &= 0 \\ \epsilon_n &= 2 & n &= 1, 2, \dots\end{aligned}$$

Thus

$$\frac{e^{-kR}}{R} = \sum_{n=0}^{\infty} \int_0^{\infty} \epsilon_n J_n(\tau\xi) J_n(\tau r) \cos n(\theta-\varphi) \frac{e^{-\gamma|z-\zeta|}}{\gamma} \tau d\tau$$

Integrating on φ from 0 to 2π , only the term for $n=0$ contributes so that we obtain

$$\bar{G}^* = \int_0^{2\pi} \frac{-e^{-kR}}{4\pi R} d\varphi = \left(\frac{-1}{2}\right) \int_0^{\infty} J_0(\tau\xi) J_0(\tau r) e^{-\gamma|z-\zeta|} \frac{\tau}{\gamma} d\tau$$

The function $\bar{F}(r, z, s)$ given by (C3.8) is composed of two terms one of which is linear in s and the other independent of s . Consider now the following Laplace transform:

$$\int_0^{\infty} e^{-st} \frac{\partial P}{\partial t} dt = -P(0) + s\bar{P} \quad (C3.12a)$$

In our case, the initial pressure and velocity are prescribed inside a closed region, outside of which they both are zero. Hence, we may invert the Green's function as if it were independent of s and for the term linear in s simply take the time derivative of the resulting expression. Thus if \bar{G}^* is the Laplace transform of the Green's function for the axisymmetric inhomogeneous Helmholtz equation which is independent of s , the response to an initial pressure p_0 and velocity \vec{u}_0 is

$$p(r, z, t) = \iint (\rho_a \vec{\nabla} \cdot \vec{u}_0 G^*) \xi d\xi d\zeta - \frac{1}{c_a} \frac{\partial}{\partial t} \iint p_0(\xi, \zeta) G^* \xi d\xi d\zeta \quad (C3.13)$$

where

$$G^*(r, z; \xi, \zeta, t) = L^{-1} \left\{ \bar{G}^*(r, z; \xi, \zeta, s) \right\}$$

is the inverse Laplace transform of \bar{G}^* .

Returning now to the axially symmetric Green's function, we found that

$$\bar{G}^* = \left(-\frac{1}{2}\right) \int_0^{\infty} J_0(\tau\xi) J_0(\tau r) e^{-\nu|z-\zeta|} \frac{\tau d\tau}{\nu}$$

Now, apply the inverse Laplace transform to this equation

$$\begin{aligned} G^* &= L^{-1}\left\{\left(-\frac{1}{2}\right) \int_0^{\infty} J_0(\tau\xi) J_0(\tau r) e^{-\nu|z-\zeta|} \frac{\tau d\tau}{\nu}\right\} \\ &= \left(-\frac{1}{2}\right) \int_0^{\infty} J_0(\tau\xi) J_0(\tau r) L^{-1}\left(\frac{e^{-\nu|z-\zeta|}}{\nu}\right) \tau d\tau \quad (C3.14) \\ &= -\left(\frac{c_a}{2}\right) \int_0^{\infty} J_0(\tau\xi) J_0(\tau r) J_0\left(\tau\sqrt{c_a^2 t^2 - (z-\zeta)^2}\right) \tau d\tau, \quad c_a t > |z-\zeta| \\ &= 0, \quad 0 < c_a t < |z-\zeta| \end{aligned}$$

We may evaluate this integral exactly (8).

$$G^* = -\frac{c_a}{4\pi\Delta} \quad (C3.15)$$

if ξ , r , $\sqrt{c_a^2 t^2 - (z-\zeta)^2}$ make up a triangle, and $G^*=0$ otherwise. Here Δ is defined as the area of the triangle whose sides are ξ , r , and $\sqrt{c_a^2 t^2 - (z-\zeta)^2}$. As for the conditions for these to compose a triangle, first, they must all be positive; second, they must satisfy the following inequalities:

$$\xi + r + \sqrt{c_a^2 t^2 - (z-\zeta)^2} \geq 0 \quad (a) \quad (C3.16)$$

$$\xi - r + \sqrt{c_a^2 t^2 - (z-\zeta)^2} \geq 0 \quad (b)$$

OEA

ORDNANCE ENGINEERING ASSOCIATES, INC.

$$r - \xi + \sqrt{c_a^2 t^2 - (z - \zeta)^2} \geq 0 \quad (c)$$

$$(r + \xi) - \sqrt{c_a^2 t^2 - (z - \zeta)^2} \geq 0 \quad (d)$$

These then are the defining equations of the region of definition of the Green's function. The region R defined by (C3.16 b, c, d) is the inside of a circle in the ξ, ζ plane having its center at (r, z) and with radius $c_a t$. If the non-zero region of initial pressure and velocity is denoted by S, then, for the response to an arbitrary p_0 and \vec{u}_0 , we have

$$p(r, z, t) = \rho_a \iint_{R \cap S} \vec{\nabla} \cdot \vec{u}_0(\xi, \zeta) G^*(r, z; \xi, \zeta, t) \xi d\xi d\zeta - \frac{1}{c_a^2} \iint_{R \cap S} p_0(\xi, \zeta) \frac{\partial G^*}{\partial t}(r, z; \xi, \zeta, t) \xi d\xi d\zeta \quad (C3.17)$$

where $R \cap S$ signifies the region common to both R and S. (See Fig. C2)

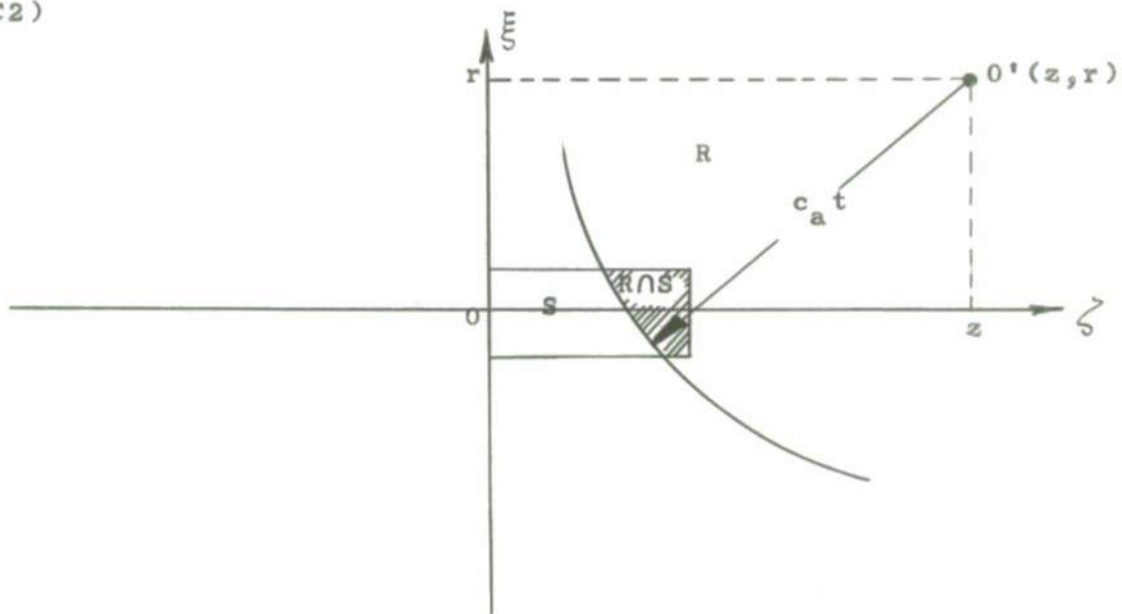


Figure C2

The explicit form of (C3.15) is

$$G^*(r, z; \xi, \zeta, t) = \frac{- (c_a / \pi)}{\sqrt{c_a^2 t^2 - (z - \zeta)^2 - (r - \xi)^2} \sqrt{(r + \xi)^2 + (z - \zeta)^2 - c_a^2 t^2}} \quad (C3.18)$$

Equation (C3.17) gives the pressure field for an arbitrary initial pressure and velocity. The velocity field may now be determined from (C3.6). This is omitted here.

C.4 Special Cases

C.4.1 Case I - Specification of Initial Velocity Distribution

Consider an axial initial velocity distribution over the cylindrical region $-\infty < z < z_0$, $0 < r < a$, i.e.,

$$\begin{aligned} \vec{u}_0 &= \vec{e}_z [V_0(1-U(z)) + V_0(1-z/z_0)(U(z) - U(z-z_0))], \quad 0 < r < a \quad (C4.1) \\ &= 0 \quad \text{otherwise} \end{aligned}$$

where $U(x)$ is the unit step function defined by

$$\begin{aligned} U(x) &= 0 & x < 0 \\ U(x) &= 1 & x \geq 0 \end{aligned}$$

The velocity distribution (C4.1) is shown in Figure C3.

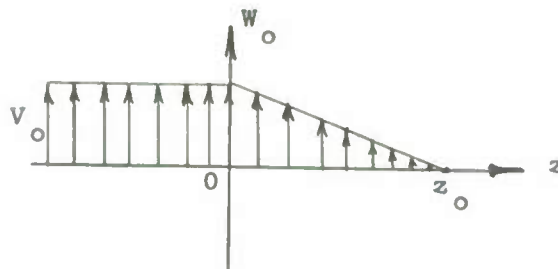


Figure C3

From (C4.1) it follows that

$$\vec{\nabla} \cdot \vec{u}_o = -\frac{V_o}{z_o} [U(z) - U(z-z_o)]$$

The region S then becomes

$$\begin{aligned} 0 \leq \zeta \leq z_o \\ 0 \leq \xi \leq a \end{aligned} \tag{C4.2}$$

From (C3.17) and (C4.1) it follows that

$$p = -\frac{\rho_a V_o}{z_o} \iint_{R \cap S} G^* \xi d\xi d\zeta \tag{C4.3}$$

This integral may be integrated with respect to ξ immediately.

$$p = \frac{c_a \rho_a V_o}{\pi z_o} \int_{\underline{\zeta}}^{\bar{\zeta}} \tan^{-1} \sqrt{\frac{\bar{\xi}^2 - A^2}{B^2 - \bar{\xi}^2}} d\zeta \tag{C4.4}$$

where

$$\begin{aligned} \bar{\xi} &= \max_{R \cap S} \xi(\zeta) \\ A &= \sqrt{c_a^2 t^2 - (z-\zeta)^2} - r \\ B &= \sqrt{c_a^2 t^2 - (z-\zeta)^2} + r \end{aligned} \tag{C4.5}$$

and $\bar{\zeta}$ and $\underline{\zeta}$ are determined by maximum and minimum ζ possible in $R \cap S$, (Figure C4). The term corresponding to the lower limit in the ξ integration vanished since $\bar{\xi}^2 = A^2$. For the case of $\sqrt{c_a^2 t^2 - (z-\zeta)^2} + r < a$ we have $\bar{\xi} = B$. Thus

$$p = \frac{c_a \rho_a V_o}{\pi z_o} \int_{\zeta_1}^{\zeta_2} \frac{\pi}{2} d\zeta = \frac{\rho_a V_o}{2z_o} c_a (\bar{\zeta} - \underline{\zeta}) \quad (C4.6)$$

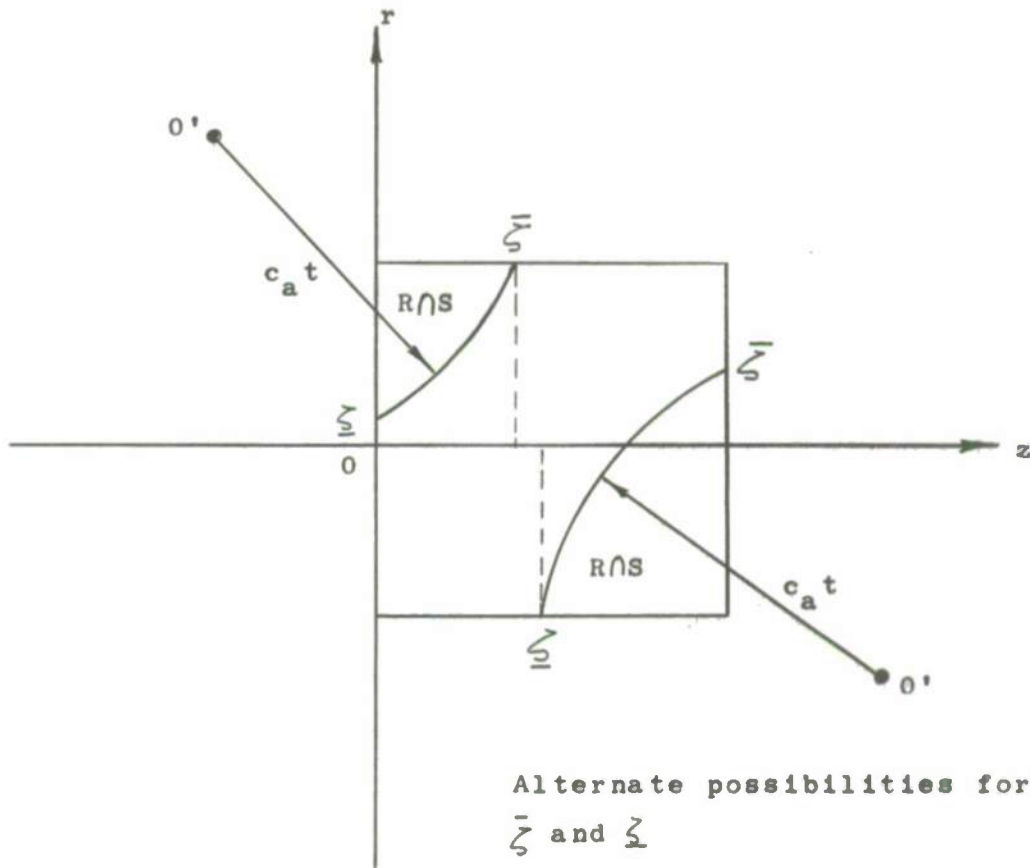


Figure C4

If, however, $B > a$ then we have $\bar{\zeta} = a$ and

$$p = \frac{\rho_a c_a V_o}{\pi z_o} \int_{\underline{\zeta}}^{\bar{\zeta}} \tan^{-1} \sqrt{\frac{a^2 - A^2}{B^2 - a^2}} d\zeta \quad (C4.7)$$

This is the case for $r > a$. In order to evaluate this integral, we integrate once by parts to obtain

$$p = -\frac{\rho_a c_a V_o}{\pi z_o} (z - \zeta) \tan^{-1} \sqrt{\frac{a^2 - A^2}{B^2 - a^2}} \Big|_{\underline{\zeta}}^{\bar{\zeta}} + \frac{\rho_a c_a V_o}{\pi z_o} \int_{\underline{\zeta}}^{\bar{\zeta}} (z - \zeta) \frac{\partial}{\partial \zeta} \tan^{-1} \sqrt{\frac{a^2 - A^2}{B^2 - a^2}} d\zeta$$

Now

$$\frac{\partial}{\partial \zeta} \tan^{-1} \sqrt{\frac{a^2 - A^2}{B^2 - a^2}} = \frac{-(z - \zeta) [c_a^2 t^2 - (z - \zeta)^2 - r^2 + a^2]}{2 [c_a^2 t^2 - (z - \zeta)^2] \sqrt{c_a^2 t^2 - (z - \zeta)^2 - (r - a)^2} \sqrt{(r + a)^2 + (z - \zeta)^2 - c_a^2 t^2}}$$

(C4.8)

and therefore,

$$p = - \frac{\rho_a c_a v_o}{\pi z_o} (z - \zeta) \tan^{-1} \sqrt{\frac{a^2 - A^2}{B^2 - a^2}} \Bigg|_{\zeta = \underline{\zeta}}^{\zeta = \bar{\zeta}}$$

$$- \frac{\rho_a c_a v_o}{2\pi z_o} \int_{\underline{\zeta}}^{\bar{\zeta}} \frac{(z - \zeta)^2 [c_a^2 t^2 - (z - \zeta)^2 - r^2 + a^2] d\zeta}{[c_a^2 t^2 - (z - \zeta)^2] \sqrt{c_a^2 t^2 - (z - \zeta)^2 - (r - a)^2} \sqrt{(r + a)^2 + (z - \zeta)^2 - c_a^2 t^2}}$$

(C4.9)

Let us examine the integral in detail. Let

$$I = - \int_{z - \underline{\zeta}}^{z - \bar{\zeta}} \frac{\lambda^2 [c_a^2 t^2 - \lambda^2 - r^2 + a^2] d\lambda}{[\lambda^2 - c_a^2 t^2] \sqrt{c_a^2 t^2 - \lambda^2 - (r - a)^2} \sqrt{\lambda^2 + (r + a)^2 - c_a^2 t^2}}$$

(C4.10)

This integral may be expressed in terms of elliptic functions.

We will make use of the following expressions (9).

$$\int_y^b \frac{\lambda^2 d\lambda}{\sqrt{(\lambda^2 - c^2)(b^2 - \lambda^2)}} = gb^2 E(\psi, k)$$

(C4.11)

$$\int_y^b \frac{(\lambda^2 - P_1) d\lambda}{(\lambda^2 - P) \sqrt{(b^2 - \lambda^2)(\lambda^2 - c^2)}} = \frac{b^2 - P_1}{(b^2 - P)} \cdot \frac{k}{a^2} \left[(a^2 - a_1^2) \pi(\psi, a^2, k) + a_1^2 F(\psi, k) \right]$$

where

$$g = \frac{1}{b} \quad k^2 = (b^2 - c^2)/b^2 \quad \text{sn}^2 u = (b^2 - \lambda^2)/(b^2 - c^2) \quad (C4.12)$$

$$\psi = \sin^{-1} \sqrt{\frac{b^2 - y^2}{b^2 - c^2}} \quad a_1^2 = \frac{(b^2 - c^2)}{(b^2 - P_1)} \quad a^2 = \frac{(b^2 - c^2)}{(b^2 - P)}$$

$F(\psi, k)$, $E(\psi, k)$ and $\pi(\psi, a^2, k)$ are the elliptic integrals of the first, second and third kind respectively, and are defined by

$$F(\psi, k) = \int_0^\psi \frac{d\theta}{\sqrt{1 - k^2 \sin^2 \theta}}$$

$$E(\psi, k) = \int_0^\psi \sqrt{1 - k^2 \sin^2 \theta} \, d\theta \quad (C4.13)$$

$$\pi(\psi, a^2, k) = \int_0^\psi \frac{d\theta}{(1 - a^2 \sin^2 \theta) \sqrt{1 - k^2 \sin^2 \theta}}$$

Applying these to equation (C4.9) we obtain

$$p = - \frac{\rho_a c_a v_o}{\pi z_o} \left[(z - \bar{\zeta}) \tan^{-1} \sqrt{\frac{a^2 - \bar{A}^2}{\bar{B}^2 - a^2}} - (z - \underline{\zeta}) \tan^{-1} \sqrt{\frac{a^2 - \underline{A}^2}{\underline{B}^2 - a^2}} \right]$$

$$\begin{aligned}
& + \frac{\rho_a c_a V_o}{2\pi z_o} \sqrt{c_a^2 t^2 - (r-a)^2} \left[E(\underline{\psi}, k) - E(\bar{\psi}, k) \right. \\
& + \frac{(r^2 - a^2)}{(r-a)^2} \frac{c_a^2 t^2}{\{c_a^2 t^2 - (r-a)^2\}} \left\{ \pi(\underline{\psi}, a^2, k) - \pi(\bar{\psi}, a^2, k) \right\} \\
& \left. + \frac{(r-a)^2}{\{c_a^2 t^2 - (r-a)^2\}} \left\{ F(\underline{\psi}, k) - F(\bar{\psi}, k) \right\} \right] \tag{C4.14}
\end{aligned}$$

where the quantities having bars above or below denote the corresponding quantities where ζ is replaced by $\bar{\zeta}$ and $\underline{\zeta}$ respectively.

C.4.2 Case II - Specification of Initial Pressure Distribution

As shown in equation (C3.12a) we need only multiply (C4.14) by $(z_o P_o / c_a^2 \rho_a V_o)$ and differentiate with respect to time to obtain the response to an initial pressure distribution

$$\begin{aligned}
p_o &= P_o [U(z) - U(z-z_o)] & r < a \\
&= 0 & r > a
\end{aligned} \tag{C4.15}$$

Thus we obtain

$$\begin{aligned}
p &= \frac{-P_o}{\pi c_a} \frac{\partial}{\partial t} \left[(z-\bar{\zeta}) \tan^{-1} \sqrt{\frac{a^2 - \bar{A}^2}{\bar{B}^2 - a^2}} - (z-\underline{\zeta}) \tan^{-1} \sqrt{\frac{a^2 - \underline{A}^2}{\underline{B}^2 - a^2}} \right] \\
& + \frac{P_o}{2\pi c_a} \frac{\partial}{\partial t} \left\{ \sqrt{c_a^2 t^2 - (r-a)^2} \left[E(\underline{\psi}, k) - E(\bar{\psi}, k) \right. \right. \\
& + \frac{(r^2 - a^2)}{(r-a)^2} \frac{c_a^2 t^2}{[c_a^2 t^2 - (r-a)^2]} \left\{ \pi(\underline{\psi}, a^2, k) - \pi(\bar{\psi}, a^2, k) \right\} \\
& \left. \left. + \frac{(r-a)^2}{[c_a^2 t^2 - (r-a)^2]} \left\{ F(\underline{\psi}, k) - F(\bar{\psi}, k) \right\} \right] \right\} \tag{C4.16}
\end{aligned}$$

It is possible to write the indicated partial differentiation in explicit forms. However, the expressions so obtained are cumbersome and for the present numerical calculations were not needed.

C.5 ASYMPTOTIC SOLUTIONS

The foregoing exact solution of the acoustic problem for a gun blast is expressed in terms of complicated elliptic functions which are not readily amenable to calculations. A limited amount of calculations, based on the exact solution (C4.14), are carried out on a digital computer and plotted in Figures C6 to C8. However, in order to gain a greater insight into the nature of the problem, it is felt that an asymptotic approach may be useful. The far field approximation is the basic theme of this article. To this end we explore the possibility of finding a Fourier integral representation to the solution of our basic equation (C3.7). We divide the space into two regions $r \leq a$ and $r > a$, and find the solutions of (C3.7) subject to

$$\bar{F} = 0 \quad \text{for } r > a \quad (\text{C5.1})$$

and that the pressure p and its partial derivative $\partial p / \partial r$ are continuous at $r = a$.

The Fourier transform $\tilde{\Phi}(s)$ of a function $\Phi(z)$ and its inverse are respectively given by

$$\begin{aligned} \Phi(\zeta) &\equiv \frac{1}{2\pi} \int_{-\infty}^{\infty} \Phi(z) e^{i\zeta z} dz \\ \Phi(z) &\equiv \int_{-\infty}^{\infty} \tilde{\Phi}(\zeta) e^{-i\zeta z} d\zeta \end{aligned} \quad (\text{C5.2})$$

We now try to find a Fourier integral representation for the solution of (C3.7) in the forms

$$\bar{p} = \int_{-\infty}^{\infty} \xi(\zeta) K_0(\gamma r) e^{-1\zeta z} d\zeta \quad r \geq a \quad (C5.3)$$

$$\bar{p} = \int_{-\infty}^{\infty} \eta(\zeta) I_0(\gamma r) e^{-1\zeta z} d\zeta - \int_{-\infty}^{\infty} \frac{f(s, \zeta) e^{-1\zeta z} d\zeta}{k^2 + \zeta^2} \quad r < a \quad (C5.4)$$

where $\xi(\zeta)$ and $\eta(\zeta)$ are two functions to be determined, $I_0(\gamma r)$ and $K_0(\gamma r)$ are the modified Bessel functions of zeroth order and

$$\gamma = \sqrt{\zeta^2 + k^2}, \quad k = s/c_a \quad (C5.5)$$

$$f(s, \zeta) = \frac{1}{2\pi} \int_{-\infty}^{\infty} \bar{F}(s, z) e^{-i\zeta z} dz$$

Here we have assumed that \bar{F} is independent of r for $r < a$.

The continuity of the pressure p and its normal gradient $\partial p / \partial r$ at $r = a$ and $t > 0$ requires that

$$\xi(\zeta) K_0(\gamma a) = \eta(\zeta) I_0(\gamma a) - f(s, \zeta) / \gamma^2$$

$$\xi(\zeta) K_1(\gamma a) = -\eta(\zeta) I_1(\gamma a)$$

Solving these two equations for ξ and η we find

$$\xi(\zeta) [K_0(\gamma a) I_1(\gamma a) + K_1(\gamma a) I_0(\gamma a)] = -\frac{f(s, \zeta)}{\gamma^2} I_1(\gamma a)$$

or

$$\xi(\zeta) = -\frac{a}{\gamma} f(s, \zeta) I_1(\gamma a) \quad (C5.6)$$

OEA

ORDNANCE ENGINEERING ASSOCIATES, INC.

where we have employed the Wronskian relation

$$K_0(x) I_1(x) + K_1(x) I_0(x) = \frac{1}{x}$$

Similarly

$$\eta(\zeta) = \frac{a}{\nu} f(s, \zeta) K_1(\nu a) \quad (C5.7)$$

The final solution is, therefore, found to be

$$p = -L^{-1} \left\{ \int_{-\infty}^{\infty} a \frac{f(s, \zeta)}{\nu} I_1(\nu a) K_0(\nu r) e^{-i\zeta z} d\zeta \right\} \quad r \geq a \quad (C5.8)$$

$$p = L^{-1} \left\{ \int_{-\infty}^{\infty} \left[a \frac{f(s, \zeta)}{\nu} I_0(\nu r) K_1(\nu a) - \frac{f(s, \zeta)}{\nu^2} \right] e^{-i\zeta z} d\zeta \right\} \quad r < a$$

It is these integrals which we will use for the asymptotic development. The pressure field will be determined at points far from the source, i.e. for

$$R \equiv \sqrt{(r-a)^2 + z^2} \gg 1$$

In general ζ and s are complex numbers such that the integrals appearing in (C5.8) are exponentially dominated. Asymptotic development of integrals of the form

$$I \equiv \int_{-\infty}^{\infty} \frac{K_0(\nu r)}{\nu} I_1(\nu a) e^{-i\zeta z} d\zeta \quad (C5.9)$$

is obtained for the region $r \geq a$. We rewrite this integral in a form convenient for our purpose.

$$I = \int_{-\infty}^{\infty} \left[e^{\nu(r-a)} K_0(\nu r) I_1(\nu a) \right] e^{-\nu(r-a) - i\zeta z} \frac{d\zeta}{\nu} \quad (C5.10)$$

OEA

ORDNANCE ENGINEERING ASSOCIATES, INC.

The quantity inside of the bracket in the integral is a slowly varying, well behaved function. Replacing the Bessel functions by their asymptotic expansions we obtain

$$\begin{aligned}
 I &\approx \int_{-\infty}^{\infty} \sqrt{\frac{\pi}{2\gamma r}} e^{-\gamma(r-a)} \frac{1}{\sqrt{2\pi\gamma a}} e^{-i\zeta z} \frac{d\zeta}{\gamma} \\
 &= \frac{1}{2\sqrt{ra}} \int_{-\infty}^{\infty} e^{-\gamma(r-a) - i\zeta z} \frac{d\zeta}{\gamma^2} \quad r > a \quad (C5.11)
 \end{aligned}$$

The method of steepest descent may now be applied to this integral to obtain its form for large R. We will find, however, that the saddle point lies close to the pole introduced by the use of the asymptotic expressions for the Bessel functions. This pole is not a part of the solution and may, therefore, be removed by the use of a Laurent series expansion. First we examine the position of the saddle point. The exponential portion of the above integrand is

$$E = -\gamma(r-a) - i\zeta z$$

At the saddle point we have

$$\frac{dE}{d\zeta} = \frac{-\zeta}{\gamma} (r-a) - iz = 0$$

The solution of this equation gives the saddle point ζ_0 .

$$\zeta_0 = \frac{-ikz}{\sqrt{(r-a)^2 + z^2}} \approx \frac{-ikz}{R} \quad (C5.12)$$

At the saddle point, γ takes the value

$$\gamma_0 = \frac{k(r-a)}{R} \quad (C5.13)$$

Since the pole corresponding to $1/\gamma^2$ is at $\zeta = -ik$, the saddle point lies between the origin and the pole as shown in Fig. C5.

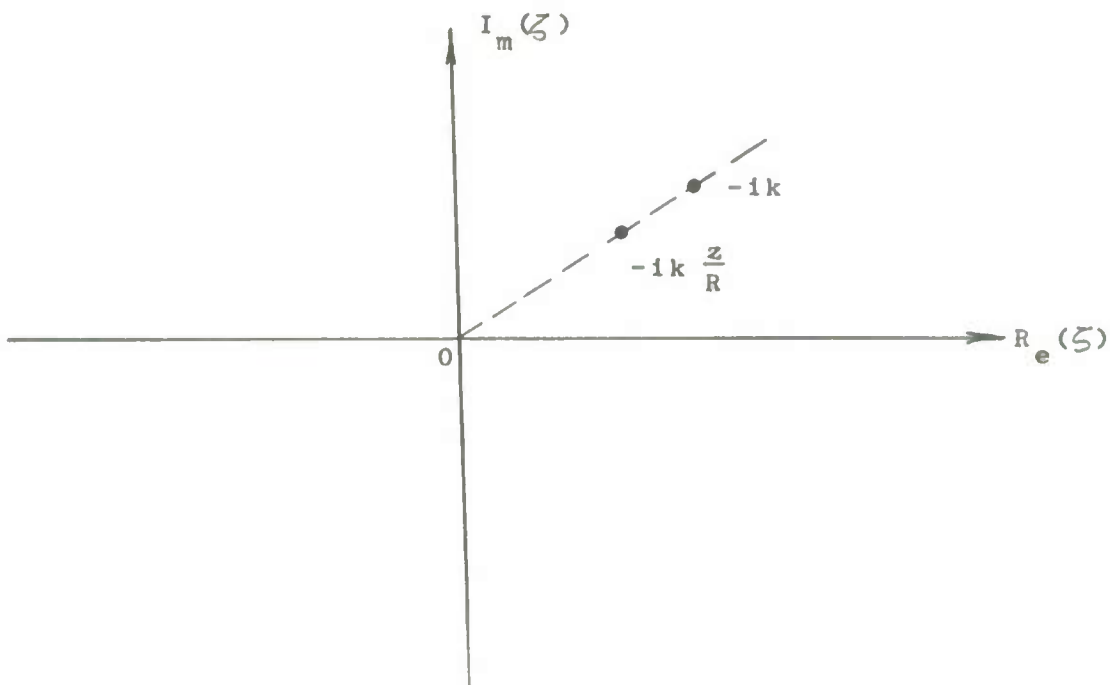


Fig. C5 - COMPLEX - PLANE

As stated above, we now remove the singularity at the pole by expanding $1/(\zeta^2+k^2)$ in a Laurent series, i.e.,

$$\frac{1}{\zeta^2 + k^2} = \frac{(-1/2)}{(\zeta + ik) ik} + \frac{1}{4k^2} + \frac{(\zeta + ik)}{8ik^3} + \dots$$

Ignoring the terms in ζ^n when $n > 0$, we obtain

$$\begin{aligned} \frac{1}{\zeta^2} &= \frac{1}{\zeta^2+k^2} = \frac{(-1/2)}{(\zeta + ik) ik} + \frac{1}{4k^2} \sum_{n=0}^{\infty} \left(\frac{1}{2}\right)^n \\ &= \frac{-1}{2ik(\zeta + ik)} + \frac{1}{2k^2} \end{aligned}$$

Integral (C5.11), with this substitution and dropping the residue contribution due to pole, gives

$$I = \frac{1}{4k^2 \sqrt{ra}} \oint e^{-kR} e^{-\left[\frac{R^3}{k(r-a)^2} \frac{(\zeta - \zeta_0)^2}{2} \right]} d\zeta$$

where we have expanded the exponent in Taylor series about the saddle point and retained only terms up to second order. Making the substitution

$$\zeta - \zeta_0 = \sqrt{k} x$$

$$d\zeta = \sqrt{k} dx$$

and extending our path of integration to infinity in both directions along the path of steepest descent we find

$$I \approx \frac{e^{-kR}}{4 \sqrt{ra} k^{3/2}} \int_{-\infty}^{\infty} e^{\frac{-R^3}{(r-a)^2} \frac{x^2}{2}} dx \quad (C5.14)$$

$$\approx \frac{(r-a)}{4k^{3/2} R^{3/2}} \sqrt{\frac{2\pi}{ra}} e^{-kR}$$

The asymptotic representation of the pressure field is, therefore, given by

$$p(r, z, t) = \frac{(r-a)}{4 \sqrt{2\pi} c_a} \sqrt{\frac{a}{r}} L^{-1} \left\{ \int_{-\infty}^{\infty} P_0(\zeta) \frac{e^{-kR}}{k^{1/2} R^{3/2}} d\zeta \right\}$$

where

$$R = \sqrt{(\zeta - z)^2 + (r - a)^2}$$

Upon exchanging the operator L^{-1} and the integral we find

$$p(r, z, t) = \frac{(r-a)}{4 \sqrt{2\pi} c_a} \sqrt{\frac{a}{r}} \int_{-\infty}^{\infty} \frac{P_0(\zeta)}{R^{3/2}} L^{-1} \left\{ \frac{e^{-s \frac{R}{c_a}}}{s^{1/2}} \right\} d\zeta$$

OE A

ORDNANCE ENGINEERING ASSOCIATES, INC.

but

$$L^{-1} \left\{ \frac{e^{-s \frac{R}{c_a}}}{s^{1/2}} \right\} = \frac{U(t-R/c_a)}{\sqrt{\pi(t-R/c_a)}}$$

where $U(t-R/c_a)$ is the unit step function. Consequently the asymptotic approximation of pressure field takes the final form.

$$p = \frac{(r-a)}{\sqrt{2}} \frac{\sqrt{a}}{4\pi} \frac{1}{\sqrt{rc_a}} \int_{-\infty}^{\infty} \frac{p_o(\zeta)}{R^{3/2}} \frac{U(t-R/c_a)}{\sqrt{t-R/c_a}} d\zeta \quad (C5.15)$$

We may now consider some special cases of pressure fields. Below is presented the case of uniform initial pressure over a finite region $(0, z_o)$, i.e.,

$$p_o(\zeta) = P_o [U(\zeta) - U(\zeta - z_o)] \quad (C5.16)$$

where P_o is a constant and $U(x)$ is the unit step function. Substitution of (C5.16) into (C5.15) gives

$$p = \frac{1}{\sqrt{2}} \frac{\sqrt{a}}{4\pi} \frac{1}{\sqrt{r}} (r-a) P_o \int_{-\infty}^{\infty} [U(\zeta) - U(\zeta - z_o)] U(t-R/c_a) \frac{d\zeta}{\sqrt{c_a t - R} R^{3/2}}$$

The first pressure arrives when

$$c_a^2 t^2 = (r-a)^2 + (z-z_o)^2$$

Therefore

$$p = \frac{1}{\sqrt{2}} \frac{\sqrt{a}}{4\pi} \frac{1}{\sqrt{r}} (r-a) P_o \int_{z - \sqrt{c_a^2 t^2 - (r-a)^2}}^{z_o} \frac{d\zeta}{\sqrt{c_a t - R} R^{3/2}}$$

until

$$c_a t = \sqrt{(r-a)^2 + z^2}$$

from then on

$$p = \frac{P_o}{\sqrt{2} 4\pi} \sqrt{\frac{a}{r}} \int_0^{z_o} \frac{d\zeta}{\sqrt{c_a^2 t - R} R^{3/2}} > c_a t \gg \sqrt{(r-a)^2 + z^2}$$

We can see quickly that the maximum of this integral occurs at $c_a^2 t^2 = (r-a)^2 + z^2$ and is given by

$$p_{\max}(r, z) = \frac{P_o}{\sqrt{2} 4\pi} \sqrt{\frac{a}{r}} (r-a) \int_0^{z_o} \frac{d\zeta}{\left[\sqrt{(r-a)^2 + (z-\zeta)^2} \right]^{3/2} \left[\sqrt{(r-a)^2 + z^2} - \sqrt{(r-a)^2 + (z-\zeta)^2} \right]}$$

Obviously most of the contribution to this integral occurs at $\zeta = 0$, hence

$$p_{\max}(r, z) \cong \frac{P_o}{\sqrt{2} 2\pi} \sqrt{\frac{a}{r}} \frac{(r-a)}{\sqrt{(r-a)^2 + z^2}} \sqrt{\frac{z_o}{z}}$$

This expression is valid for $z \geq z_o$. Similar ones may be obtained for $0 < z < z_o$ and $z < 0$. These asymptotic solutions do not have a well defined domain of validity. However, we may make the qualitative statement that they break down for $z \gg r$. This is caused by the use of the asymptotic form of the Bessel functions. An approximate region of validity is indicated by the dotted lines in Fig. C11. Plots of the isobars for the peak in the pressure distribution are given in Fig. C11.

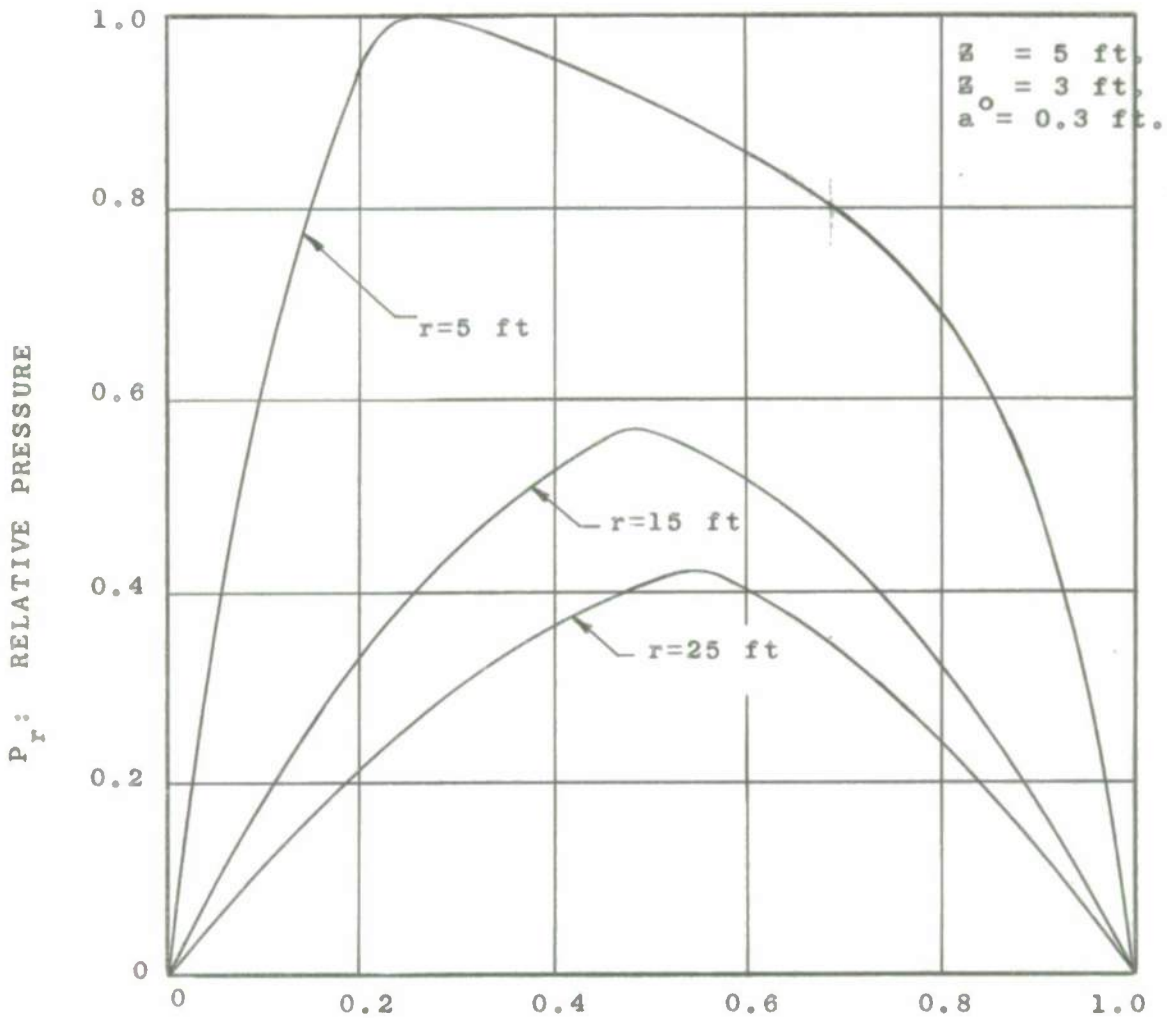
C.6 CONCLUSIONS AND SUGGESTIONS

The results of the numerical work done on this problem are given in Figs. C6 to C12. Figures C6 and C7 show the waveforms obtained from equations (C4.14) as a function of the radial and axial coordinates. Note that the decay in the z direction is more rapid than in the radial direction. This is a manifestation of the development of cylindrical waves. This phenomenon is shown clearly in Fig. C8 in which the isobars for the peak in the

waveform are given. Figures C9 and C10 are the waveforms obtained from the asymptotic development. It should be noted that these are infinite in extent although they decay in time. The isobars for the asymptotic development are shown in Fig. C11. Here the region of doubt for these are indicated by dashed lines. The decay along the z axis for specified initial velocity distribution is given in Fig. C12.

The analytical work presented here can be applied to other types of initial velocity and pressure distributions. Further numerical work will no doubt cast better light into the nature of the problem. The acoustical problem of gun blast with muzzle brake can also be formulated and solved with the technique employed here. The effects of the presence of the gun and the reflection of the wave from the ground need novel considerations not included in the present analysis.

Finally a work or two may not be out of order in regard to the nonlinear problem involving strong shocks. From the above solution of the acoustical problem it is clear that the exact solution of the correct nonlinear problem, presently, is out of our reach. However an approximation in the form of spherical shock waves emanating from a point explosion with a given energy can be treated. While certain solutions of this problem are found in the literature, (2), (3), (4), they are not directly applicable to the problem at hand since no directionality is inherent in these solutions. The final solution of the nonlinear problem requires a skillful combination of analytical and computer work.



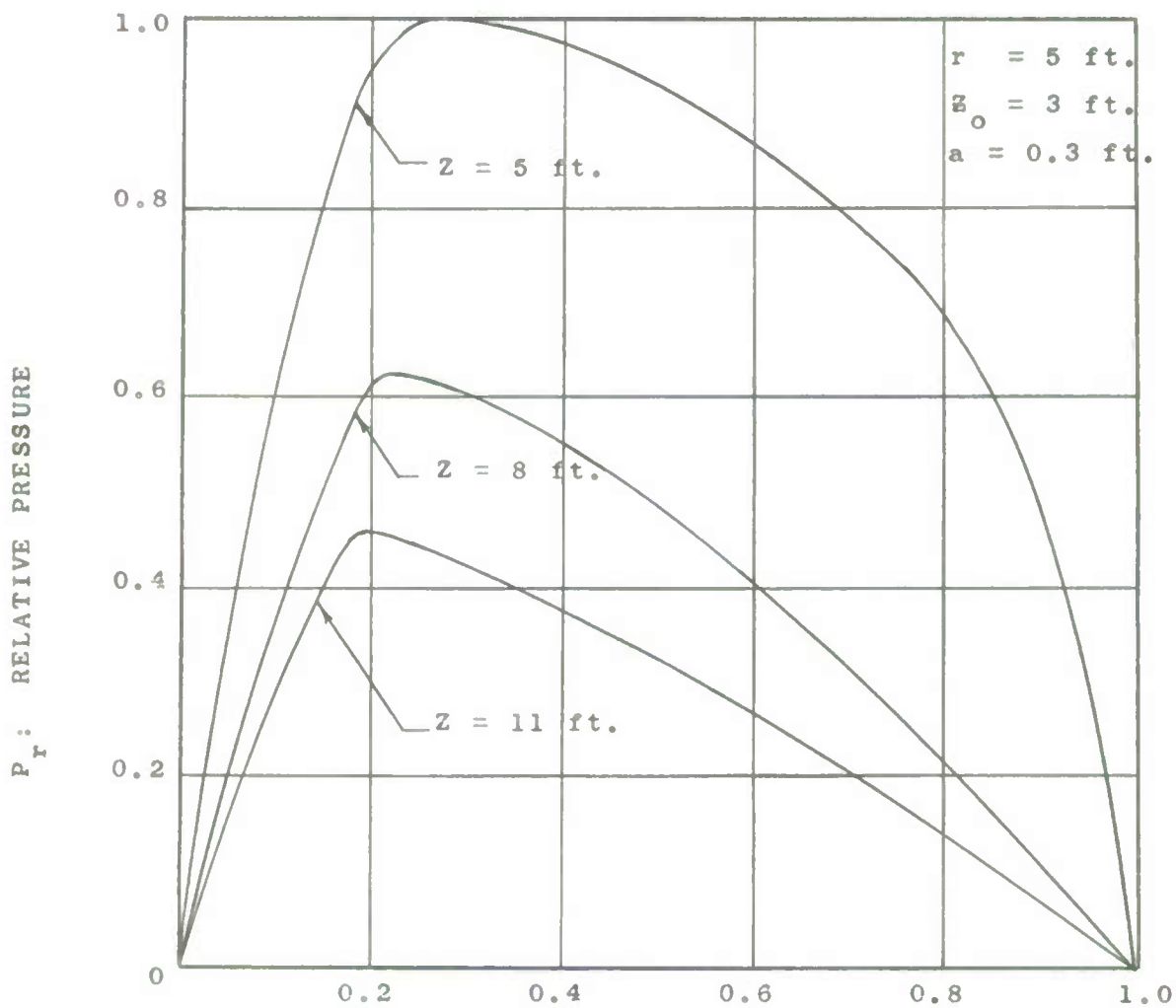
$$t^* = \frac{c_a t - \sqrt{(r-a)^2 + (z-z_0)^2}}{\sqrt{(r+a)^2 + (z)^2} - \sqrt{(r-a)^2 + (z-z_0)^2}}$$

Fig. C6 - EXACT WAVEFORMS

$$P_r = \frac{\text{(Pressure at } r \text{ and } z\text{)}}{\text{(Pressure at } r=5', z=5'\text{)}}$$

OEA

ORDNANCE ENGINEERING ASSOCIATES, INC.



$$t^* = \frac{c_a t - \sqrt{(r-a)^2 + (z-z_0)^2}}{\sqrt{(r+a)^2 + (z)^2} - \sqrt{(r-a)^2 + (z-z_0)^2}}$$

Fig. C7 - EXACT WAVEFORMS

$$P_r = \frac{(\text{Pressure at } r \text{ and } z)}{(\text{Pressure at } r=5', z=5')}$$

OEA

ORDNANCE ENGINEERING ASSOCIATES, INC.

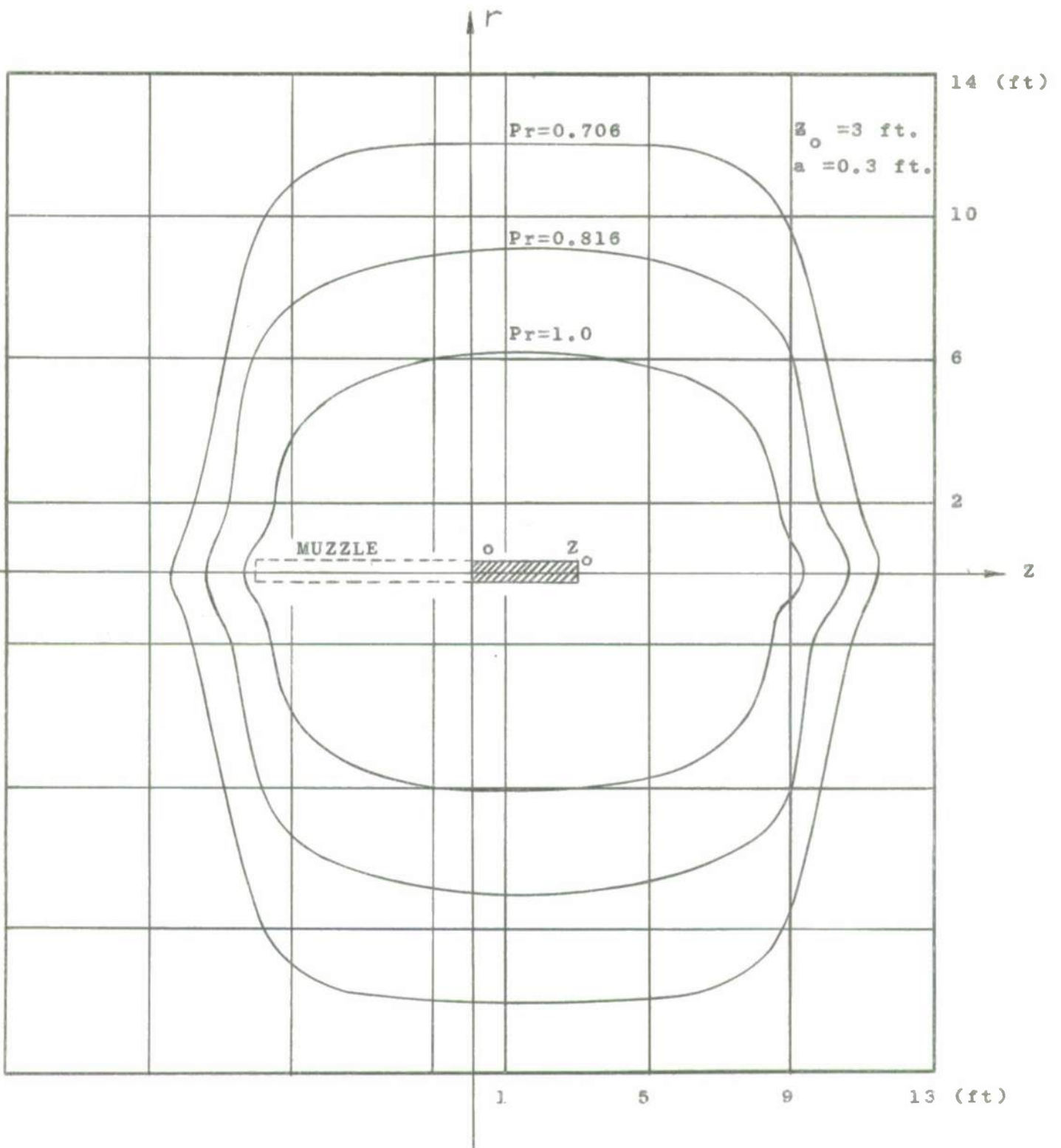


Fig. C8 - PEAK PRESSURE ISOBARS

OEA

ORDNANCE ENGINEERING ASSOCIATES, INC.

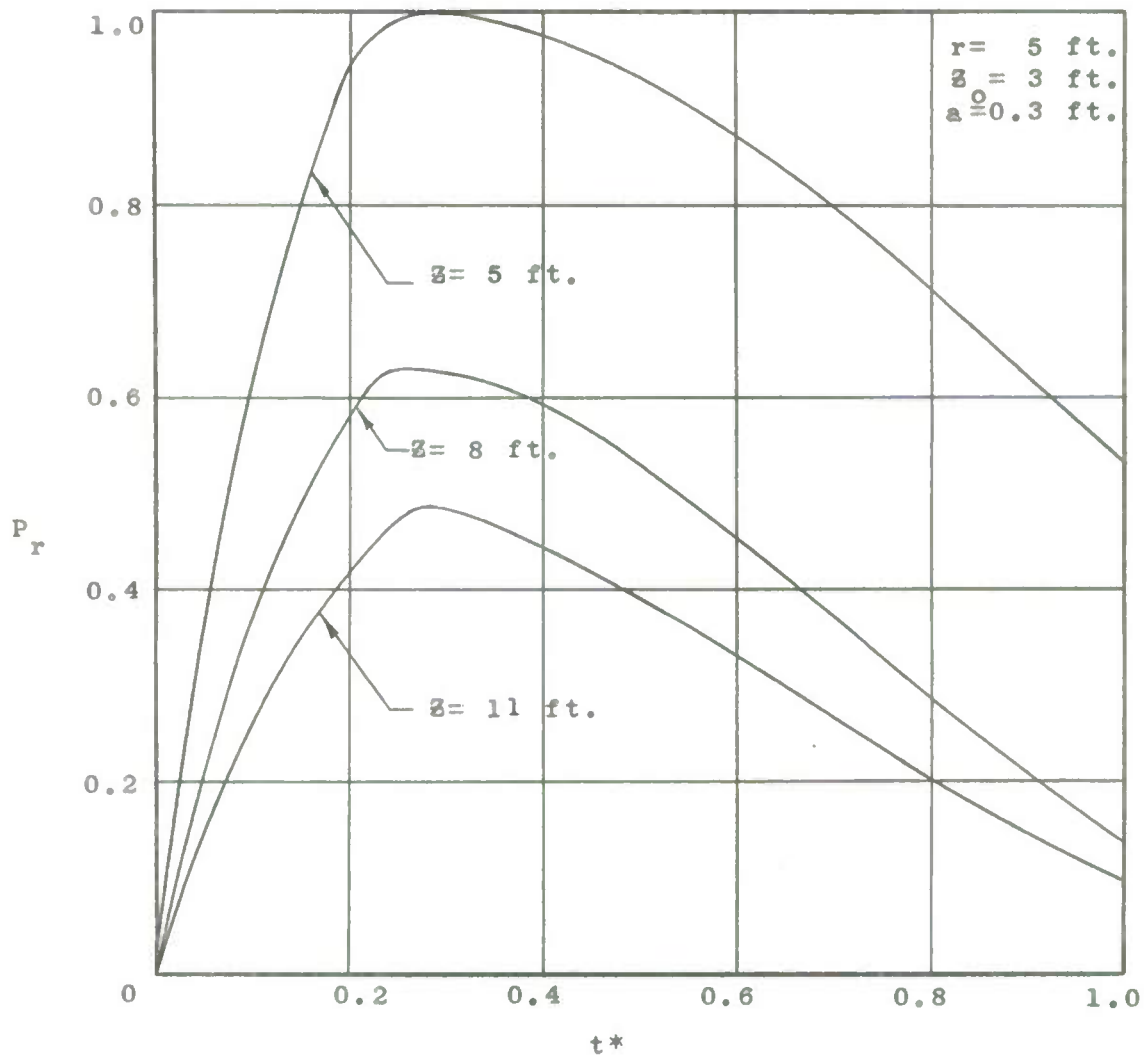


Fig. C9 - ASYMPTOTIC WAVEFORMS

$$P_r = \frac{(\text{Pressure at } r \text{ and } z)}{(\text{Pressure at } r=5', z'=5')}$$

OEA

ORDNANCE ENGINEERING ASSOCIATES, INC.

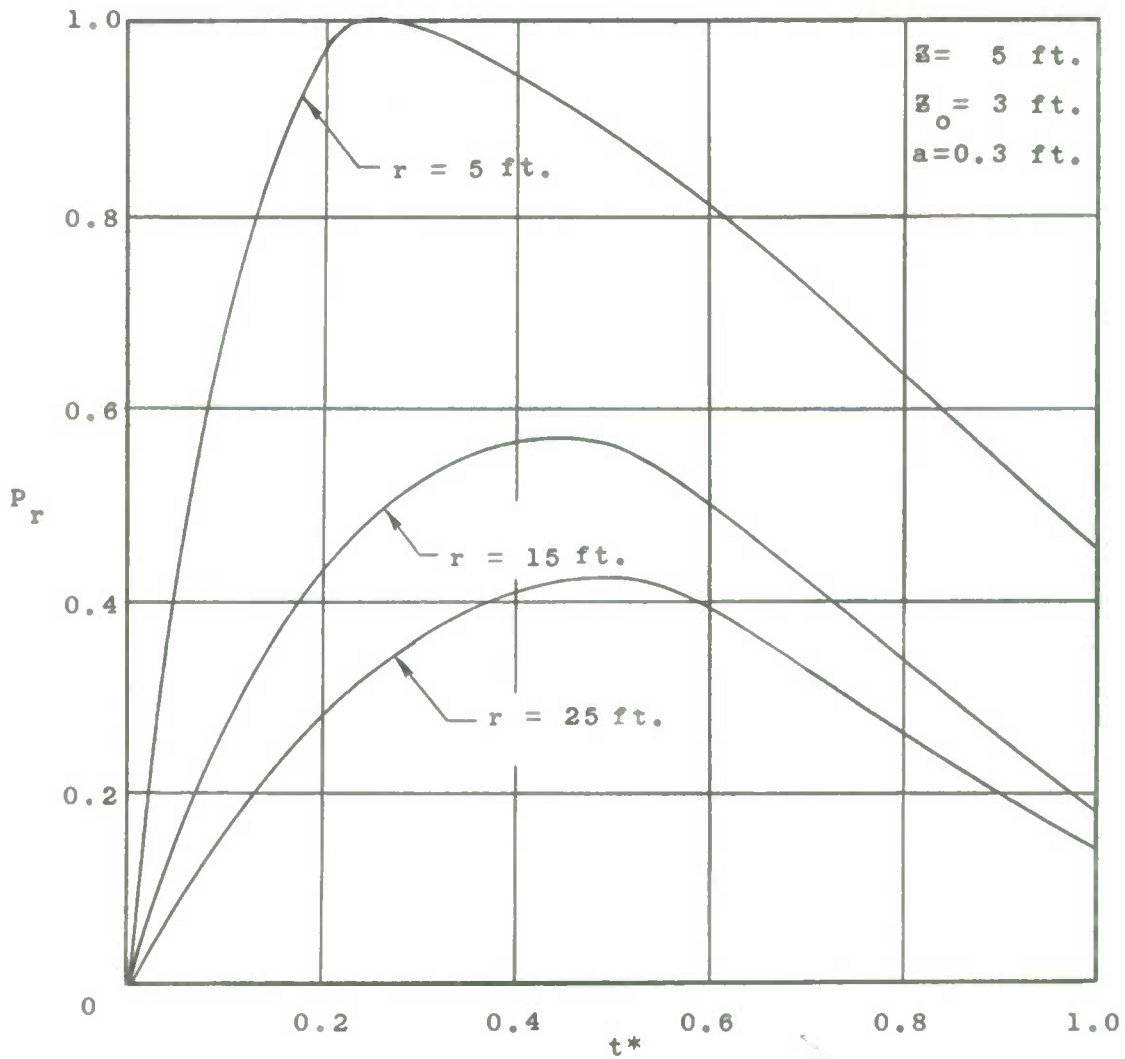


Fig. C10 - ASYMPTOTIC WAVEFORMS

$$P_r = \frac{(\text{Pressure at } r \text{ and } z)}{(\text{Pressure at } r=5', z=5')}$$

OEA

ORDNANCE ENGINEERING ASSOCIATES, INC.

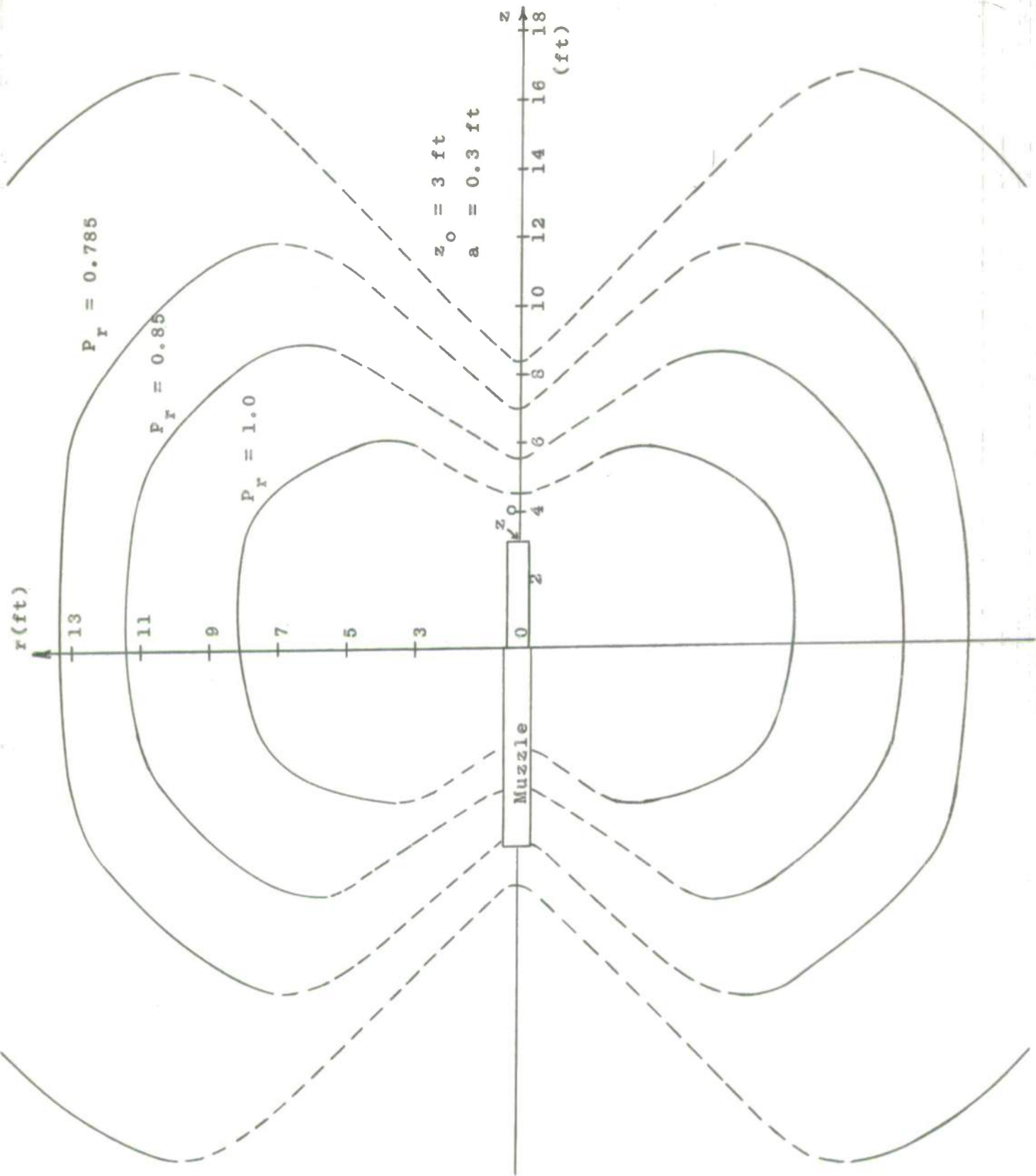


FIG. C11 - ASYMPTOTIC PEAK PRESSURE ISOBARS



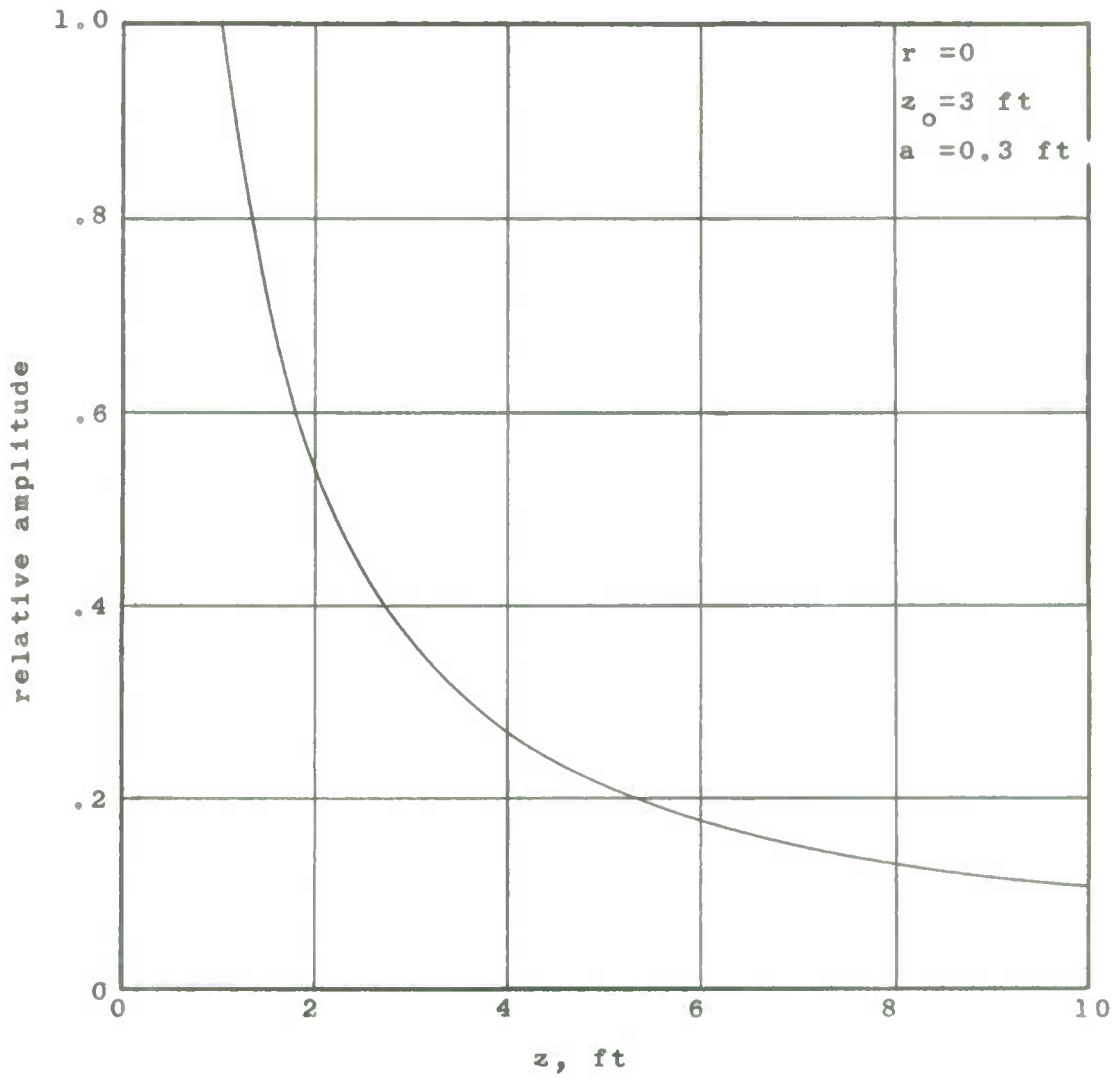


Fig. C12 - PEAK DECAY ALONG z AXIS; INITIAL VELOCITY

REFERENCES

- (1) Howard, Hollard H., Jr., Muzzle Blast Measurements on Howitzer, 105mm, XM103E1. Technical Memo 23-62, U.S. Army Human Engineering Laboratories, Aberdeen Proving Ground, Maryland.
- (2) Stanyukovich, K.P., Unsteady Motion of Continuous Media. Pergamon Press, 1960.
- (3) Courant, R. and Friedrichs, K.O., Supersonic Flow and Shock Waves. Interscience Publishers, 1948.
- (4) Howarth, L. (edit), Modern Developments in Fluid Dynamics. Vol. I, Oxford, 1953.
- (5) Brode, H.L., Space Plots of Pressure, Density and Particle Velocity for the Blast Wave From a Point Source. RM1913-AEC, The Rand Corporation, 1957.
- (6) Cole, J. D., Note on Directional Effects of Pressure Fields of Moving Blast. RM-848, The Rand Corporation, 1952.
- (7) Churchill, R. V., Operational Mathematics. McGraw-Hill, 1958.
- (8) Watson, G. N., A Treatise on the Theory of Bessel Functions. Cambridge: 1922, p. 411.
- (9) Byrd, P.F., and Friedman, M. D., Handbook of Elliptic Integrals for Engineers and Physicists. Berlin: Springer, 1954, pp. 56, 57, and 205.
- (10) Berning, W. W., Investigation of Blast Waves Over Relatively Large Distances and the Damaging Possibilities of Such Propagation. Rep. No. 675, Ballistic Research Laboratories, November 1948.
- (11) Schlenker, G., Contribution to the Analysis of Muzzle Brake Design. Report 62-1794, Rock Island Arsenal Research and Development Division, May, 1962.
- (12) Levin, S., and Kafadar, A. D., Concept and Feasibility Studies of Muzzle Brake Blast Suppression Devices for 105mm and 155mm Howitzers. Ordnance Engineering Associates, Inc., 27 December 1962.
- (13) McShane, E.J., Kelley, J.L., Reno, F.V., Exterior Ballistics. The University of Denver Press, 1953.

OEA

O R D N A N C E E N G I N E E R I N G A S S O C I A T E S , I N C .